N77-22483

FINAL REPORT

A FUNDAMENTAL APPROACH TO ADHESION: SYNTHESIS, SURFACE ANALYSIS, THERMODYNAMICS AND MECHANICS

by

David W. Dwight and James P. Wightman

Prepared for

National Aeronautics and Space Administration

February, 1977

Grant NSG-1124

NASA-Langley Research Center
Hampton, Virginia 23665
Materials Division
Donald J. Progar

Department of Chemistry
Virginia Polytechnic Institute and State University
Blacksburg, Virginia 24061

NOTICE

TABLE OF CONTEN

ACKNOWLEDGMENT

Most of the work described in this report was performed on samples supplied by Norm Johnston's Polymer Group at NASA-LaRC. Our studies would not have been possible without their efforts, especially Terry St. Clair and Paul Hergenrother in polymer synthesis and Don Progar in adhesive testing. Also gratefully acknowledged is the expert SEM operation of Frank Mitsianis.

LIST OF TABLES

LIST OF FIGURES

Page

GLOSSARY

TECHNIQUES

SEM - Scanning Electron Microscopy
EDAX - Energy Dispersive Analysis of X-ray Fluorescence
ESCA - Electron Spectroscopy for Chemical Analysis (X-ray photoelectron spectroscopy)
SRIRS - Specular Reflectance Infra-Red Spectroscopy
ISS - Ion Scattering Spectroscopy
SIMS - Secondary Ion Mass Spectroscopy
AES - Auger Electron Spectroscopy
FIM - Field Ion Microscopy

CHEMICALS, SOLVENTS, ETC.

BTDA - Benzophenone Tetracarboxylic Acid Dianhydride
DABP - Diaminobenzophenone
PMDA - Pyromellitic Dianhydride
ODPA - Oxydiphthalic Anhydride
EAH-13 - m,m''-Diamino Terbenzylone
DG - Diglyme
DMAC - Dimethylacetamide
DMF - Dimethylformamide
HT-S - Hercules Graphite fiber
P13N - Ciba-Giegy Addition Polyimide
PPQ - Polyphenylquinoxaline
LSS - Lap Shear Strength

I. Introduction

The trends in new materials research and development for advanced aerospace vehicles emphasize the use of composites of high-strength fibers and polymers. Surface characterization is especially important for optimizing properties of these systems, not only because adhesive bonding is the preferred method for fabrication, but also the bulk properties of composites depend critically upon interactions at the interface between the fibers and the polymer matrix. During the current grant period the majority of experiments were performed to elucidate the microscopic failure mechanisms of selected lap-shear tested specimens of several NASA-LaRC adhesive formulations on composite substrates composed of three different matrix polymers and HT-S graphite fiber.

Earlier work emphasized synthesis and strength-testing of novel high-temperature polymers, including variations in solvent, amine and anhydride in the adhesive formulation; high temperature aging and strength-testing; and aluminum powder adhesive filler (1-3). Surface characteristics associated with joint strength were evaluated with ESCA, SEM/EDAX, SRIRS and contact angles in a variety of preliminary experiments (4-7), and SEM/EDAX stood out as most effective. Detailed analysis of the surface structures of fractured joints revealed unique characteristics typical of specific adhesive formulations and test conditions*, and a "fracture mechanics" model was developed to promote

---

*This is not surprising; before the popularity of scanning electron microscopy, one reads, "The use of microscopy and associated techniques provides a great deal of information about fracture phenomena and in particular about fracture mechanisms and must always be an important tool in the study of this subject."...E. H. Andrews, Fracture in Polymers, American Elsevier, New York, 1968.

correlations between macroscopic shear strength and the microstructure of fracture surfaces (8).

Fractographic analysis of NASA-LaRC samples clearly identifies the major constituents of adhesive-bond strength and weakness, serving as a practical guide to the most likely means to improvements. Literature research and personal consultation have established a comprehensive program to predict and control the relevant polymer and interfacial properties. A unique series of international meetings on surface and polymer science provided the opportunity to present these results and refine our methods as well as to get an update from the other leading workers in the field (9-14).

Although the principal effort during the current grant period was directed toward understanding the effects of composites as adherends, several other variables were studied by fractography: aluminum powder adhesive filler, fiber glass cloth "scrim" or adhesive carrier, new adhesives PPQ-413 and LARC-13, and strength-test temperature. When the new results were juxtaposed with previous work, it appeared that complex interactions between adhesive, adherend, bonding and testing conditions govern the observed strength and fracture-surface features. Table I lists the design parameters likely to have a significant effect upon strength-test results.

A. Background

Qualitative application of fracture mechanics or theories of strength-of-materials identified the main factors to be (1) inherent flaws (e.g. voids), (2) interfacial failure, (3) viscoelastic and plastic deformation and (4) crazing and crack propagation. These are the four main categories of microscopic phenomena observed in fracture. For any test specimen, the observed strength results from the

Table I

Experimental Design Parameters

I. Adhesive Formulation

A. Polymer*
B. Solvent*
C. Al filler
D. Carrier cloth

II. Adherend

A. Ti6-4
B. Al
C. Composite*
D. Surface Treatment*

III. Bonding

A. Cure cycles*
B. Glue-line thickness

IV. Testing

A. Durability*
B. Geometry
C. Temperature
D. Rate

*Several parameters have been included under one category.

combination of these mechanisms. Variations in strength are accompanied by changes in the relative extent and specific nature of each of the four mechanisms.

In systems of interest to NASA LaRC, generally strength is diminished when either initial flaws or interfacial failure increase. Reversible (viscoelastic) and irreversible (plastic) deformations in the adhesive or adherends absorb energy and thus increase strength proportionally. Systematic study of microstructure and composition of fracture surfaces (fractography) provides qualitative analysis of the proportions of the constituent failure mechanisms. SEM/EDAX is the most powerful single technique because the microtopography can be observed with great depth-of-field, and qualitative elemental analysis of micron-thick layers can be obtained. In many cases of low strength, bulk flaws or causes for interfacial separation are immediately obvious. Further details on the chemical bonding and structures at the surface can be obtained with ESCA, SRIRS, and contact angles leading to positive identification of contaminants and weak boundary layers. High strength in NASA-LaRC samples must be obtained by absorbing strain energy through combinations of deformation, crazing and cracking. Although the effect of these mechanisms can be observed by SEM, dynamic mechanical tests are necessary for even semi-quantitative accounting for rheological factors. Table II diagramatically illustrates the interrelationships described above.

For improvements in practical, adhesive-bonding technology, it is expedient to know whether to make changes in the materials of construction, the methods of fabrication or in the interfaces. Fractographic study of the locus of failure usually identifies which is the weakest link.

The findings of the initial phase of our interdisciplinary program, using titanium 6-4 adherends, have been published (9). The main factor to limit strength and reproducability appeared to be voids in the glue-line that were generated during cure, either by residual solvent or water of imidization. Voids reduced the area of adhesive drawing and fracture and were nucleation sites for crack initiation.

Strength decreased when the test temperature increased. Photomicrographs showed a corresponding increase in interfacial failure and void area, and a decrease in the amount of plastic and brittle mechanisms. Apparently interfacial bonding was weakened by differential thermal expansion of the titanium and polyimide. Filling the adhesive with aluminum powder doubled the high-temperature shear

Table II

Relationships Among Surface and Polymer Analysis, Fracture Mechanics and Lap Shear Strength Test

ANALYTICAL METHOD AND RANGE OF APPLICATION		FAILURE MECHANISM	LAP SHEAR CHARACTERISTIC
SEM/EDAX	ESCA, SRIRS, Contact Angles	1. Initial Flaws	WEAKNESS
		2. "Interfacial" Separation	
	Dynamic Mechanical Tests ("WLF" Rheology)	3. Viscoelastic & Plastic Deformation	STRENGTH
		4. Crazing & Crack Propagation	

strength, and surface analysis showed that interfacial failure was eliminated and fracture-surface features were an order of magnitude smaller. Since the 20 kV electron beam in the SEM should penetrate about 1μm of organic polymer, we were able to show with the EDAX* accessory that fracture propagates farther from the interface at high-temperature.

The use of the solvents diglyme and dimethylformamide promoted good wetting by the adhesive, but diglyme resulted in plastic deformation while dimethylformamide gave high-area, brittle fracture. Dimethylacetamide solvent produced lower strength; surface analysis showed little deformation or brittle fracture-surface area and considerable interfacial failure, indicating that this solvent gave poor contact with the adherend. Changes in solvent probably effect polymer physical properties through variations in chain conformation or entanglement.

Adhesive formulations with either the anhydride PMDA or para-structures in the amine appeared more brittle than when anhydrides BTDA or ODPA or meta-amines were used. These conclusions were based on the fact that plastic deformation decreased and both interfacial failure and low-area brittle cracking (without extensive louvering) increased in the former cases. The totally pre-imidized "flow-bonding" adhesive film, made with EAH-13 amine, produced no voids and gave good strength despite apparent interfacial failure and the absence of brittle and plastic mechanisms. Here, elastic deformation (undetectable by SEM) is the probable cause of strength, and polymer rheology measurements are necessary to evaluate this contribution.

---

*Acronym for <u>E</u>nergy <u>D</u>ispersive <u>A</u>nalysis of <u>X</u>-ray fluorescence.

B. Literature Survey

Research reports in the areas of high-performance materials, surfaces, and adhesive bonding are increasing, and contributions were made during the grant period (10-14). The following highlights are relevant to NASA-LaRC problems.

Fundamental work on the characterization of solid surfaces is a continuing activity at the NASA Lewis Research Center and at the Wright-Patterson Air Force Base/University of Dayton Research Institute. Using field-ion microscopy, transfer of both polyimide and polytetrafluoroethylene was observed following simple touch contact with atomically clean tungsten emitter tips (in vacuo) (5). Chemical bonding between metal and polymer was suggested since imaging voltages of over 20 kV were needed to desorb the last atomic layer of transferred polymer. Surprisingly, deformation of the tungsten occurred if a 0.75 mg loading was used. Further details on the atomic nature of polymer-metal interactions in adhesion, and especially friction and wear, were analyzed by Auger electron spectroscopy (AES) (16). Combined with electron-induced desorption, the results indicated metal-to-carbon bonding in polytetrafluoroethylene and no participation of fluorine. Polymer adhesion to weaker metals (aluminum) in sliding contact was sufficient to transfer metal fragments to the polymer.

A variety of titanium and aluminum adherends have been characterized via a combination of Auger spectroscopy, Ion Scattering Spectroscopy (ISS), Secondary Ion Mass Spectroscopy (SIMS) and Scanning Electron Microscopy (SEM) (17). Also krypton adsorption isotherms and heats were used for surface characterization of high modulus graphite fibers used in composites. Consistent with our results on titanium, a phosphate/fluoride surface treatment altered the chemical and physical surface composition, whereas sodium hydroxide, nitric acid/hydrofluoric acid, ammonium bifluoride, and sulfuric acid/chromic acid treatments made little change compared with simple degreasing. In-depth profiles of elemental composition, obtained by simultaneous Auger analysis and argon-ion sputtering, show surface oxide layers with thickness (25-40 Å) independent of surface treatment (18). The data suggest that the anatase structure is stabilized by impurity ions. Durability should be promoted thereby; reversion to the rutile structure is accompanied by an 8% volume change which migh lower bond strength.

A new approach to understanding the properties of filled polymers identified the relative acid-base interactions between filler surface, polymer and solvent as the primary controlling factor (19). To characterize this interaction, electrokinetic potential measurements were made with fillers and polymers in low dielectric constant solvents. Correlations were demonstrated with modulus, tensile strength and SEM photos of the fracture surfaces. Perhaps the most significant observation was that without proper adjustment of the acid/base nature of all three components, it was <u>impossible to produce uniform films for testing</u>.

The difficulty of solvent and water removal would require a careful study of the transport of small molecules in polymeric glasses (20). However, some general and practical suggestions come from this type of study (21). Thermal and solvent annealing techniques have been successful in some homogeneous glassy polymers. Additive methods, similar to the procedures of paint or adhesive formulators, making use of binary solvents, thickeners and tackifiers, may be especially useful in forming practical adhesively-bonded joints. If the additives can be removed from the film without disruption, perhaps specimens could be prepared for fundamental physical property tests.

Brittle failure modes were consistent features of our previous work, and become even more prominent in the work reported here on composite substrates. This is predictable for fracture in glasses, and improvements in epoxy resins have been made by the addition of reactive rubber under carefully controlled conditions (22). SEM identified plastic deformation in the vicinity of numerous spherical inclusions of rubber particles. Particle size varied between 1 and 100 μm, and showed a dependence on the conditions of preparation. Maximum toughness was produced by a combination of large particles that favor tensile crazing with microcavitation and small particles that favor shear banding (23). Fracture energies required to drive a planar crack through the polymers in a double cantilever beam were determined. With exact control of precipitation, particle size and reactivity, values some 1500% of control were obtained with bisphenol A epichlorohydrin (DGEBA) resin and carboxyl-terminated acrylonitrile-butadiene (CTBN) liquid rubbers. Two disinclinations to this technology are that the toughened blends have lower heat-distortion temperatures, and more cross-linked (higher Tg) epoxys showed only modest toughening (24). Moreover, when adhesive bonds are subject to shear and tensile forces, improvements in strength may be much less spectacular than in fracture energy (25). Yet, it is a sound "micro-engineering" approach to somehow blend a more viscoelastic component into systems that are too brittle. Surprisingly, even an incompatible dispersed phase like poly(tetrafluoroethylene) (PTFE) seems to toughen some thermosets (26), although probably by a different mechanism than CTBN rubbers.

How to test adhesively-bonded joints is a matter of guesswork and opinion, but the fracture mechanics approach mentioned above has become popular. Proponents claim that failure always occurs due to the extension of some initially present, crack-like flaw in the glue-line. Therefore, limitations of bonded structures are defined by estimating the "flaw tolerance" or the force required to open a pre-formed crack (27). An additional complication is the need to assess the durability of the adhesive bond under service conditions. From the viewpoint of continuum mechanics, the most difficult problem is to determine the interaction between the surroundings and the material decomposing at the crack tip, where properties cannot be determined. Moreover, the experimental basis of mechanics has to do with rate-insensitive metals and ceramics, where propagation of cracks contributes little to fracture energy compared to crack-initiation. Generally, the reverse is true for polymers (28). Refined theoretical treatment predicts that "the rate-dependent fracture energy is the product of the intrinsic fracture energy of the polymer, presumably of molecular origin, and a non-dimensional function which embodies the (viscoelastic) rheology of the material surrounding the crack tip.." This approach clearly provides useful qualitative insight for adhesive bonding problems, and more quantitative results will evolve. For example, in poly(methyl methacrylate) dependence of fracture energy upon molecular weight was predicted directly from a theoretical, Griffith-type equation derived on the assumption that only molecules with molecular weight greater than 1×10^5 contribute to plastic deformation (29).

Although restricted to small strains (linear viscoelastic region), dynamic mechanical tests provide information on modulus, crystallinity, stress relaxation, and the effectiveness of additives (30). Fundamental to modern polymer characterization, these measurements provide a link between practically useful properties and basic molecular structure, where the synthetic polymer chemist has unprecedented facility to vary macromolecular architecture. On the other hand, the critical dependence of final properties upon processing conditions was emphasized in recent work that showed a marked dependence of the modulus on the solubility parameter of the casting solvent (31).

The implication for the development of high-performance adhesives and composites is that accurate characterization of most of the parameters in Table I is required to determine the predominant factors and interactions in each case. However, to approach the problem on a practical time frame, most of the variables are assumed (tacitly) negligible. Fractography is useful in both approaches: by providing a rapid check on assumptions of the technologist, and an insight into the components of failure important to the materials scientist.

Our new results include examples of (1) a surprising cause of weakness, inadvertently left on the adherend during surface preparation, (2) failure in the adherend when HT-S graphite fiber/ polymer matrix composites are used, (3) corresponding effects of fiber glass adhesive-carrier cloth or "scrim" on strength and fractography, and several other factors. These observations help in the design of improvements in adhesively bonded systems.

In our earlier studies, ESCA provided basic core-level binding energy or oxidation state data on the elements present in titanium and aluminum adherends, as well as changes that occur during various surface treatments (4-8). Also attempts were made to study fracture surfaces of lap-shear strength specimens.

Primary consideration was given this year to the quantitative aspects of ESCA peak intensities in terms of stoichiometry of the surface region. This is a most important and controversial area in electron spectroscopy currently, and leading authorities hold divergent opinions in some cases (32-34). A number of factors must be taken into account when interpreting ESCA intensity ratios (complications of interpreting absolute intensities eliminate practical utility today). Table III outlines roughly what the experimentalist must consider before attempting even semi-quantitative surface analysis (35,36).

Briefly, inorganic samples present greater difficulty than organic samples in general, although the latter class suffers more from X-ray beam damage and limited range of binding energy and chemical shift information. Other factors are minimized by comparing intensities of photoelectrons with very similar kinetic

TABLE III

Factors Influencing Relative ESCA Intensities

I. Class of Sample	II. Other Parameters
A. Organic	A. Contamination
B. Inorganic	B. Line Sensitivities
C. Smooth Film	C. Intrinsic and Matrix Effects
D. Rough: Film, Fiber, Fabric, or Particle	1. Shake-up and Shake-off Satellites 2. Energy Loss Satellites 3. Scattering
E. Atom distribution: lateral and depth	

energy. Sample roughness and instrumental beam geometry have been shown experimentally to alter even relative intensity ratios in ESCA (37). The effect has been predicted theoretically, and thus ratios may be corrected by accurate knowledge of the respective geometrical factors (38, 39). Either assumptions must be made or independent experimental evidence invoked to take both lateral and in-depth distribution of elements in the specific sample matrix into account.

Intensity of primary ESCA peaks is diminished by interactions of the photoelectron. "Extrinsic" processes such as inelastic scattering, phonon excitation, etc. and "intrinsic" mechanisms such as shake-up and shake-off phenomena must be considered explicitly (40). This means that the entire photoelectron spectrum must be recorded and all significant peaks included in calculations of relative atomic composition of the sampled volume. These computations require knowledge of the relative sensitivity or cross-section for photoionization for each peak; tables of values have been published, but there is a disturbing lack of agreement in some cases (32, 41, 42). Hydrocarbons deposit on the sample surface during most practical ESCA measurements; correction for contamination must be made.

Fortunately there are a variety of ways to obtain corroborative information to facilitate quantitative applications of ESCA, although the experimental time required may increase many-fold. The use of measurements on standards and model compounds, combined with theoretical calculations based on chemical and physical structure models, is the classical analytical approach (43). In situ cleaning (or depth-profiling) by ion beams or plasmas can remove contamination and other surface layers (44). Data on the spacial distribution of elements within the sampled volume can be obtained from variation in take-off angle ("grazing-angle" ESCA), and by using intensity ratios from two photoelectrons ejected from different core levels of the same element (45). Table IV summarizes these methods. The field remains very active with frequent publications in the areas of absolute calibration (46-48), relative intensities (49-51), and quantitative analysis (52).

D. T. Clark and co-workers have published a series of papers pioneering applications of ESCA to elucidate structure and bonding in polymers (53-55). Absolute and relative binding energies, and relative peak areas (intensities) were the primary sources of information capable of elucidating many polymer-surface chemistry problems, especially when coupled with model compound studies and *ab initio* MO calculations (53). Recently satellite peaks were reported in aromatic polymers, and attributed to shake-up processes involving $\pi^* \leftarrow \pi$ transitions (55). Thus ESCA shows a feature that may uniquely identify the local aromatic character in some polymers.

During the current grant period, quantitative use of ESCA peak intensities was studied, especially as an aid to fundamental characterization of polymers. We also show that "wide scan" ESCA spectra of metal adherends, before and after *in situ* ion bombardment, provide unique structural "fingerprints".

TABLE IV

Corroborative Techniques for Quantitative Electron Spectroscopy

I. Theoretical Calculations

   A. Chemical } Structural Models
   B. Physical

II. Etching *In Situ*

   A. Ion beam
   B. Plasma

III. Escape Depth *vs*. Electron Energy

IV. Angular Distribution

V. Standards and Model Compounds

II. Experimental

A. Apparatus and Procedures

1. Scanning Electron Microscopy/Energy Dispersive Analysis of X-rays (SEM/EDAX)

Photomicrographs were obtained using a polaroid camera back attached to the oscilloscope on the Advanced Metals Research Corporation Model 900 scanning electron microscope. Operating at 20 kV, high magnification views (500X-5000X) gave information on the details of surface features, while survey scans at 20X-200X provided a check on the distribution of representative features that describe the surface. For convenience in studying the results, approximate vertical dimensions of each photomicrograph appear at the right in the figures, and the corresponding magnification is listed in each caption. Specimens were cut to approximately 1 x 1 cm with either a high pressure cutting bar (titanium substrates) or a hack saw (composite substrates), and fastened to SEM mounting stubs with conductive, adhesive-coated, copper tape. To enhance conductivity of insulating samples, a thin (∿ 200 Å) film of Au/Pd alloy was vacuum-evaporated onto the samples. Photomicrographs were taken with the sample inclined 70° from the incident electron beam. Rapid, semi-quantitative elemental analyses were obtained with an EDAX International Model 707A energy-dispersive X-ray fluorescence analyzer attached to the AMR-900 SEM. A Polaroid photographic record of each spectrum was made using a camera specially adapted for the EDAX oscilloscope output. Tracings of the spectra are juxtaposed in the figures to facilitate interpretation.

2. Electron Spectroscopy for Chemical Analysis (ESCA)

Titanium and composite samples were cut as above, but to a size of approximately 5 x 20 mm to match the ESCA probe mount, and fastened with non-conductive, double-stick adhesive tape. Thin film samples of polyamic acids were cast from 15% diglyme solutions, and polycarbonate and polysulfone cast from ∿ 1% chloroform solutions directly on the ESCA probe. An AEI ES-100 X-ray photoelectron spectrometer with Al Kα radiation (1486.6 eV) operating at 15 kV and 20 mA excited the samples and the ESCA data were punched on paper tape using the AEI DS-100 Digital Data Aquisition System. A Digital PDP-8e computer/plotter provided flexible, graphic display of the spectra.

B. Materials

The Polymer Section of the Materials Division at NASA-LaRC synthesized the three adhesive resins designated LARC-3, LARC-13 and PPQ 413, formulated and applied them to various adherends and conducted lap shear strength measurements according to ASTM D1002-64. Details have been published (1-3, 56-58).

Professor J. E. McGrath, Chemistry Department, V.P.I.& S.U., kindly supplied the polysulfone and polycarbonate samples.

III. Results and Discussion

A. Scanning Electron Microscopy/Energy Dispersive Analysis of X-ray Fluorescence (SEM/EDAX).

1. Adherend Surfaces

a. HT-S Graphite Fiber/Polymer Matrix Composites

Three polymers were studied as the matrix component for HT-S graphite fibers: P13N, Skybond 710 and NR-150B2. Only sanding was employed for surface preparation, and in Figures 1-5, each of the composite adherends is shown at different magnifications both as received and after sanding. At low magnification in Figure 1, all of the composites appear rough on a large scale, both before and after sanding. The NR-150B2 and Skybond 710 samples look essentially identical at this level, while P13N looks smoother although basically similar. The graphite fibers are barely covered by the P13N resin as shown in Figure 2; sanding appears to scrape open voids near the surface and gouge out irregular pits between 5μm and 50μm in size. Particle (1-10μm) population on the surface appears as dense before as after sanding.

A relatively thick, bumpy polymer overlayer as received, and more extensive sanding effects are characteristic of the NR-150B2 (Figure 3) and Skybond 710 (Figures 4 and 5) matrix composites. Before sanding the topography indicates that a non-uniform layer (<25μm) of polymer covers the upper ply of HT-S graphite fibers, and it became imprinted by a release cloth used during the hot-press cure of the composite. In later studies of fracture surfaces with NR150-B2 composite adherends, we will show that the matrix resin at the surface contained the element silicon, probably deriving from a silicone mold-release agent. Sanding shatters the matrix resin surface, leaving behind a lot of particulate debris, fractured polymer surfaces, and some exposed and broken HT-S fibers. Although the two Skybond 710 samples were taken from the same stock and do have basically similar features, close inspection of Figure 5 reveals a curious, new microporosity.

These observations suggest that sanding may not be the optimum preparation for bonding to composite substrates. Perhaps a solvent treatment would be more effective to remove debris and allow molecular blending with the adhesive by swelling the adherend matrix surface. Most failures described in succeeding sections occur in the surface layers of the composite adherends; potential contaminants, stress concentrations or other fracture nuclei in this zone must be taken into account for improved strength in these systems.

FIGURE 1.

Wide-area views (20X) of
HT-S graphite fiber composite substrates
typical of this study.

Figure 1. Wide-area views (20X) of HT-S graphite fiber composite substrates typical of this study.

One-half of each sample is as received and the other half is after sanding. All composite adherends are rough before and after sanding.

P13N (top left)	NR-150B2 (top right)
Skybond 710 (1975) (bottom left)	Skybond 710 (1976) (bottom right)

2-12

5mm

5mm

21b

5mm

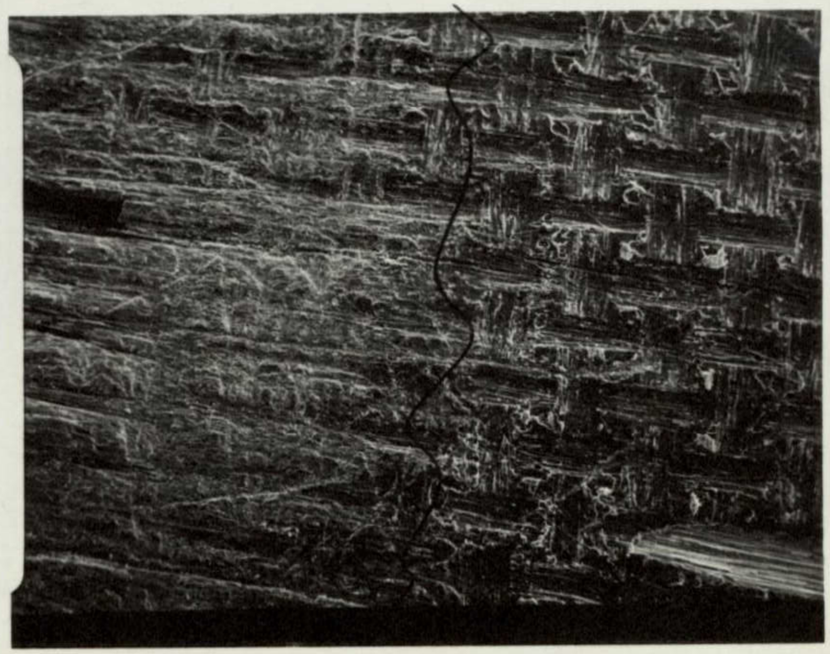

5mm

FIGURE 2.

Two higher magnifications (200X, 1000X) of
HT-S graphite fiber/P13N matrix composite;
as received on the left and
after sanding on the right.

Figure 2. Two higher magnifications (200X, 1000X) of HT-S graphite fiber/P13N matrix composite; as received on the left and after sanding on the right.

Smoothest composite as received. The upper layer of fibers is barely covered with resin. Sanding appears to scrape open surface voids and gouge out irregular pits between 5μm and 50μm in size. Some debris (1-10μm), but less than the other two types.

0.5mm

0.5mm

100 μm

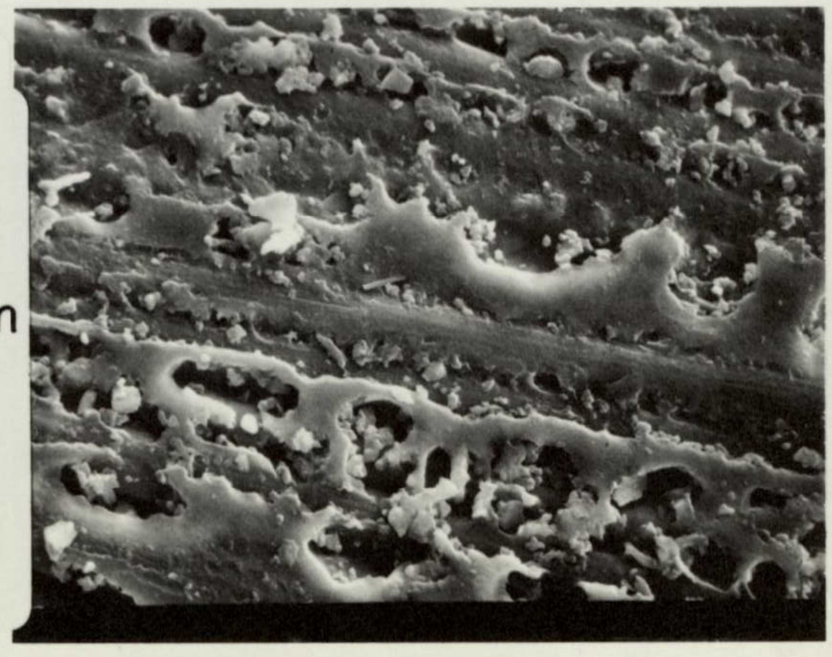

100 μm

FIGURE 3.

Two higher magnifications (200X, 1000X) of
HT-S graphite fiber/NR-150B2 matrix composite;
as received on the left and
after sanding on the right.

Figure 3. Two higher magnifications (200X, 1000X) of HT-S graphite fiber/NR-150B2 matrix composite; as received on the left and after sanding on the right.

Relatively thicker, bumpy polymer overlayer as received, bearing what appears to be the imprint of release cloth used during fabrication of the composite. EDAX shows a silicon signal from matrix areas, but not fiber surfaces (Figure 22). A silicone (e.g. mold release agent) is indicated rather than a silicon glass, because the latter always shows a calcium peak. Sanding shatters the matrix surface leaving 1-10μm size debris, and some exposed and broken fibers.

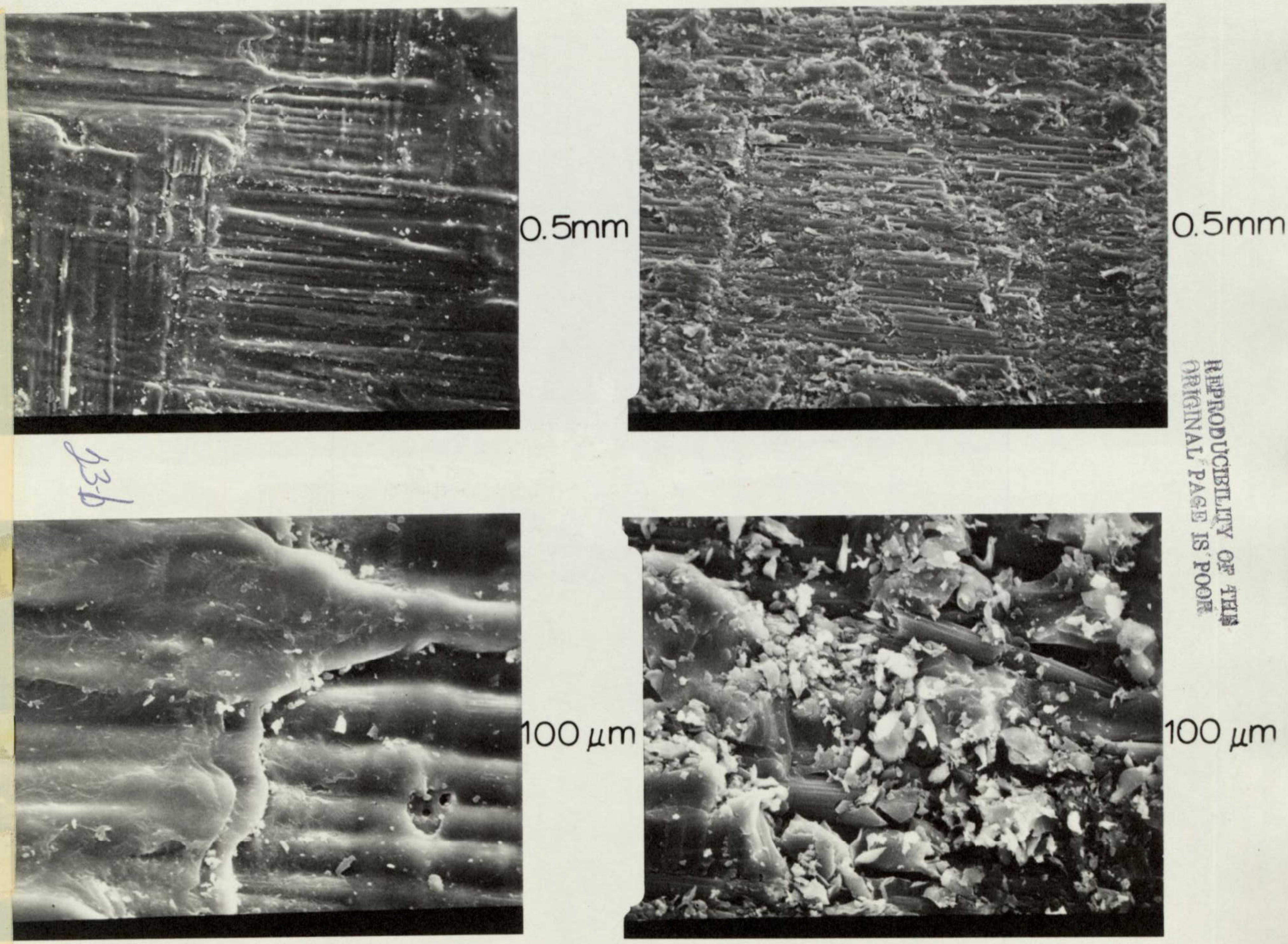

23-b

FIGURE 4.

Two higher magnifications (200X, 1000X) of
HT-S graphite fiber/Skybond 710 matrix composite;
as received on the left and
after sanding on the right. (1975)

Figure 4. Two higher magnifications (200X, 1000X) of HT-S graphite fiber/Skybond 710 matrix composite; as received on the left and after sanding on the right. (1975)

Relatively thickest polymer overlayer as received, also showing release-cloth imprint. Very similar to NR150-B2 composite after sanding.

24-a

0.5mm

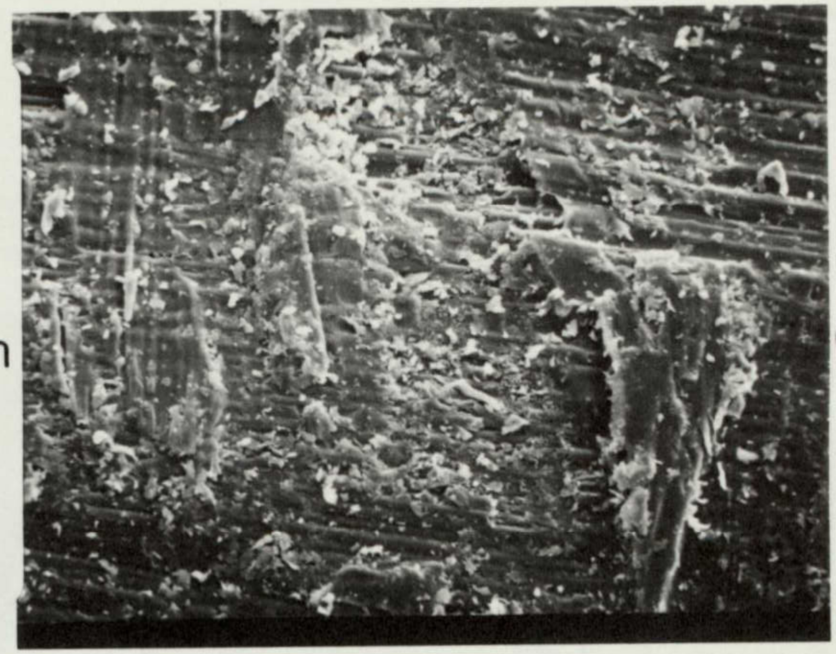

0.5mm

24b

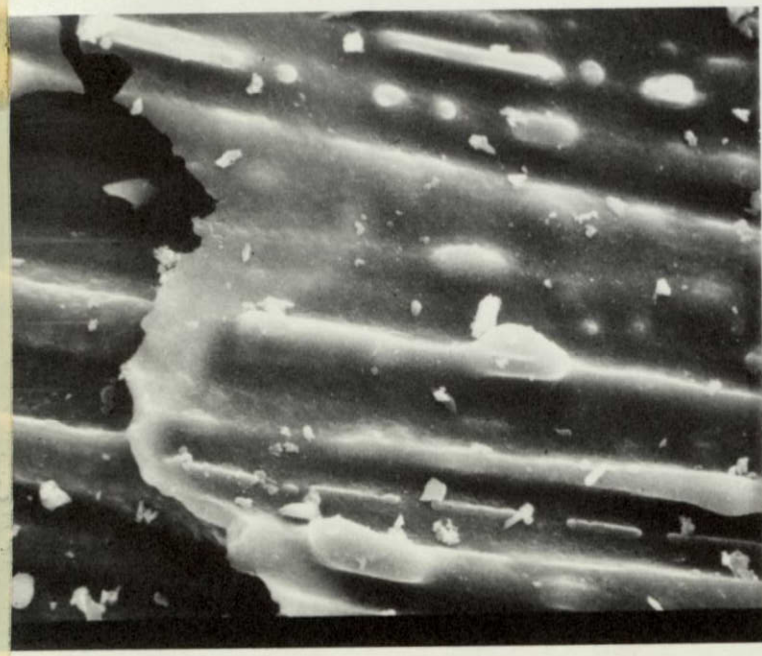

100 μm

100 μm

FIGURE 5.

Two higher magnifications (200X, 1000X) of
HT-S graphite fiber/Skybond 710 matrix composite;
as received on the left and
after sanding on the right. (1976)

Figure 5. Two higher magnifications (200X, 1000X) of HT-S graphite fiber/Skybond 710 matrix composite; as received on the left and after sanding on the right. (1976)

Note crack extending into substrate as received. Also there appears to be a microporosity (< 1μm) that didn't show in the earlier examination in Figure 4.

22a

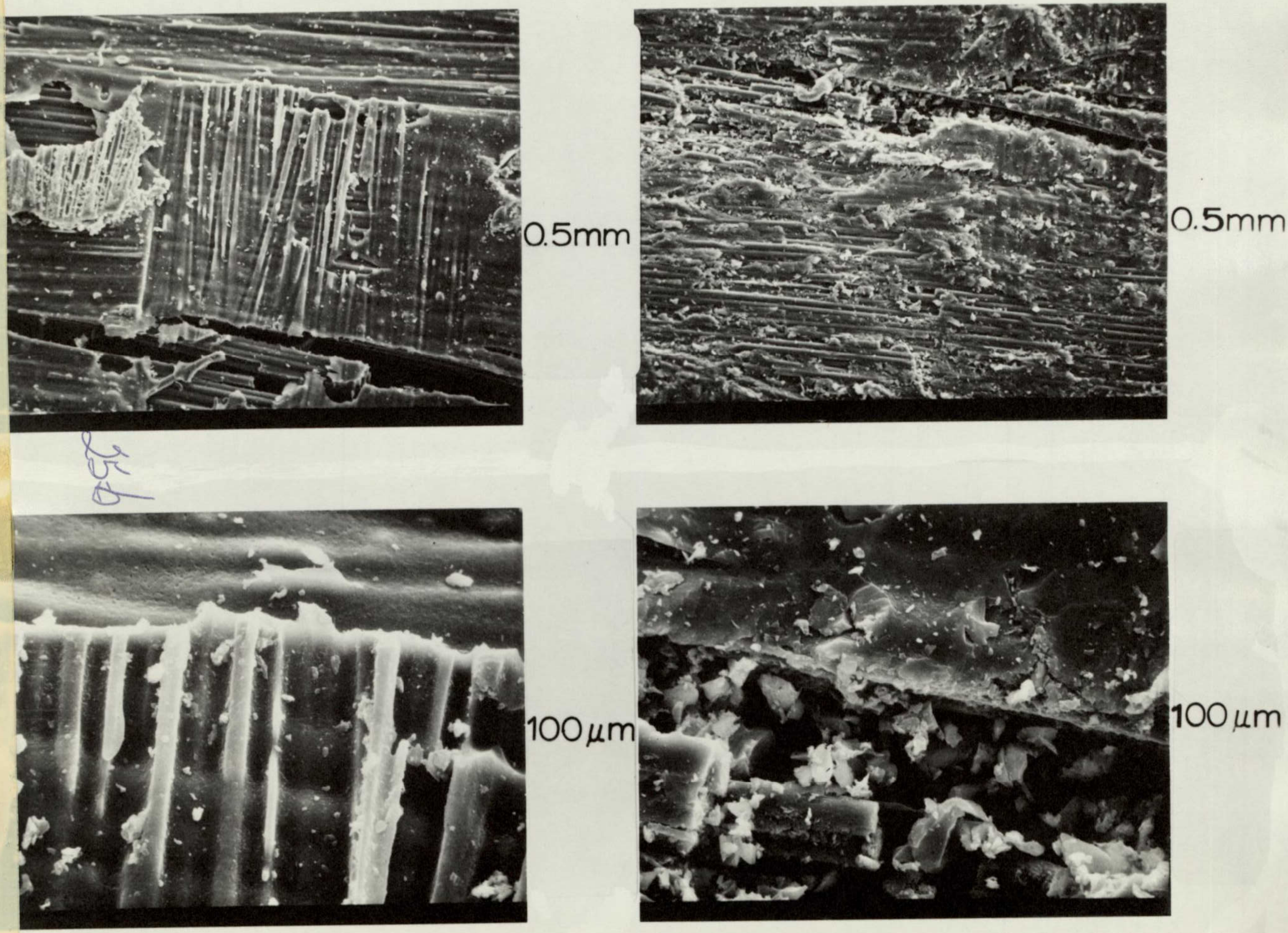
0.5mm
0.5mm
100 μm
100 μm

b. Titanium 6-4

Consistently low lap shear strengths on recent titanium 6-4 adherends treated by the phosphate/fluoride process was a cause for concern at NASA-LaRC. During this period, samples with a proprietary Boeing anodized surface were tested. The unique surface morphology of the latter is shown in Figure 6. The oxide surface layer is penetrated by many very irregular micro-pits about 0.5μm to 3μm in dimensions, with a pattern of roughly hemispherical, overlapping indentations 10-20μm in diameter. Seen at higher magnification is a dense population of spherical nodules of uniform diameter less than 0.5μm. These features lead one to anticipate that anodizing would lead to good mechanical interlocking if the adhesive wets and spreads intimately. On the other hand, there is potential difficulty in the removal of adsorbed contaminants.

Figure 7 displays the representative features of recent phosphate/fluoride treated titanium 6-4, and the irregular white, beta phase particles and rough, pitted, gray alpha phase resemble photomicrographs shown in the previous report (8). However, an important new feature is the distribution of 5-25μm, jagged particles on top of the substrate. Fracture surfaces (Figure 11) show a similar size and distribution of particles when these adherends were used. By focusing the SEM electron beam to a very small diameter, separate elemental analysis was performed on the particle and the adjacent substrate with the EDAX attachment. The results in Figure 8 show primarily aluminum from the particle and titanium from the adjacent matrix. During subsequent conversations with LaRC personnel we learned that a grit-blast step had recently been added to the procedure before the phosphate/fluoride treatment. Undoubtedly the particles are residual aluminum oxide grit.

These two examples make it clear that with titanium the surface topography may differ significantly even though chemical structure and bonding may be virtually identical. Furthermore, surface preparations such as roughening by grit blast may lead to anomalous results. Routine surface analysis provides a useful quality control monitor.

2. Fracture Surfaces

a. PPQ 413/Titanium 6-4

Polyphenylquinoxaline (PPQ) adhesives were synthesized by P. Hergenrother and became available during the current grant period. This section describes the results using standard titaniu 6-4 adherends with three different surface preparations, and also notes some effects of using scrim cloth.

Some details of the failure mechanisms responsible for low strength on 1976 (grit blasted) phosphate/fluoride adherends are seen in Figures 9-11. Failure is almost entirely interfacial although there is a little, curious delamination in the center of the bond line. The prime factor initiating polymer/metal separation appears to be residual, inadvertent grit particles seen on the adherend initially (Figure 7) and again in the center of interfacial eruptions in Figure 10. The polymer surface appears to replicate the grosser features of the adherend, but not the finer features. More adhesive was squeezed out of the bond line with PPQ 413 relative to LARC polyimides.

Representative EDAX spectra for elemental identification on each of the components of these fracture surfaces are juxtaposed in Figure 11. The bottom line shows the expected result from the adherend-side of the interfacial failure: an intense titanium doublet and a small aluminum peak from the substrate alloy, and two very small peaks from the 200 Å Au/Pd coating required for good conductivity in SEM. The relatively poor signal-to-noise ratio in spectra A.-C. is a direct indication of reduced atomic abundance in the latter areas. A wide-area survey of the adhesive-side of the interfacial failure showed titanium and aluminum peaks of similar magnitude to the Au/Pd peaks (Figure 11A). Line B shows the aluminum signal was localized to the particles in the center of eruptions. No aluminum signal was found in areas like Figure 10, top right, but a significant titanium signal persisted. Virtually no titanium signal appears in line C, obtained on the flat polymer surface generated by bond-line delamination seen in Figure 9, bottom right. The implication is that very thin patches of surface oxide transferred to the adhesive during interfacial failure.

Another series of tests used anodized Ti 6-4 adherends and fiber glass "scrim" cloth to support the adhesive film. All of the samples showed "near interfacial" and scrim cloth failure in different proportions depending on strength and temperature. Representative features of this series are illustrated in Figures 12 and 13. At lowest strength, failure is mostly "near-interfacial", while at highest strength, more than half the fracture surface involves scrim cloth, with cracks perpendicular to the adherends, leaving patches of the adhesive layer on each side. Fracture proceeds cohesively (Figure 12, top right) through the middle of the scrim cloth at high temperature, leaving half the adhesive layer covering each adherend. The appearance of so much bare fiber glass surface leads to the conclusion that the resin did not penetrate thoroughly between the individual filaments, thereby creating loci for failure initiation. However, the flexibility and toughness of the unencapsulated fabric undoubtedly provided the increased strength. High magnification views of the opposite surfaces from "near interfacial" failure are shown in Figure 13, bottom (left-adherend, right-adhesive). It appears that a thin primer layer covers the adherend, almost obscuring the anodized Ti 6-4 surface features. Flakes and chunks of bulk adhesive were pulled out and remain attached to the primer. In general this series suffered from poor wetting and spreading of the adhesive, leading to weakness at the interfaces between primer and adhesive tape, and between the adhesive matrix and the filaments of the fiber glass scrim cloth.

Rather high strength at room temperature was obtained in a test using 1975 phosphate/fluoride Ti 6-4 adherends. Figure 14 shows the opposite, mating fracture surfaces, and it is clear that the PPQ 413 achieved much better penetration into the scrim cloth than in previous examples. Failure is 100% in the scrim cloth, very close to the glass surface in one ply of the fabric. The opposing surface is predominantly matrix resin with channels that match the glass fibers on the other adherend. Thus, the weak link was still fiber/resin interfaces, but strength improved because of the high-area, louvered, brittle fracture of the PPQ 413 between the filaments and in the interstices of the cloth.

FIGURE 6.

Three magnifications (500X, 2000X, 5000X) of an anodized Ti 6-4 adherend surface.

Figure 6. Three magnifications (500X, 2000X, 5000X) of an anodized Ti 6-4 adherend surface.

At the level of 10μm to 20μm there appears a pattern of overlapping, roughly hemispherical indentations. The surface oxide layer is full of micro-pits of very irregular shape, and about 0.5μm to 3μm in size. Also there is a dense population of nodules $<$ 0.5μm in diameter. The latter two features are unique to the anodized Ti 6-4 surface.

31-a

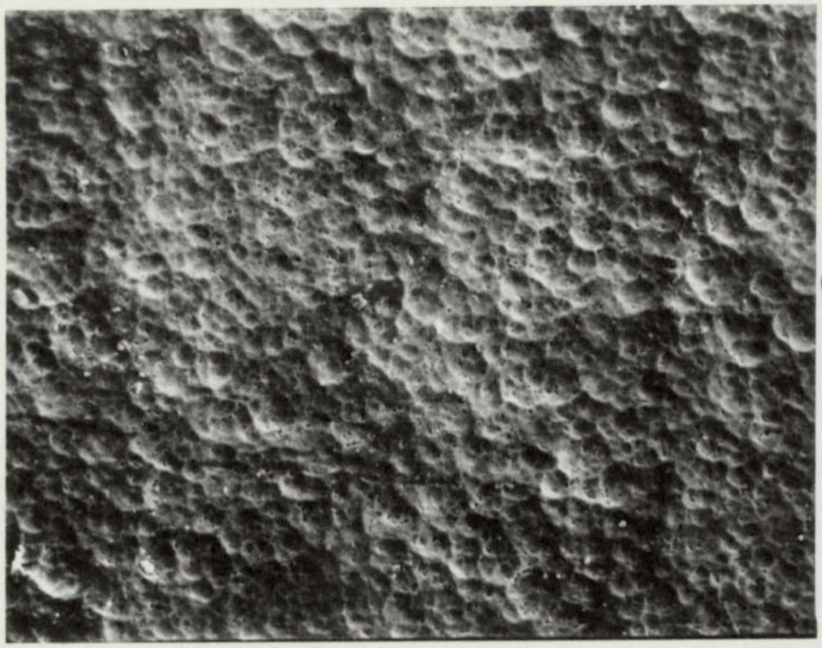
0.2mm

31-b


50 µm

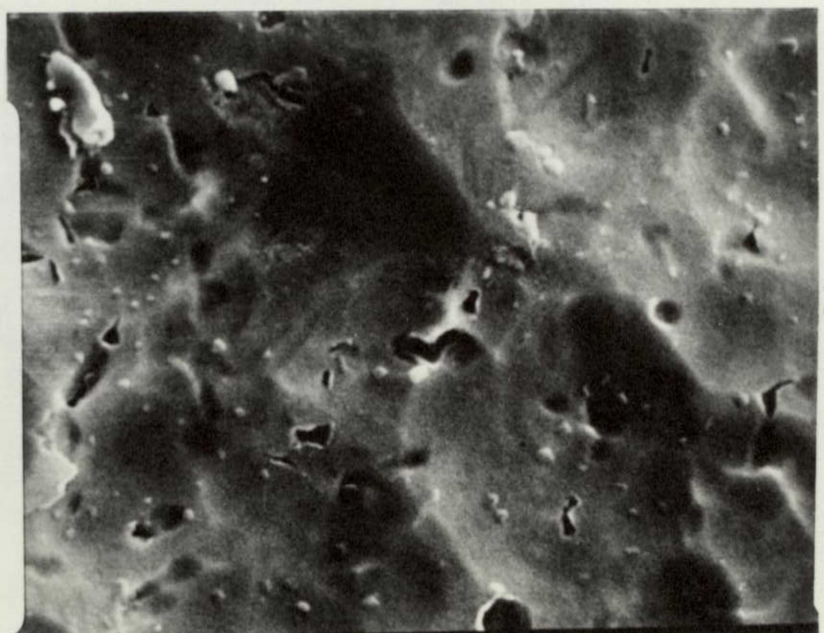
20 µm

FIGURE 7.

Four magnifications (200X, 1000X, 2000X, 5000X) of recent phosphate fluoride treated Ti 6-4.

Figure 7. Four magnifications (200X, 1000X, 2000X, 5000X) of recent phosphate/fluoride treated Ti 6-4.

The substrate has much finer features than the anodized surface and appears like the phosphate/fluoride-treated Ti 6-4 reported earlier(8): irregular, white beta phase particles ($\sim 0.5\mu m$ to $2\mu m$ in size) densely scattered, protruding from a very rough, pitted, gray matrix of alpha-phase alloy. A new feature is the larger, jagged particles about $5\text{-}25\mu m$ in size, seen most clearly on the right. Close inspection of the top left photomicrograph shows the particle density to be about one per $2000\mu m^2$. EDAX (Figure 8) shows an intense aluminum signal from the particles, but a titanium peak from the adjacent matrix. These substrates gave low strength joints, and the role of the particles is illustrated in Figure 11.

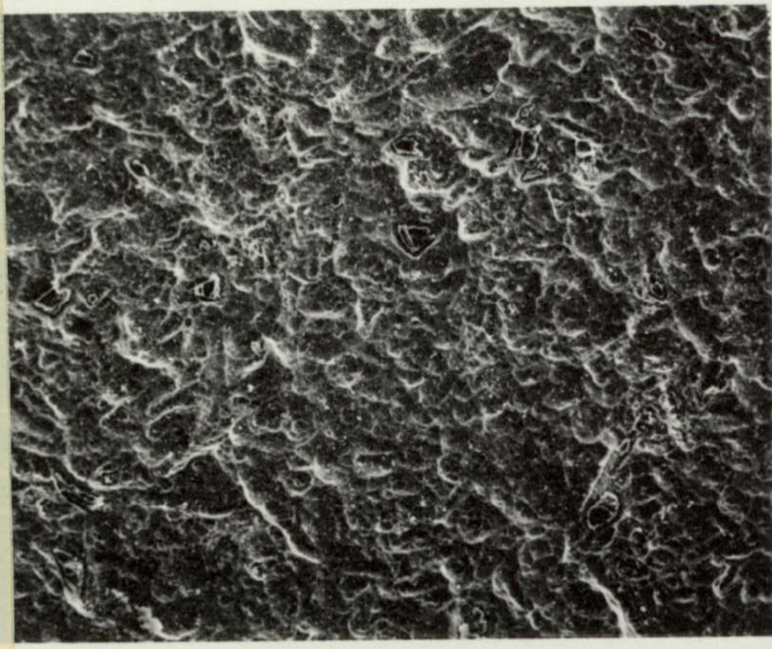
0.5mm

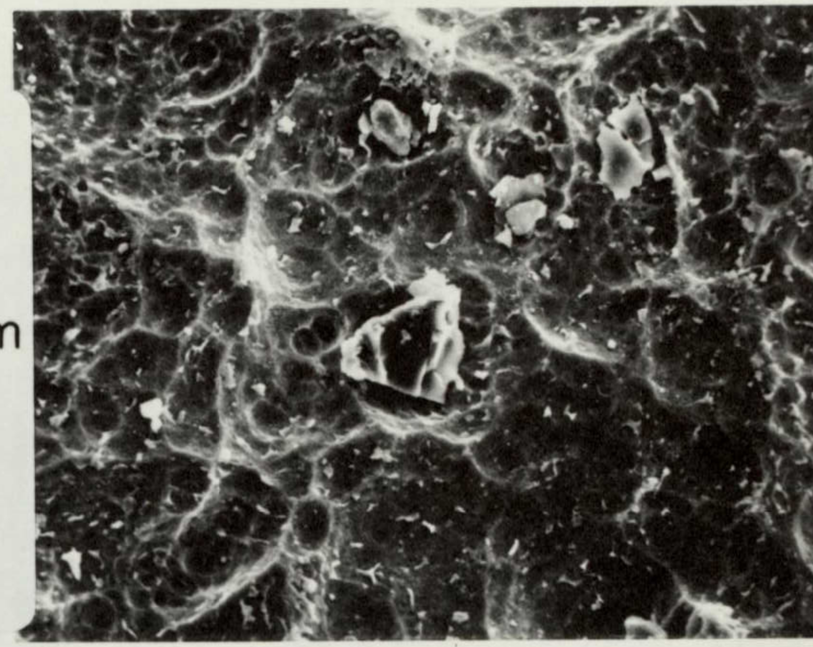
100 μm

32b

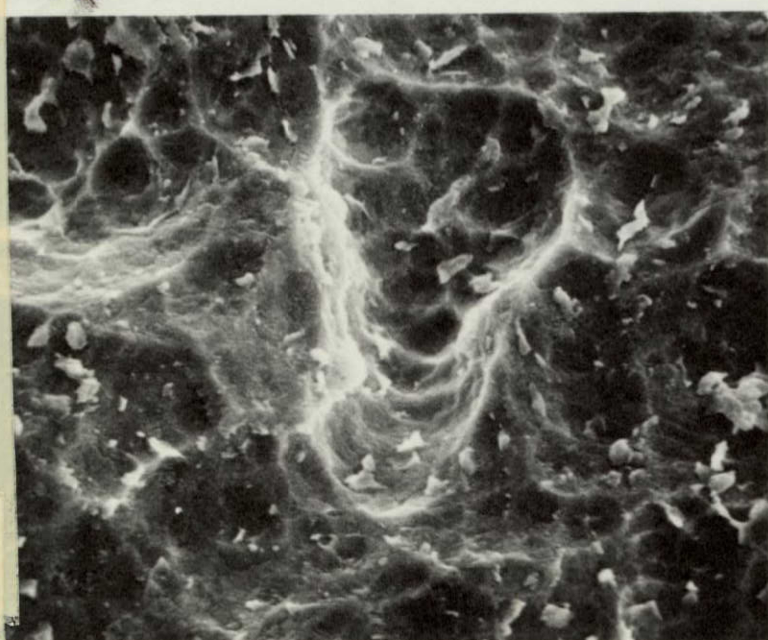
50 μm

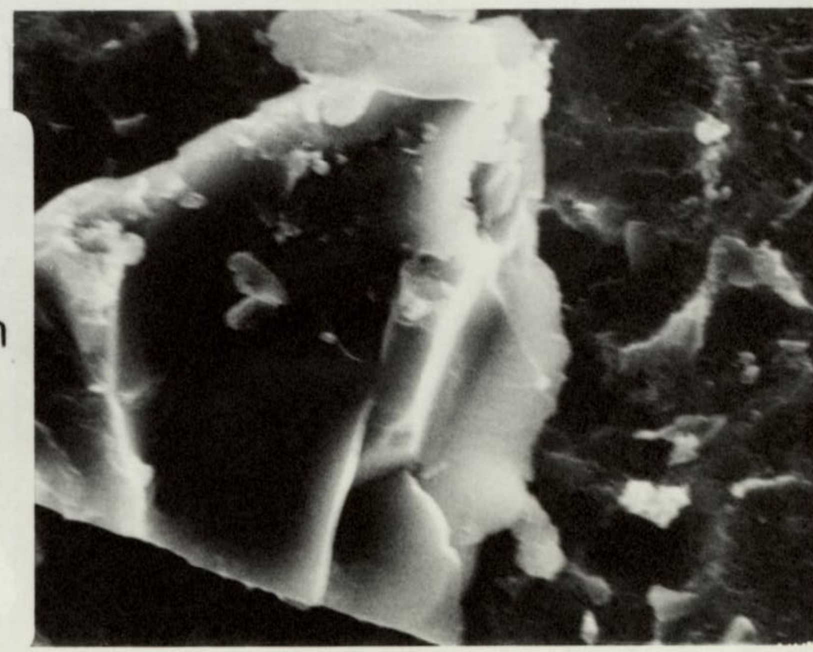
20 μm

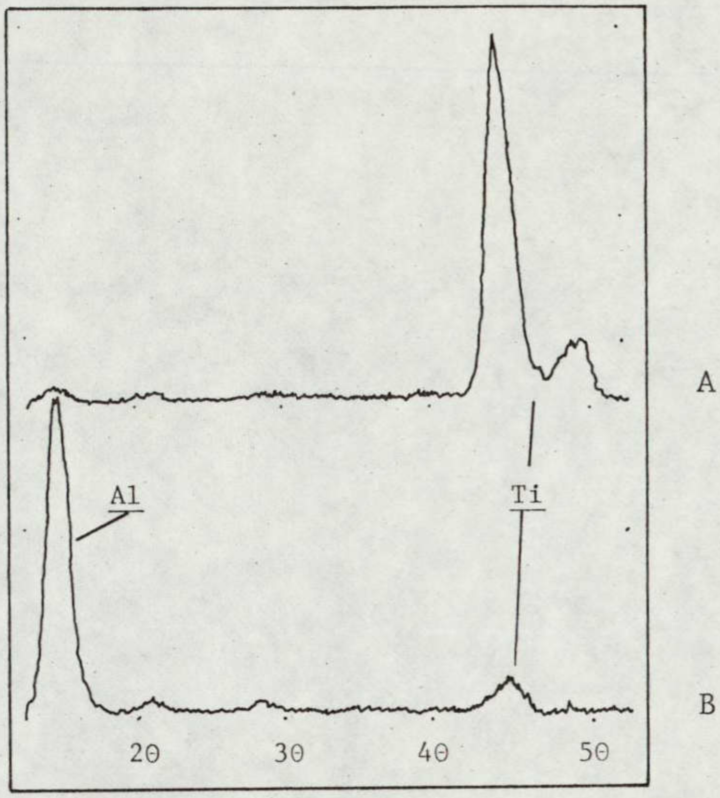

Figure 8. EDAX spectra obtained from recent phosphate/ fluoride treated Ti 6-4, seen in the photomicrographs of Figure 7 (right). A. Substrate, B. Particle.

FIGURE 9.

Three magnifications (20X, 500X, 1000X) of the fracture surface of a PPQ 413/Ti 6-4 (phosphate/fluoride) sample that gave 1400 psi lap shear strength at room temperature.

Figure 9. Three magnifications (20X, 500X, 1000X) of the fracture surface of a PPQ 413/Ti 6-4 (phosphate/fluoride) sample that gave 1400 psi lap shear strength at room temperature.

95% interfacial failure with one main perpendicular fracture through the adhesive layer, leaving about half the adhesive on each adherend; about 5% delamination in the middle of the adhesive layer, shown in high magnification on the bottom right. Note that the total glue line appears to be about 30-40μm thick. Visual inspection of the joints indicated more "flash" or glue squeezed out of the bond line with PPQ 413 than with LARC-type adhesives. ?

34-a

5mm

34b

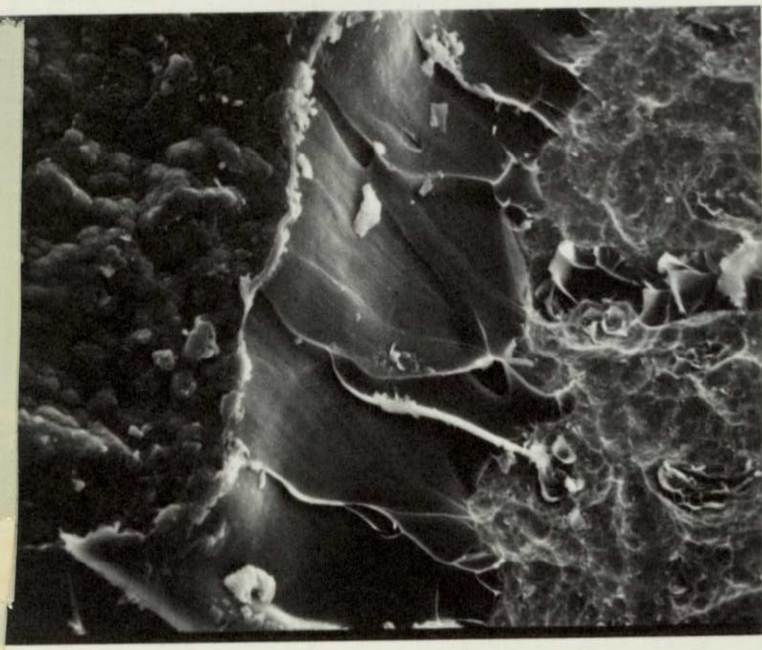

0.2mm

100 μm

FIGURE 10.

Four magnifications (200X, 1000X, 2000X, 5000X) of
the fracture surface of a PPQ 413/Ti 6-4 (phosphate/fluoride)
sample that gave 1400 psi lap shear strength
at room temperature.

Figure 10. Four magnifications (200X, 1000X, 2000X, 5000X) of the fracture surface of a PPQ 413/Ti 6-4 (phosphate/fluoride) sample that gave 1400 psi lap shear strength at room temperature.

These are representative of the polymer side of the interfacial failure, seen at the top of Figure 8. The PPQ 413 replicates the gross (10-75μm) features of the adherend, but not the finer features, perhaps due to incomplete spreading and wetting. Numerous eruptions (about one per $2000\mu m^2$) are scattered randomly about the polymer surface and higher magnifications reveal one jagged particle penetrating through from center of each eruption. Note the correspondence between these particles on the fracture surface and those on the substrate before bonding (Figure 7), suggesting that the contaminant played an important role in initiating failure at low stress. EDAX (Figure 10) shows a uniform titanium signal from the "polymer" surface, indicating the probable transfer of very thin patches of oxide from the adherend to the adhesive during interfacial failure. The particles show a strong aluminum signal in EDAX.

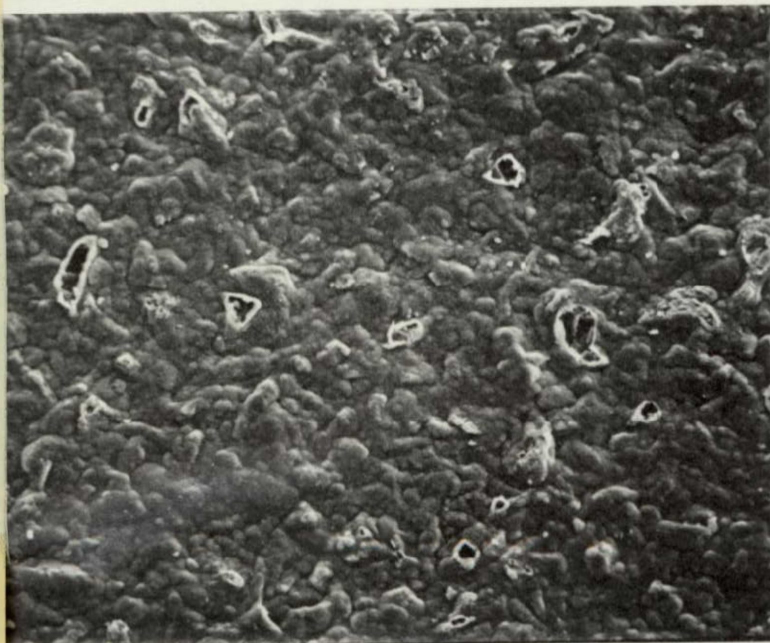

0.5mm

100 µm

35b

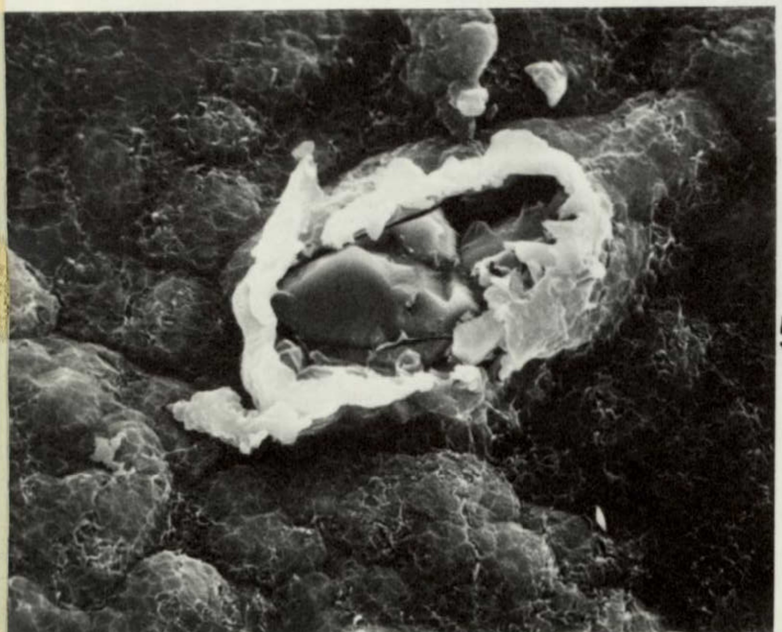

50 µm

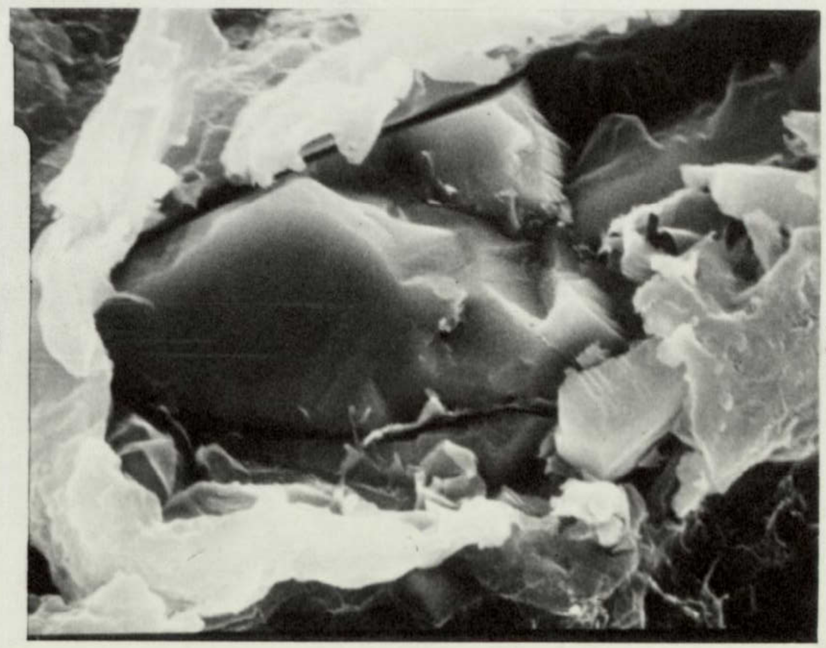

20 µm

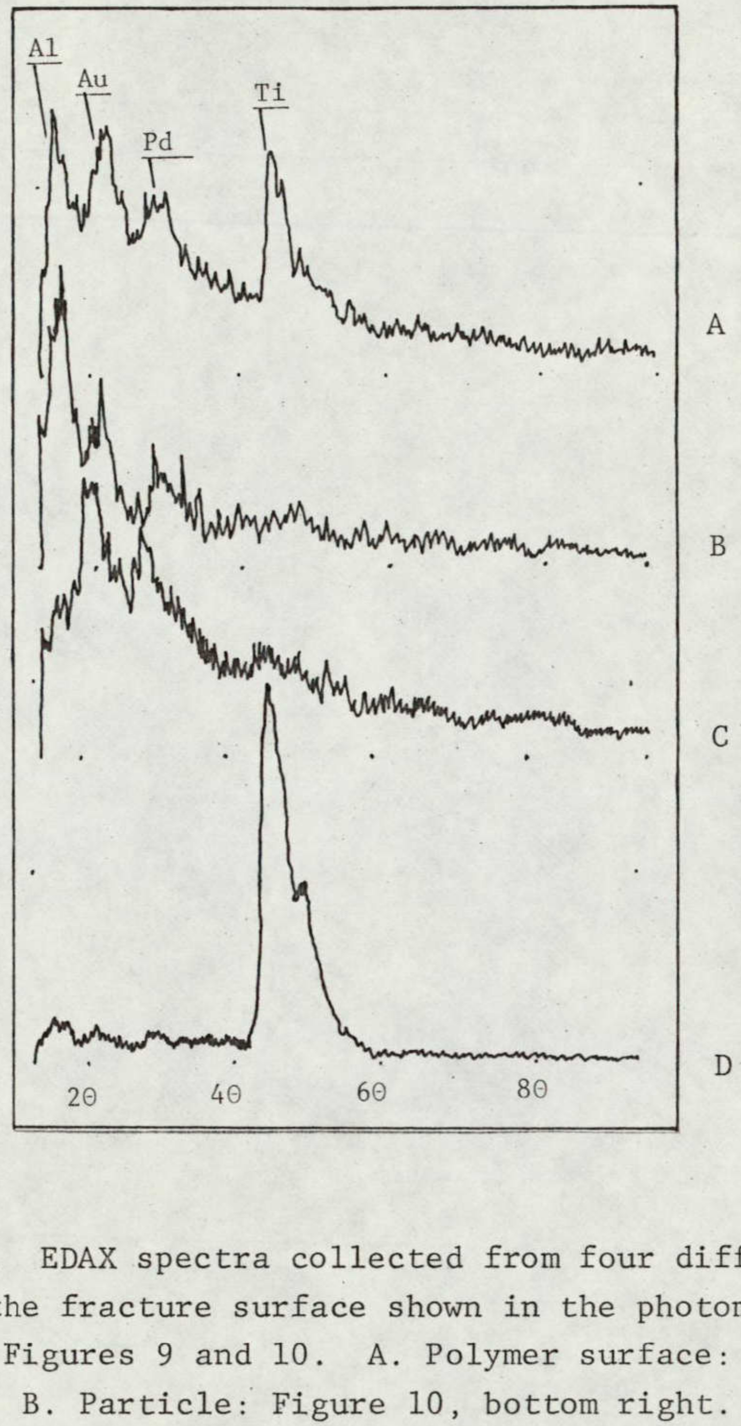

Figure 11. EDAX spectra collected from four different areas of the fracture surface shown in the photomicrographs of Figures 9 and 10. A. Polymer surface: Figure 10, top left. B. Particle: Figure 10, bottom right. C. Delaminated surface: Figure 9, bottom right. D. Adherend surface: Figure 9, top. The Au and Pd signals arise from ∿ 200 Å of alloy vacuum deposited on the sample.

FIGURE 12.

Four magnifications (20X and 3 @ 200X) of the fracture surface of a PPQ 413 (with scrim cloth)/Ti 6-4 (anodized) sample that gave low strength at room temperature.

<u>Figure 12.</u> Four magnifications (20X and 3 @ 200X) of the fracture surface of a PPQ 413 (with scrim cloth)/Ti 6-4 (anodized) sample that gave low strength at room temperature.

In contrast to the previous example, a fiber glass "scrim" or carrier cloth was used. At low strength, failure is 95% interfacial, shifting to about 60% failure in the scrim cloth at higher strength. At 550°F, there is 100% cohesive failure in the middle of the scrim cloth. Figure 13 shows higher magnification views of these fracture surfaces. It appears that the resin did not penetrate thoroughly into the cloth threads and encapsulate the individual glass filaments. Part of the adhesive layer remains on each adherend, cracked in two by low-area brittle cleavage through a polymer layer ∿ 100μm thick on each side of the cloth and through the cloth by resin/fiber interfacial failure and brittle fracture of the glass fibers.

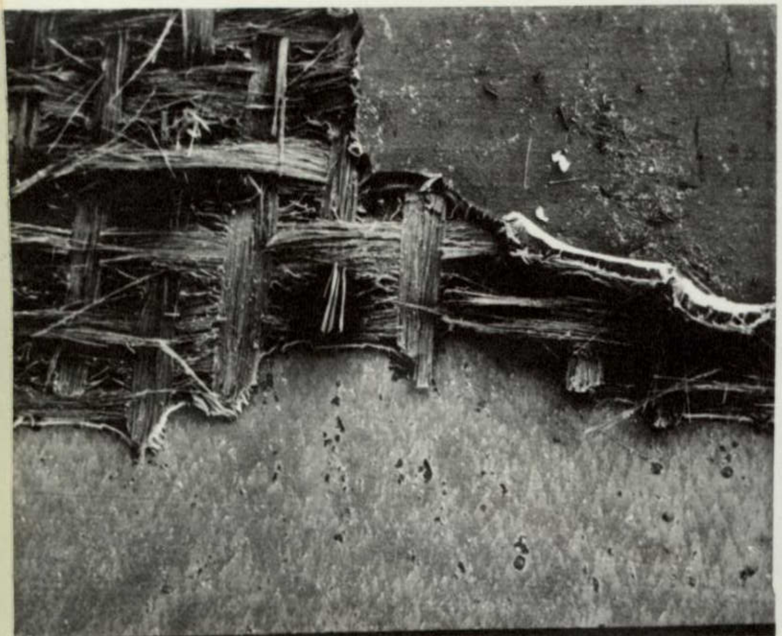

5mm

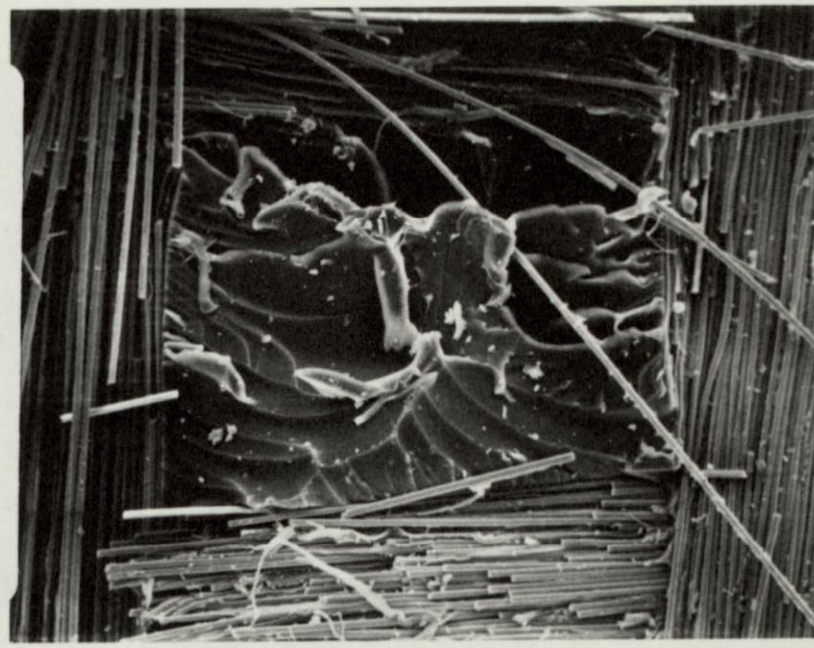

0.5mm

37b

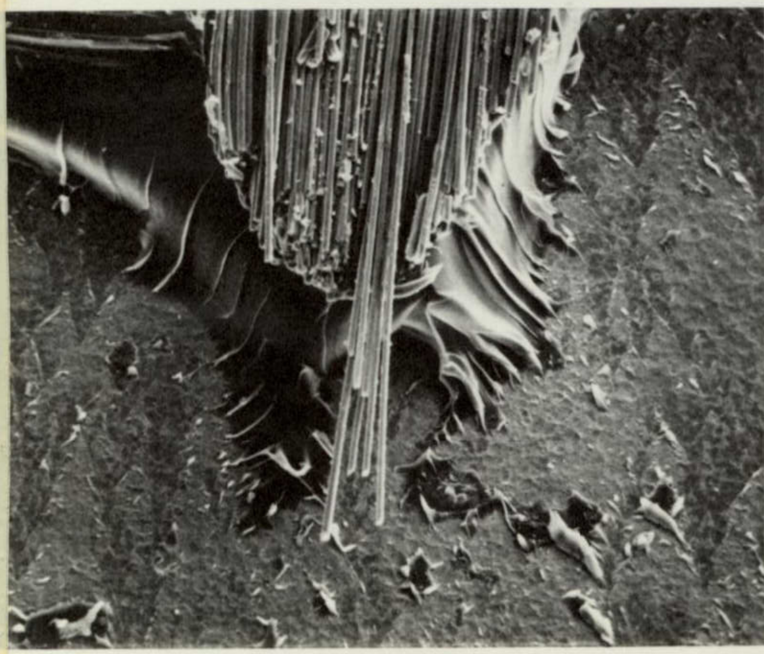

0.5mm

0.5mm

FIGURE 13.

Four magnifications (2 @ 500X, 1000X, 2000X) of the same samples shown in Figure 12.

Figure 13. Four magnifications (2 @ 500X, 1000X, 2000X) of the same samples shown in Figure 12.

Glass fiber/resin interfacial failure and $\sim$ 100μm glue line are confirmed. Comparing the bottom left photomicrograph with Figure 6, a thin, pinhole-filled overlayer of primer plus some flakey fragments of the bulk adhesive remain below. The adhesive side of the fracture interface, on the bottom right, shows the eruptions where fragments were plucked out by the substrate. The overall impression is that low flow and interfacial incompatibility weakened bonds at adherend/primer, primer/adhesive, and adhesive/fiber glass cloth interfaces.

38-a

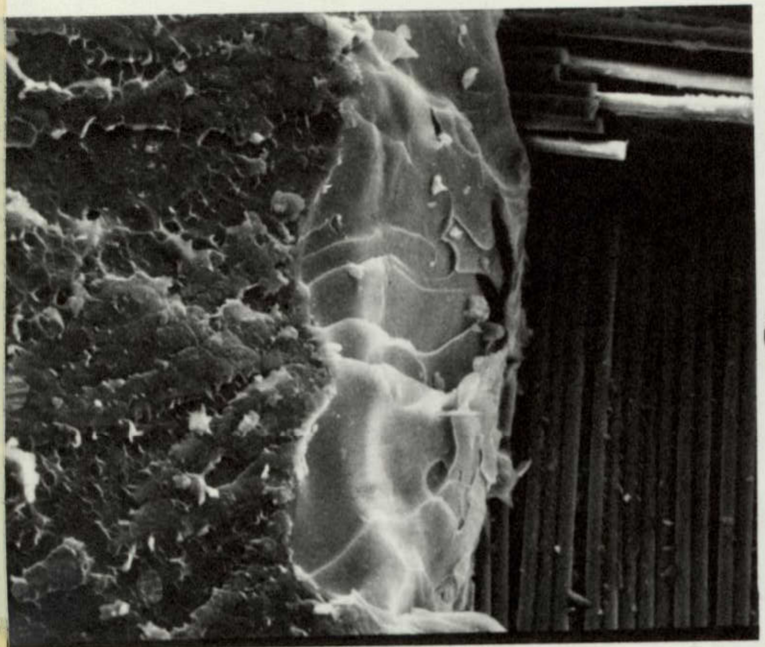
0.2mm

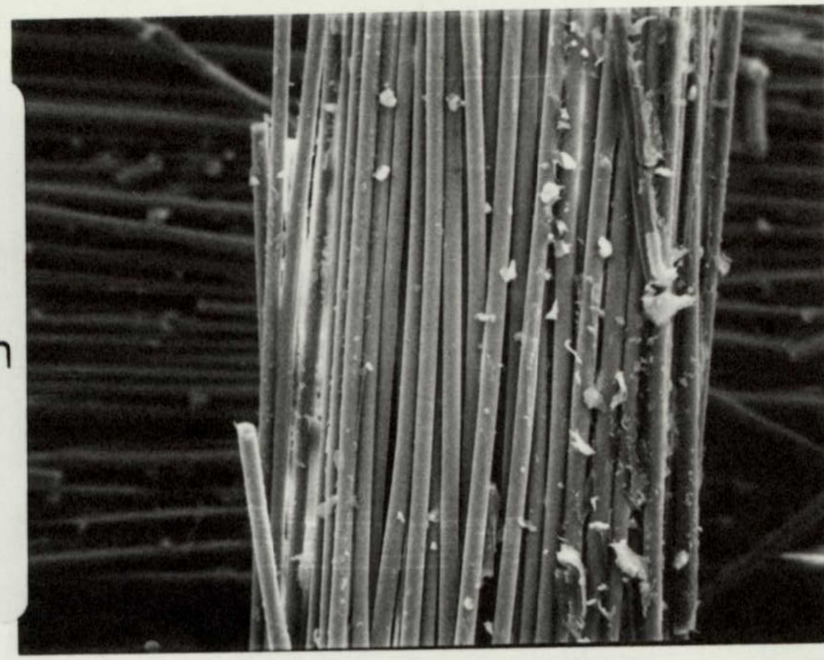
0.2mm

38b

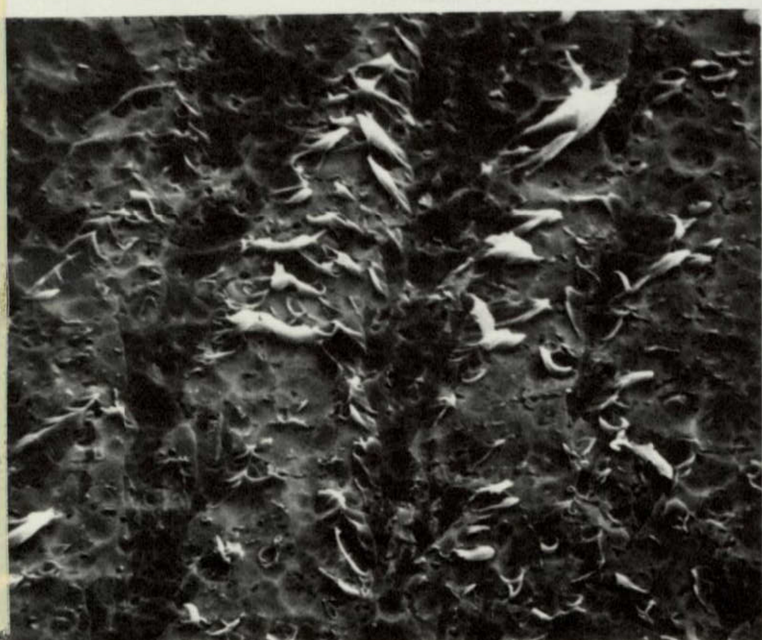
100 μm

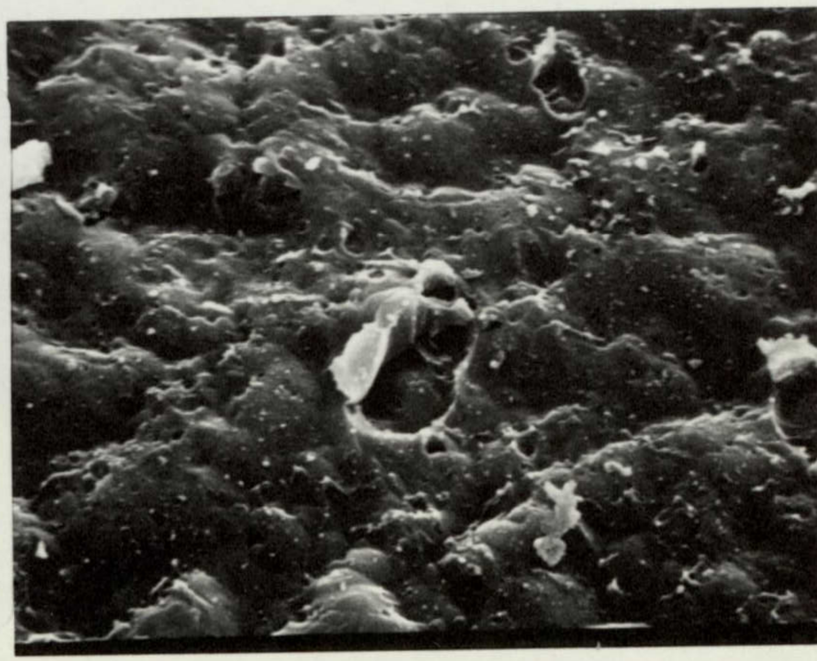
50 μm

FIGURE 14.

Four magnifications (2 @ 20X, 2 @ 200X) of the fracture surface of a PPQ 413 (with scrim cloth)/Ti 6-4 (phosphate/fluoride) sample that gave 4400 psi lap shear strength at room temperature.

Figure 14. Four magnifications (2 @ 20X, 2 @ 200X) of the fracture surface of a PPQ 413 (with scrim cloth)/Ti 6-4 (phosphate/fluoride) sample that gave 4400 psi lap shear strength at room temperature.

Fracture is entirely in the scrim cloth, but in this case penetration by the PPQ 413 was achieved. Voids are apparent. Mostly fiber glass shows on one adherend (right) and resin is predominant on the left, plus glass/resin interfacial failure. Between fibers and in the windows, resin fractures in a high-area, louvered, brittle mode.

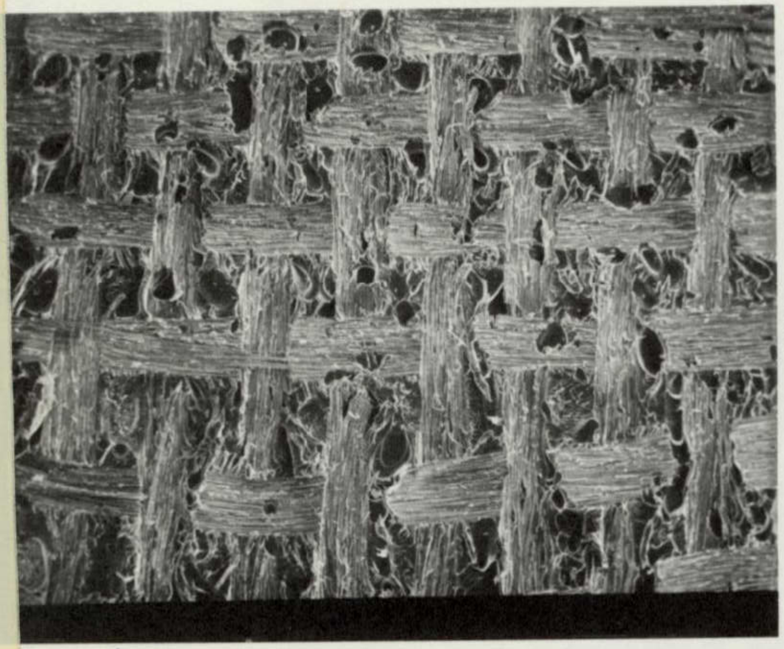

5mm

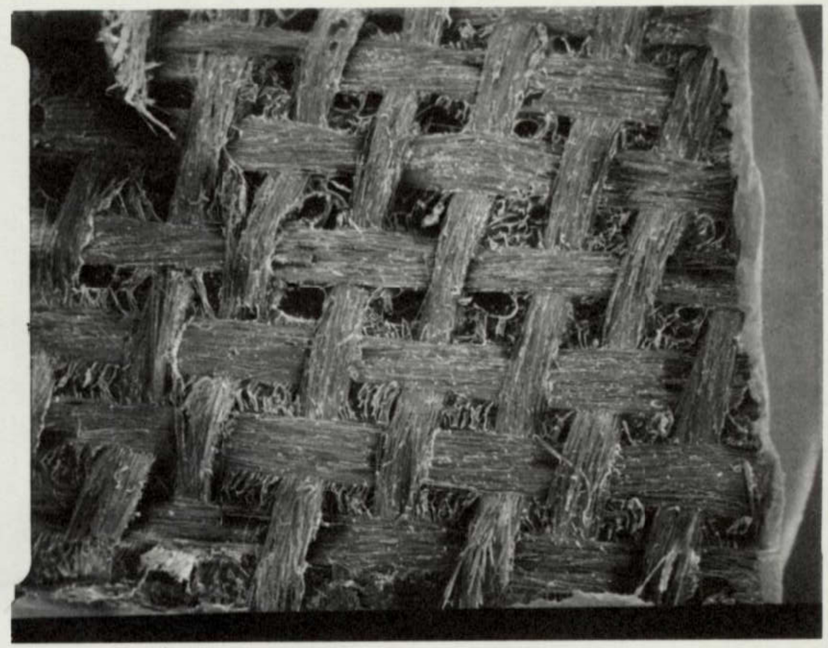

5mm

38-b

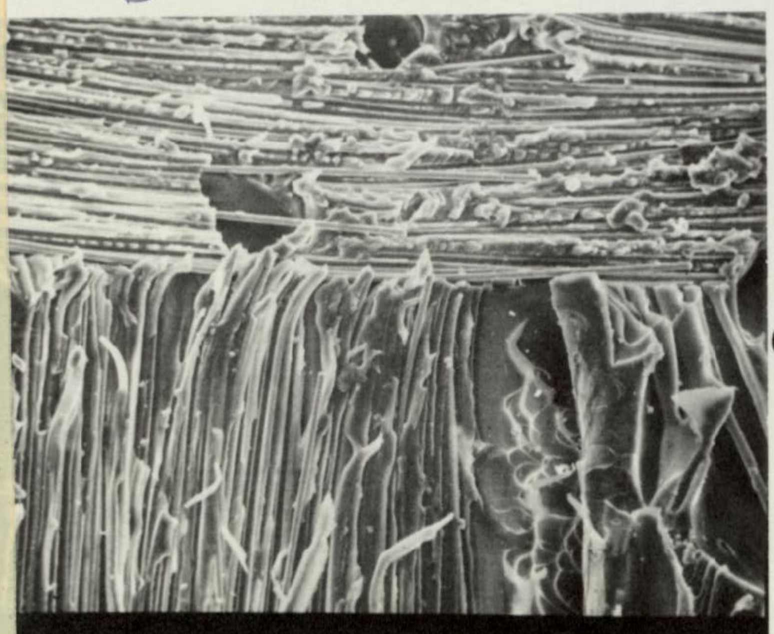

0.5mm

0.5mm

b. PPQ 413/NR-150B2 Composite

The effect of testing temperature on strength and fracture-surface features was observed for this bonded pair (and the following three pairs). The effect of using scrim cloth was also noted:

At room temperature (Figure 15) fracture relatively deep in the adherends is dominant. A few cracks proceed through the brittle 0.1 mm thick bond line leaving patches of one adherend on the other. At the level of about 5-25μm, composite failure is distributed between matrix resin/HT-S fiber interfacial separation and high-area, brittle cleavage cracking of the matrix resin.

High temperatures result in plastic deformation of the PPQ bond line and an average locus of failure very near the original composite/adhesive interface. Figure 16 shows that at 286°C the glue line stretches to ∿ 0.2mm before a low-area, brittle crack propagated basically perpendicular to the adherends and stress direction, leaving part of the adhesive layer on each adherend. Close inspection of the interfacial line shows the adhesive pulling away from the surface of the adherend. Fracture area is mainly in the composite, near the surface, by mixed failure at fiber/matrix interfaces and rather large, brittle cleavage cracks. Perhaps there is also a plastic component in the deformation of louvers in the stress direction, and a contribution from fiber fracture. Figure 17 clearly shows voids (presumably due to residual solvent) and fluid-flow at 316°C. The glue line is now about 0.5 mm, penetrated by numerous cracks that leave yellowed flakes of adhesive on each adherend. The majority of the fracture area appears to be close to the first layer of HT-S fibers, leaving the adhesive layer patterned with channels representing fiber/matrix separation, with ductile matrix fracture between the fibers. The yellow flakes of adhesive may be due to precipitation of the PPQ by residual N-methylpyralidone in the composite.

When scrim cloth was used to support PPQ413 adhesive for bonding to NR-150B2 composite adherends, room temperature strength dropped about 30%. Figure 18 shows a corresponding decrease in composite fracture area, because significant failure occurs now in the scrim, which appears poorly penetrated with adhesive. Also note that over 0.1mm of adhesive are on each side of the scrim cloth.

c. PPQ413/Skybond 710 Composite

Failure in the adherends at all temperatures and a surprising morphology for the composite matrix resin are the important features in this series. At room temperature, Figure 19 shows that fracture alternates between plies in the adherend and from one adherend to the other via brittle cracks through the adhesive layer. Close inspection of the composite failure shows that the Skybond 710 matrix resin is not a uniform solid, but appears to be a porous aggregate of chunks about 5-10μm in size. This is seen even more clearly in Figure 20, where the chunks seem to have a lumpy <0.4μm substructure at the higher temperature. Failure is predominantly in one adherend and there is one crack through the glue line where plastic deformation has apparently taken place. At the highest temperature, further deformation of the glueline is the only different feature (Figure 21). In each case the composite adherend was the weakest member. Interfacial separation between fibers and matrix, and polymer fracture mechanisms are limited by the void-filled structure.

An unexpected silicon peak in the EDAX spectrum (Figure 22B) arose from both the composite matrix and adhesive polymer, but not from bare HT-S fiber surfaces. Although we have not used EDAX analysis routinely on all samples, we have not seen silicon previously in composites. Perhaps in the present case, a silicone release agent was used in the preparation of the composite adherend and migrated into the polymer resin phases. In future studies EDAX analysis will be a routine part of basic data on surface characterization. More systematic investigation should elucidate such apparent anomalies as the silicon signal above and the titanium signal from the polymer surface (Figure 11).

FIGURE 15.

Four magnifications (20X, 200X, 500X, 2000X) of the fracture surface of a PPQ 413/NR-150B2 HT-S graphite fiber composite sample that gave 6200 psi lap shear strength at room temperature.

Figure 15. Four magnifications (20X, 200X, 500X, 2000X) of the fracture surface of a PPQ 413/NR-150B2 HT-S graphite fiber composite sample that gave 6200 psi lap shear strength at room temperature.

Part of failure in one adherend with brittle cracks through the bond line parallel to stress, and rest of failure in opposite adherend. Fracture modes are between HT-S fiber/NR-150B2 interface and high-area, louvered, brittle matrix fracture with some plastic deformation.

413-2

5mm

0.5mm

43b

0.2mm

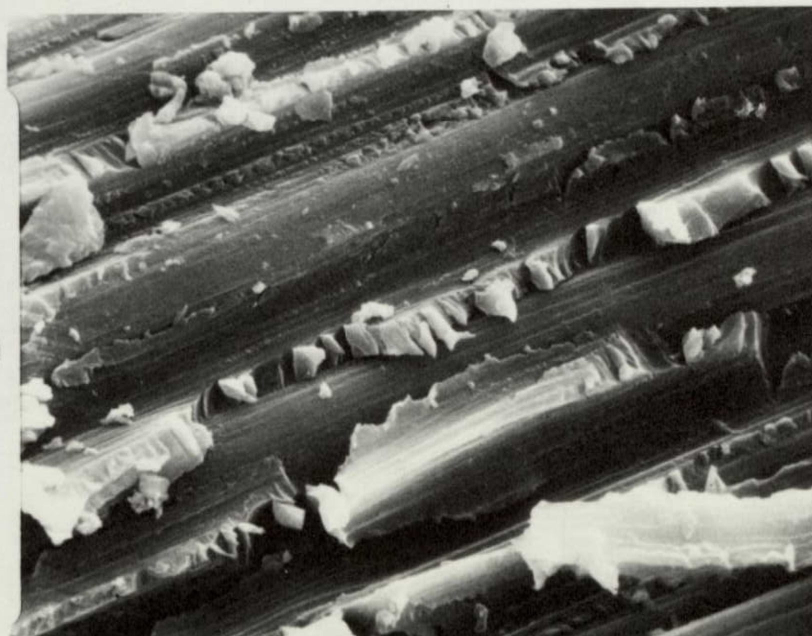

50 μm

FIGURE 16.

Four magnifications (20X, 100X, 500X, 2000X) of the fracture surface of a PPQ 413/NR-150B2 sample that gave 2500 psi lap shear strength at 286^{o}C.

Figure 16. Four magnifications (20X, 100X, 500X, 2000X) of the fracture surface of a PPQ 413/NR-150B2 sample that gave 2500 psi lap shear strength at 286^{o}C.

Failure in each adherend, and one fracture through the glue-line, mostly perpendicular to the stress direction. Plastic deformation in PPQ 413 glue-line, $\sim$ 0.2 mm thick. Adherend failure is closer to the adhesive interface than in Figure 15. Composite surface failure is basically similar to the previous, room-temperature sample, although there appears to be more broken fibers and plastic deformation and larger brittle-cleavage louvers. Also there is prominent resin/fiber interfacial failure.

5mm

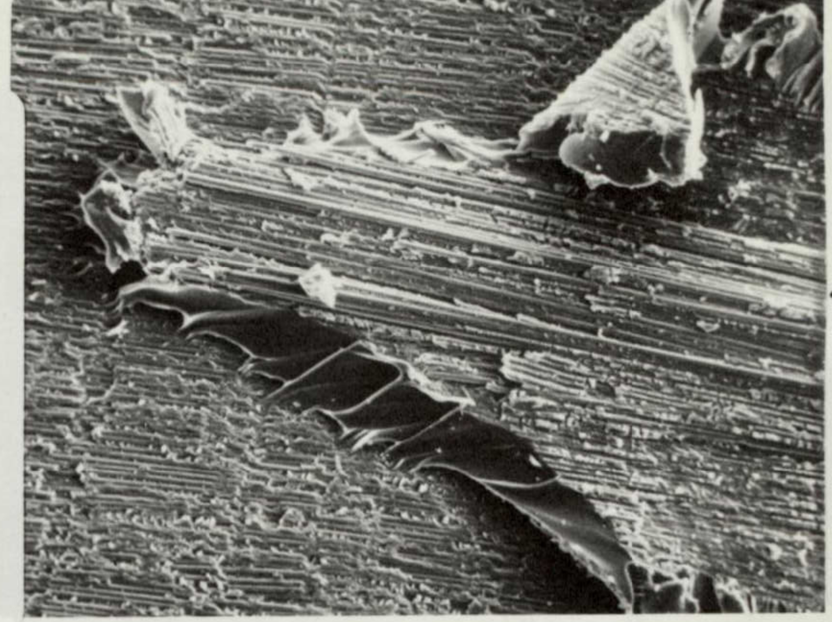

1mm

D44b

0.2mm

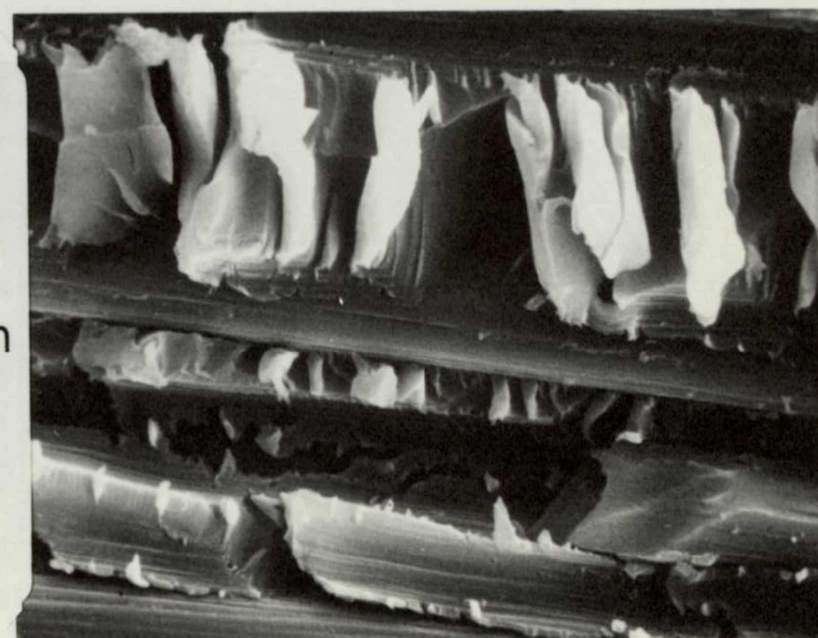

50 μm

FIGURE 17.

Four magnifications (20X, 100X, 200X, 2000X) of the fracture surface of a PPQ 413/NR150-B2 sample that gave 1000 psi lap shear strength at 316°C.

Figure 17. Four magnifications (20X, 100X, 200X, 2000X) of the fracture surface of a PPQ 413/NR150-B2 sample that gave 1000 psi lap shear strength at 316°C.

Failure is primarily in the composite surface between the resin and the first layer of fibers. Plastic deformation and decomposition are obvious in the ∿ 0.5 mm, stretched, bond line. Numerous cracks through the bond line leaving patches of adhesive on each adherend.

1mm

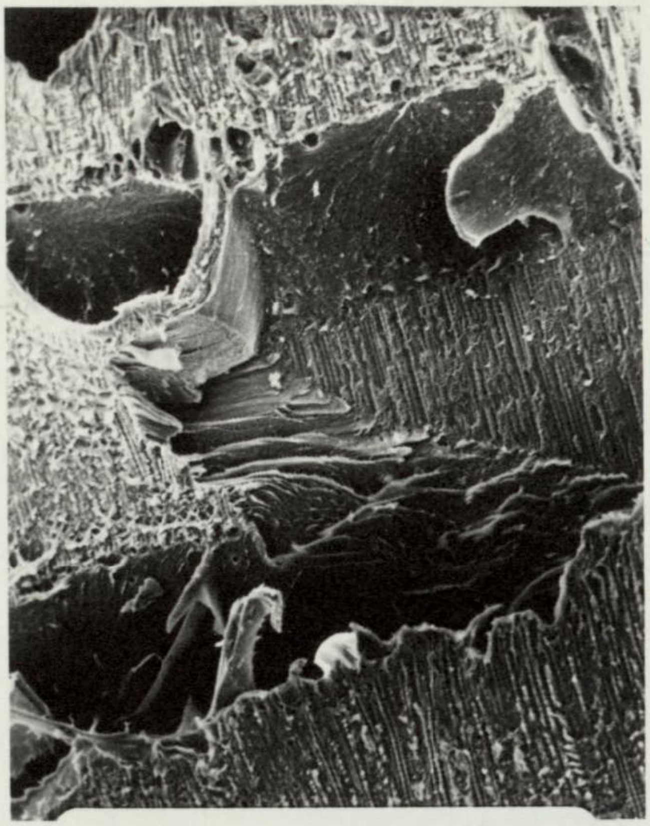

50 μm

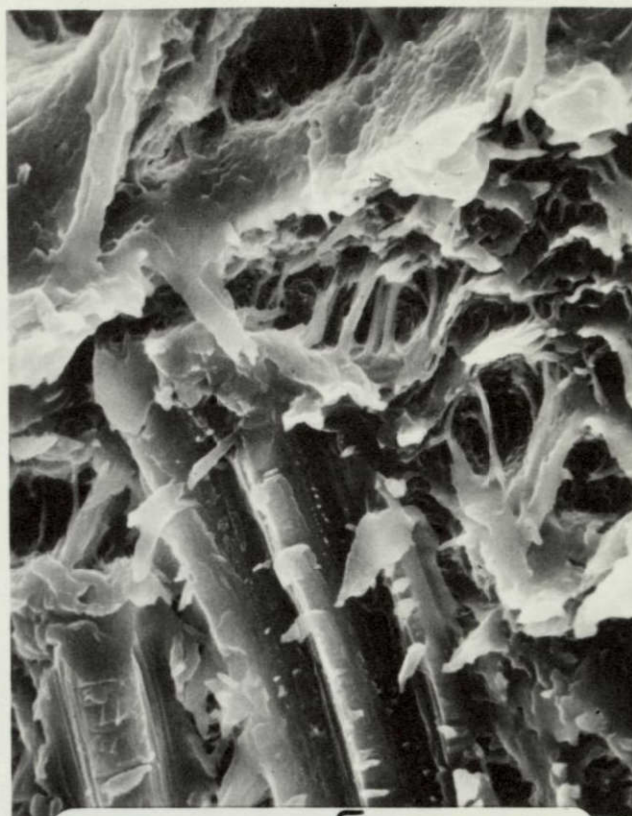

5mm

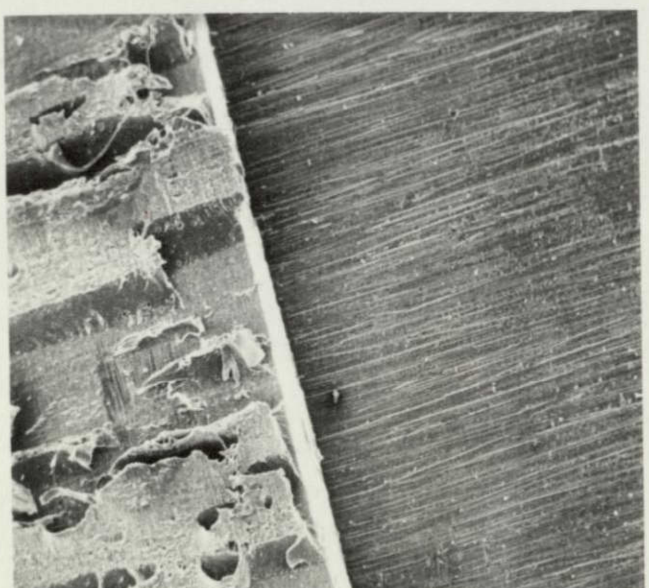

0.5mm

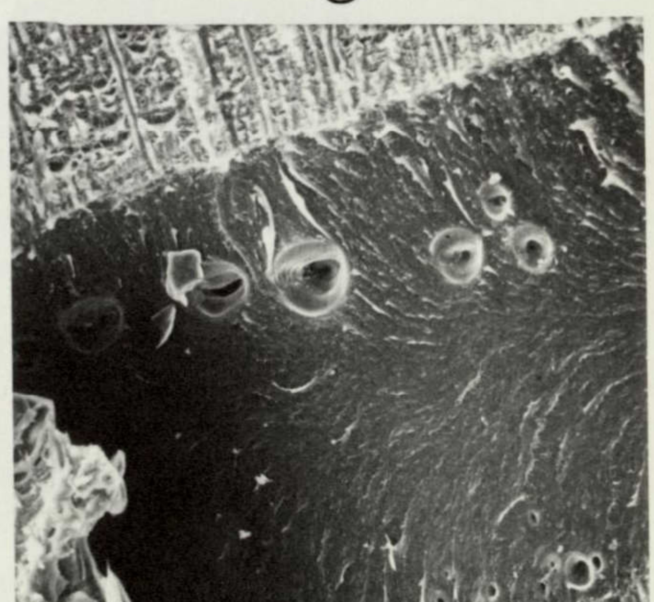

FIGURE 18.

Four magnifications (20X, 200X, 500X, 2000X) of the fracture surface of a PPQ 413 (with scrim cloth)/NR150-B2 sample that gave 4000 psi lap shear strength at room temperature.

Figure 18. Four magnifications (20X, 200X, 500X, 2000X) of the fracture surface of a PPQ 413 (with scrim cloth)/NR150-B2 sample that gave 4000 psi lap shear strength at room temperature.

The use of a scrim cloth is the only obvious difference from the example of Figure 15. About 30% failure is in the scrim cloth and strength is correspondingly less; apparently poor flow of resin into scrim and perhaps interfacial incompatibility also. Glue between scrim cloth and adherend is > 0.1 mm thick. Composite surface fracture shows the same characteristics of previous, high strength samples; high-area, brittle cleavage cracking and fiber/resin interfacial failure.

2-97

5mm

0.5mm

46b

0.2mm

50 μm

FIGURE 19.

Four magnifications (20X, 100X, 500X, 2000X) of the fracture surface of a PPQ 413/Skybond 710 sample that gave 3400 psi lap shear strength at room temperature.

Figure 19. Four magnifications (20X, 100X, 500X, 2000X) of the fracture surface of a PPQ 413/Skybond 710 sample that gave 3400 psi lap shear strength at room temperature.

Failure is essentially in the composite, alternating frequently from one adherend to the other via brittle cracks through the bond line (lower left). The Skybond 710 matrix is porous; discontinuous "chunks" about 5-10 μm in size seem to be packed tightly around the graphite fibers. Interfacial failure between the fibers and lumpy matrix particles is predominant.

47-A

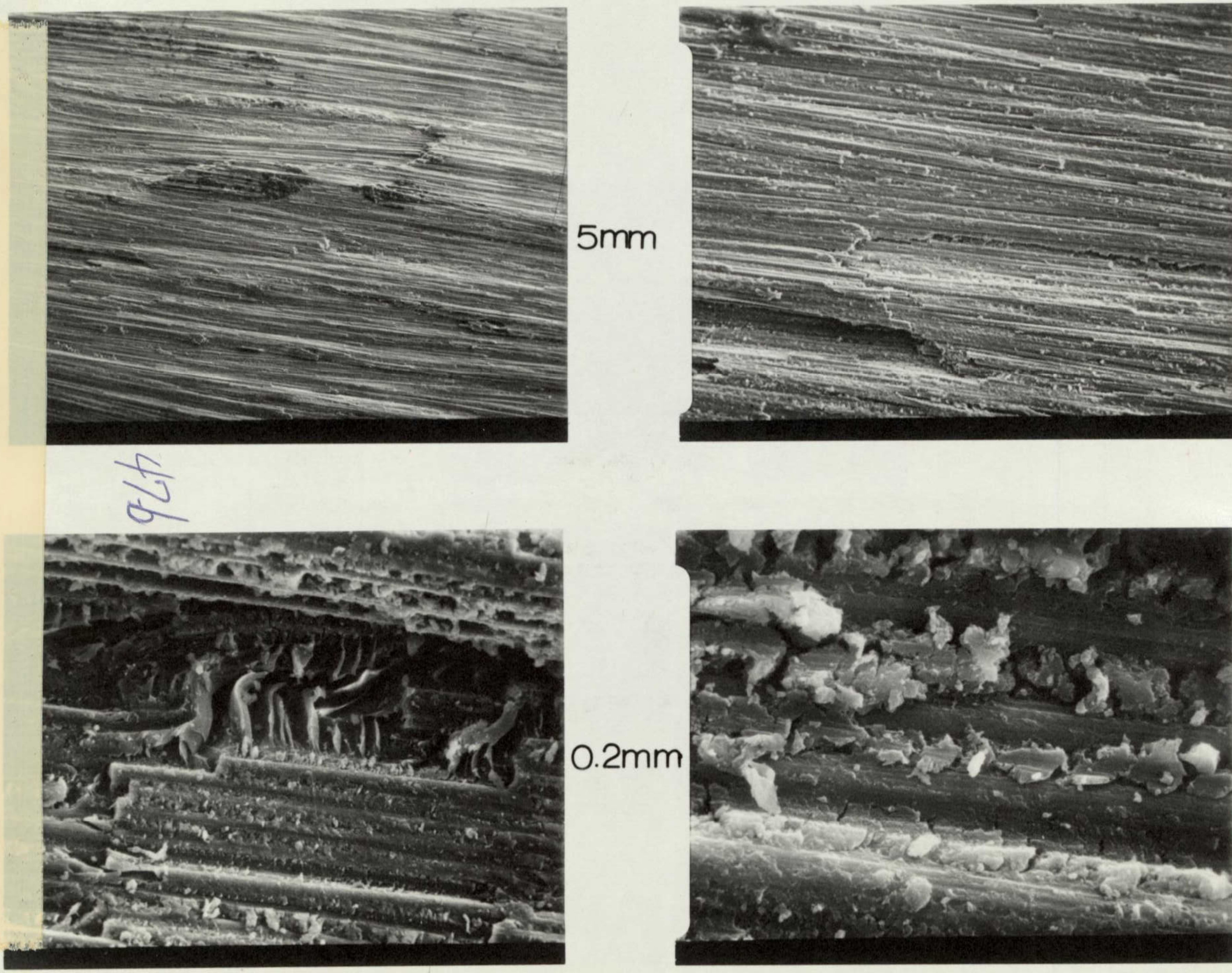
5mm
1mm
0.2mm
50 µm

FIGURE 20.

Four magnifications (20X, 200X, 2000X, 5000X) of the fracture surface of a PPQ 413/Skybond 710 sample that gave 4200 psi lap shear strength at 286°C.

Figure 20. Four magnifications (20X, 200X, 2000X, 5000X) of the fracture surface of a PPQ 413/Skybond 710 sample that gave 4200 psi lap shear strength at 286^{o}C.

Failure is primarily in the composite adherend surface on one side, leaving a rough surface because of fracturing through fibers and plys. Some low-area, brittle fracture through the adhesive to the opposite adherend, and the glue line appears to have deformed plastically to a thickness of about 0.2 mm (upper right). The "chunky" Skybond 710 matrix is even more apparent and shows a lumpy substructure < 0.4μm. Interfacial failure between the HT-S fibers and the Skybond 710 matrix is again the major fractographic feature.

48a

5mm

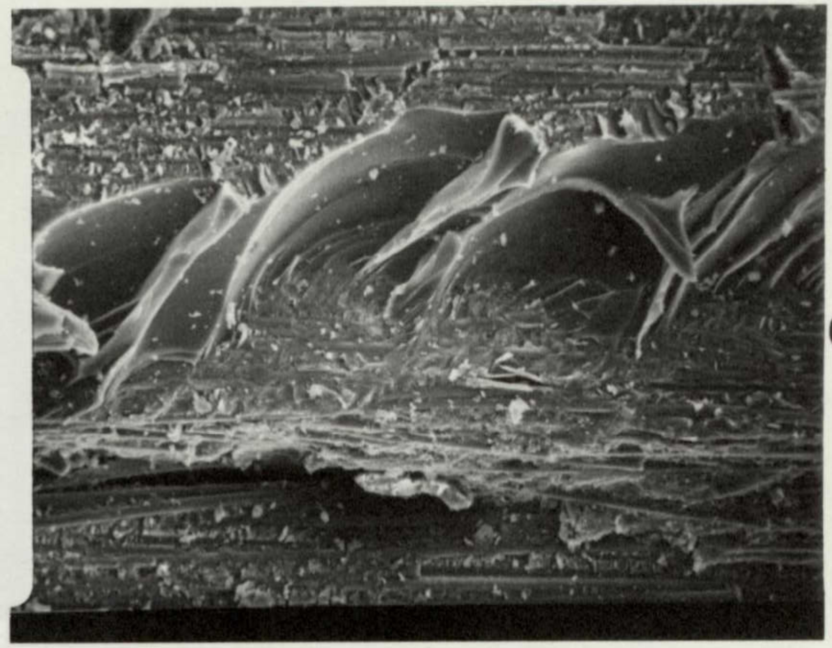

0.5mm

50 μm

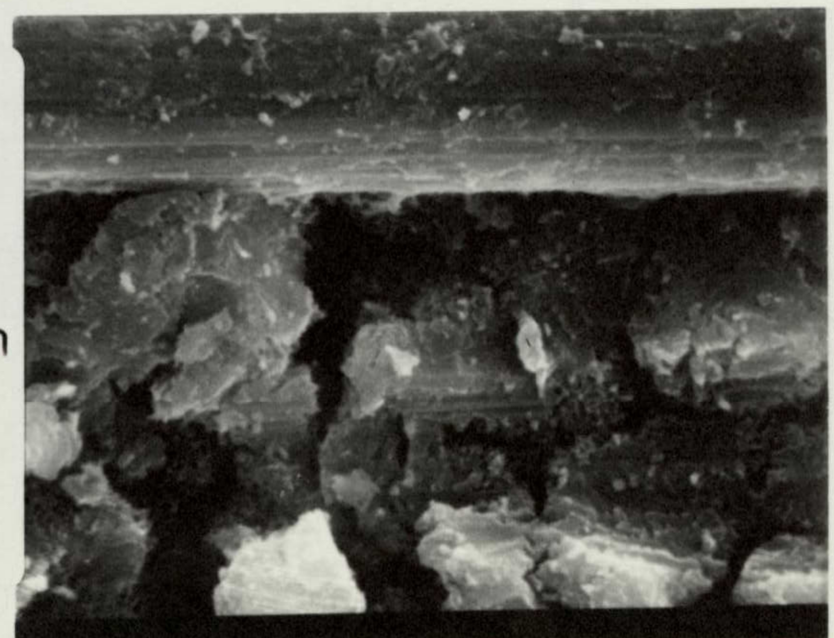

20 μm

FIGURE 21.

Four magnifications (20X, 200X, 500X, 2000X) of the fracture surface of a PPQ 413/Skybond 710 sample that gave 3000 psi lap shear strength at 316^{o}C.

Figure 21. Four magnifications (20X, 200X, 500X, 2000X) of the fracture surface of a PPQ 413/Skybond 710 sample that gave 3000 psi lap shear strength at $316^{\circ}C$.

Fracture is nearly identical to the previous example, except the glue line has deformed further to about 0.5 mm. Interfacial failure between HT-S fibers and Skybond 710 matrix is the predominant failure mechanism. EDAX (Figure 22) shows a silicon signal from the PPQ 413 and Skybond 710 resins, but not from HT-S fiber surfaces; possibly a residual mold release silicone. There was no calcium signal, ruling out glass.

49-a

5mm

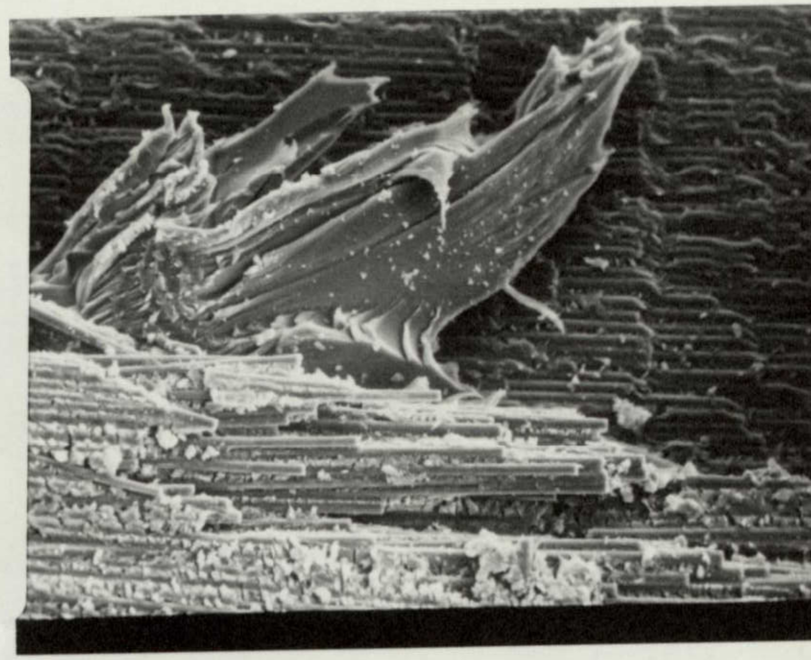

0.5mm

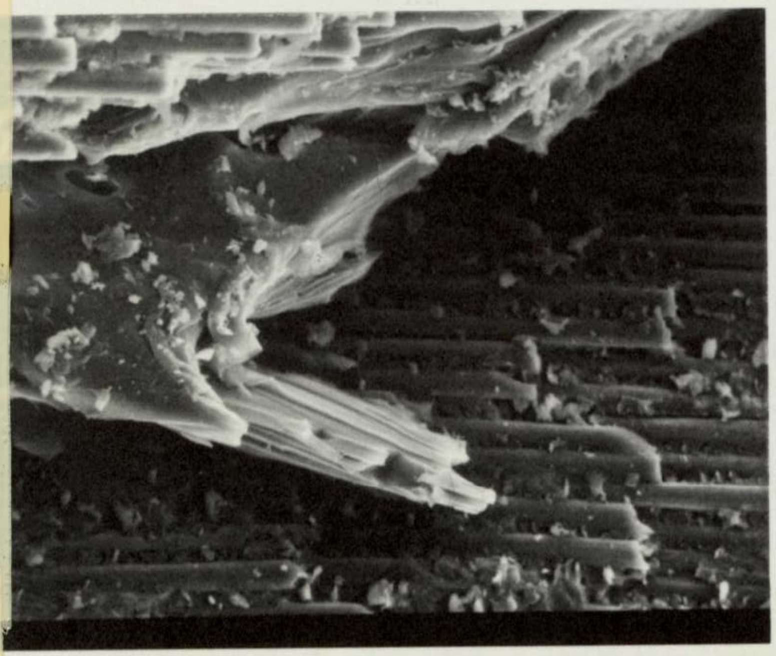

0.2mm

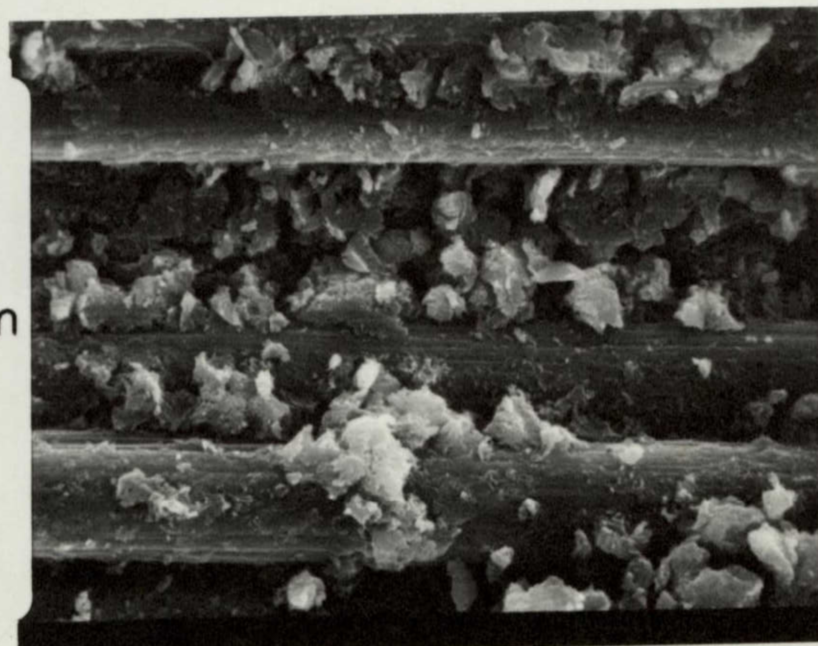

50 μm

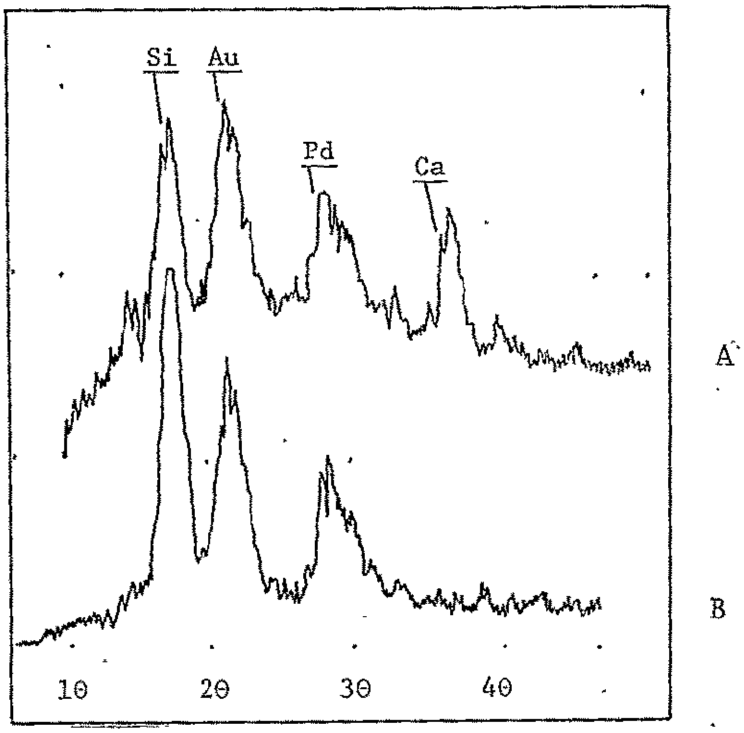

Figure 22. EDAX spectra that show a calcium and silicon peak from a fiber glass (SiO_2) containing substrate (A), while only silicon was found on adhesive and matrix resin fracture surfaces (B).

d. LARC-13/NR-150B2 Composite

Another synthetic approach to high-performance adhesives involves a cure mechanism in which olefinic end groups on an imide prepolymer crosslink at high temperature, thus avoiding the water evolved when the polyamic acid cures (57). An adhesive formulation of this type, synthesized with nadimide end groups (about 25% solution in diglyme) and filled with 30% aluminum powder, was obtained for the first time during the current grant period. SEM/EDAX analysis of the fracture surfaces obtained when this adhesive, supported on scrim cloth was used on NR-150B2/HT-S graphite fiber composite adherends is displayed in Figures 23-26.

Failure is entirely in one adherend at varying depths at room temperature (Figure 23). Apparently poor flow, insufficient polymer or both operated to cause the large voids ∿ 0.5mm at the interface between the adherend and the interstices of the scrim cloth. Surely the voids lower strength via stress concentration and limit the area available for strength-producing mechanisms. Adherend fracture mechanisms are basically the same as seen in NR-150B2/PPQ studies: interfacial failure between fiber or resin and brittle fracture of the matrix between the fibers.

At higher temperatures the locus of failure shifts toward the surface of the scrim cloth. Figure 24 indicates that about half the failure is in the adherend and the remainder in the voidy scrim cloth surface at 286°C. In the latter areas, patches of glass fibers have been removed from the scrim cloth and remain on the adherend. High-area, brittle cleavage cracking occurs in the

LARC-13 matrix around the glass fibers, and the adherend fracture mechanisms are identical to the previous case. At 316°C (Figure 25), failure is predominantly in the scrim cloth which has fractured in two, leaving one half the adhesive layer on each adherend. Closer inspection of the adhesive matrix resin between the smooth glass fibers reveals numerous voids about 5 to 20μm in size, and the fracture surfaces have no brittle cleavage cracks, indicating the possibility of thermal decomposition and softening at the highest temperature. The small amount of composite adherend failure still has the same fractography as at room temperature.

A preliminary experiment with EDAX on these three samples confirmed the photomicrographic indication that the fiber glass cloth became a more prominent feature as the test temperature increased.

Control of voids and increased polymer thermal stability and interfacial bonding with glass and aluminum are indicated for improvements in strength.

FIGURE 23.

Four magnifications (20X, 200X, 2 @ 2000X) of the fracture surface of a LARC-13 (with scrim cloth)/NR-150B2 sample that gave 5000 psi lap shear strength at room temperature.

Figure 23. Four magnifications (20X, 200X, 2 @ 2000X) of the fracture surface of a LARC-13 (with scrim cloth)/NR-150B2 sample that gave 5000 psi lap shear strength at room temperature.

Failure is in the composite adherend, at varying depths. Large ($\sim$0.5 mm) voids seen in top left coincide with the interstices of the scrim cloth yarns. The fracture surfaces are similar to the NR-150B2/HT-S fiber composite failure seen earlier: interfacial failure between fiber and resin, and brittle fracture of the matrix between the fibers.

53b

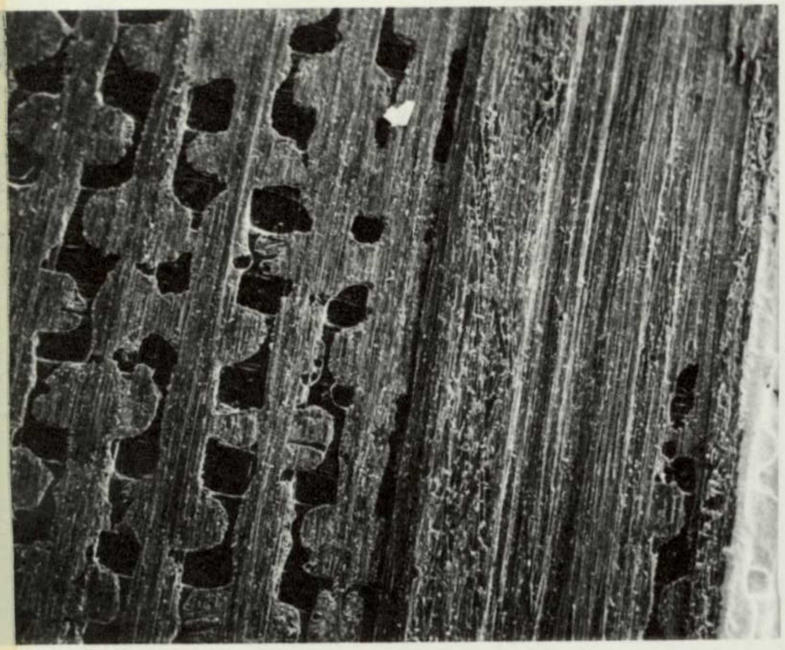

5mm

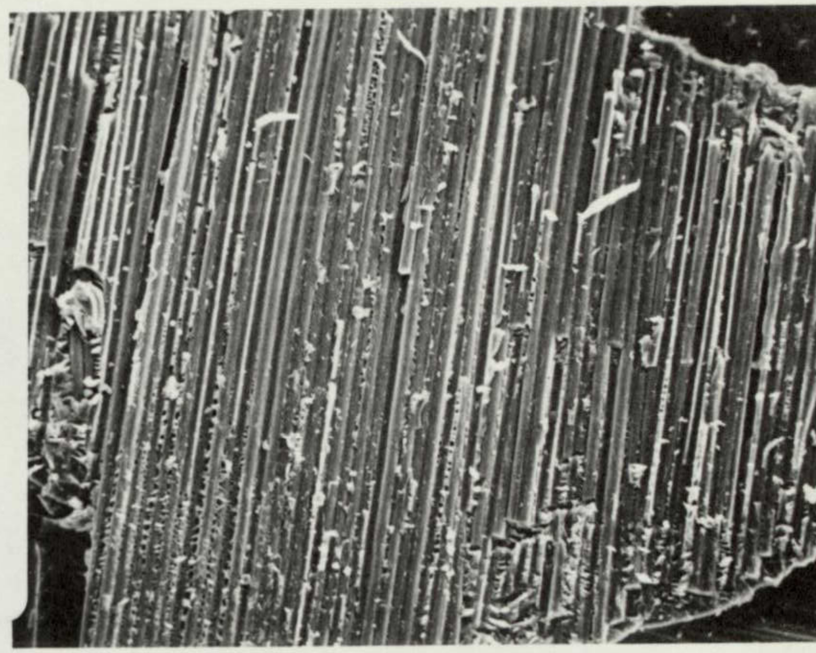

0.5mm

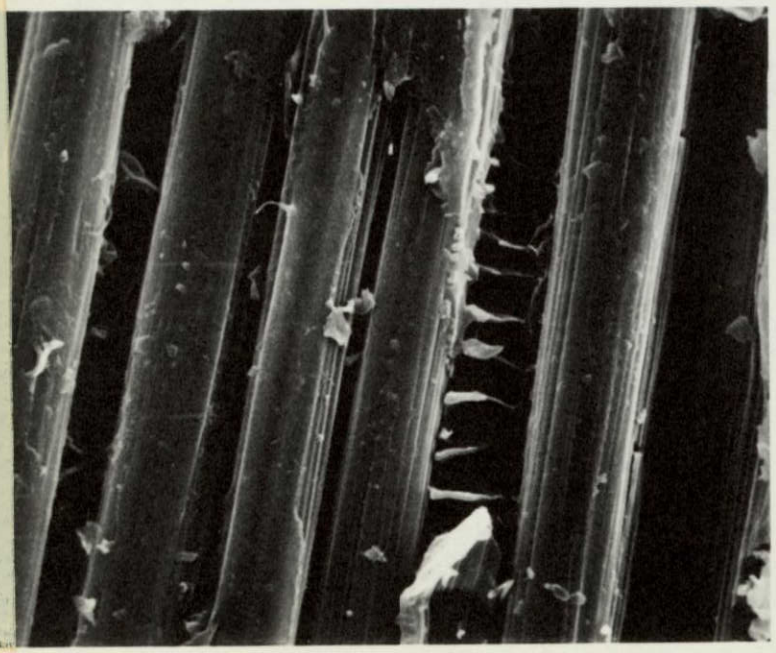

50 μm

50 μm

FIGURE 24.

Four magnifications (20X, 200X, 2 @ 1000X) of the fracture surface of a LARC-13 (with scrim cloth)/NR-150B2 sample that gave 3200 psi lap shear strength at 286°C.

Figure 24. Four magnifications (20X, 200X, 2 @ 1000X) of the fracture surface of a LARC-13 (with scrim cloth)/NR150-B2 sample that gave 3200 lap shear strength at 286°C.

About 50% failure in the composite adherend and 50% in the scrim cloth surface and voids. Lumps of aluminum powder filler are clearly visible under the resin surface on the bottom right, as well as a glue line of about 25μm between the void bottom and the composite. Patches of the surface of the scrim cloth are transferred; glass fibers and aluminum particles are seen on the lower left. The composite failure is the same as before. Adhesive resin fracture is by high-area, louvered, brittle modes with perhaps some plastic deformation. EDAX shows silicon and calcium from areas like bottom left, but not elsewhere.

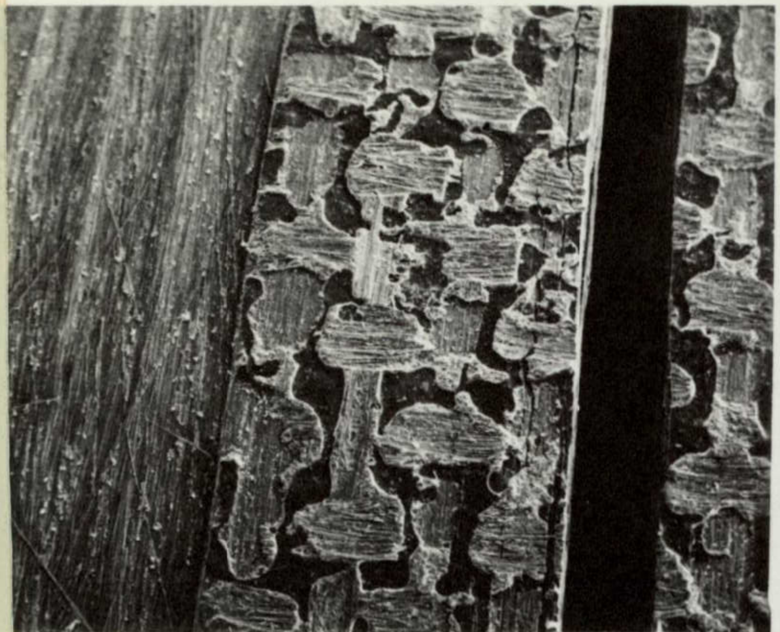

5mm

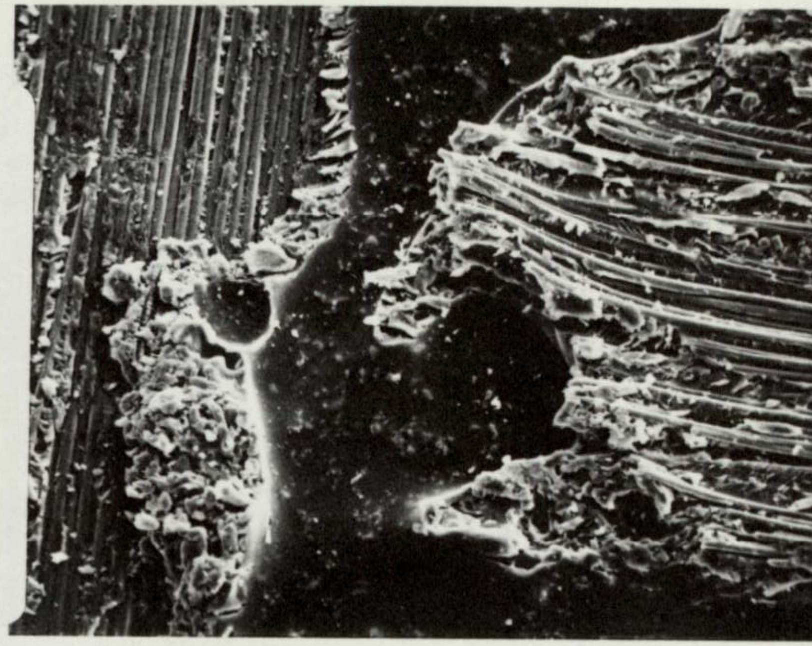

0.5mm

546

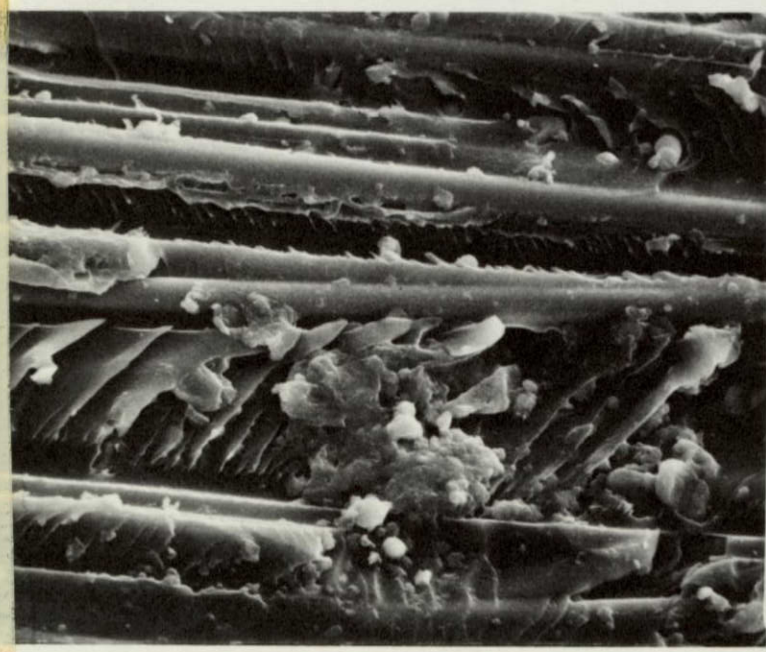

100 μm

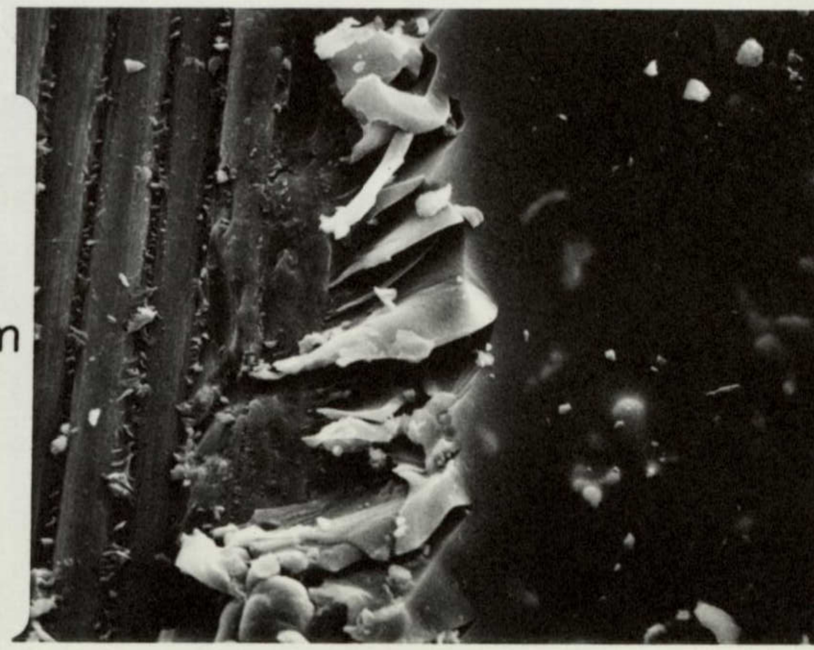

100 μm

FIGURE 25.

Four magnifications (20X, 500X, 1000X, 2000X) of the fracture surface of a LARC-13 (with scrim cloth)/NR150-B2 sample that gave 1700 psi lap shear strength at 316^{o}C.

Figure 25. Four magnifications (20X, 500X, 1000X, 2000X) of the fracture surface of a LARC-13 (with scrim cloth)/NR150-B2 sample that gave 1700 lap shear strength at 316°C.

Mostly failure in the scrim cloth surface, with a vertical fracture through the scrim leaving about half the adhesive layer on each adherend. Considerable glass fiber apparent, confirmed by EDAX (Figure 26). Fracture through the adhesive matrix reveals many small (5-20μm) voids; perhaps a result of decomposition by the combined effects of temperature and stress. About 10% of failure is in the composite, with familiar features as seen on the bottom right.

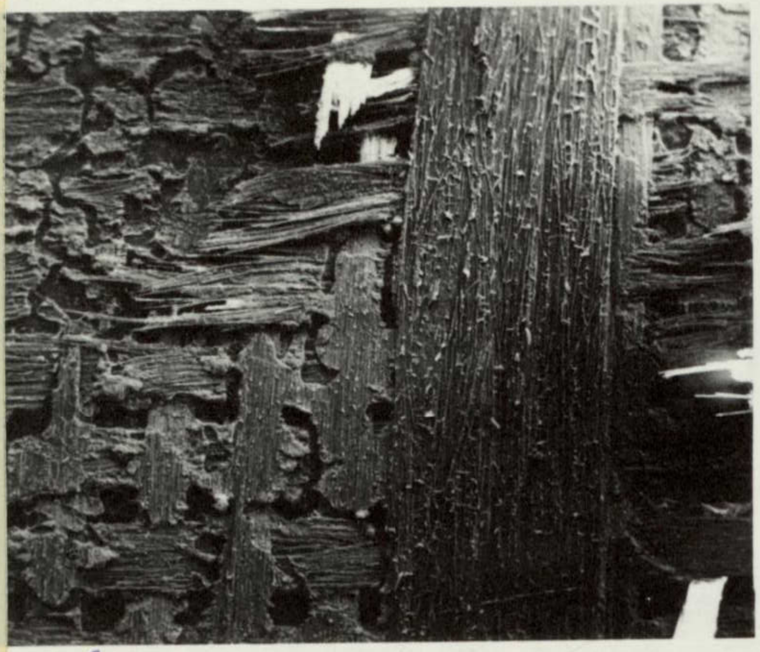

5mm

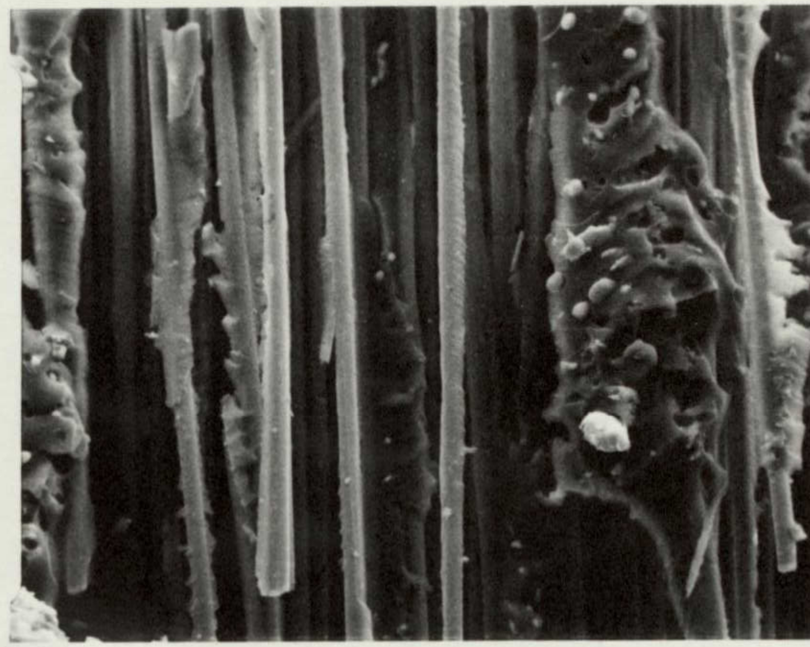

0.2mm

G55

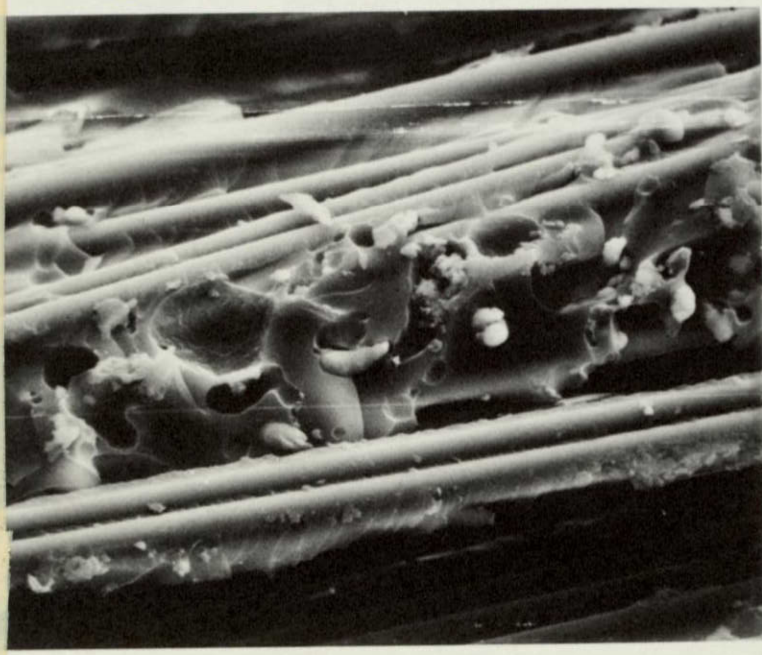

100 μm

50 μm

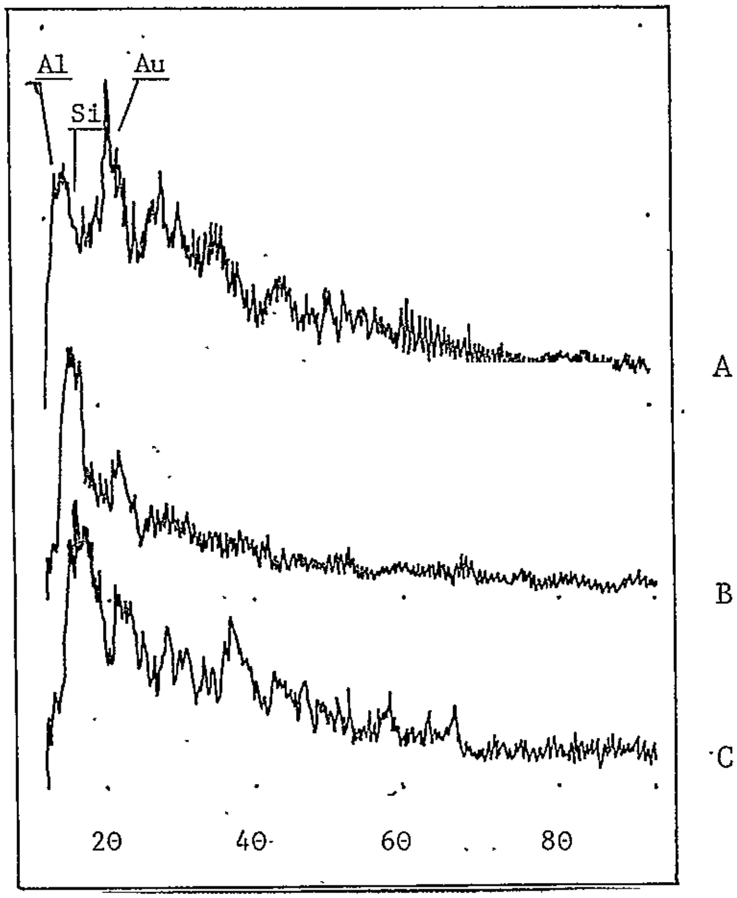

<u>Figure 26.</u> EDAX spectra taken from a wide area (50X) of the samples shown in Figures 23-A.,24-B., and 25-C.. Although there is overlap of the aluminum peak from the adhesive filler with the silicon peak from the fiber glass scrim cloth, the peak increases on the right-hand side (silicon) in going from A. to C.. Also C. shows the strongest calcium peak.

e. LARC-3 Adhesive and Variable Adherend, Formulation and Testing.

This adhesive was a principal development of the earlier work (1-3), and fractography on titanium 6-4 adherends of various LARC-3 type formulations has been published (9). In this section HT-S graphite fiber composite adherends with either Skybond 710 or P13N as the matrix resin were used, and tests run with and without aluminum powder filler and scrim cloth. A slight change in geometry for the strength test was made by removal of a shim from the grip in a few cases.

Single lap-shear specimens are usually mounted with a shim in one grip to direct most of the stress parallel to the adherend surfaces. Contrary to experience with titanium, Figure 27 shows that most of the failure occurred in an irregular plane through one composite adherend. The chunky, discontinuous Skybond 710 matrix seen before is even more evident here. Most fracture surfaces look like HT-S fiber/matrix resin interfacial failure, and strength was only moderate. A 50% improvement in strength was obtained without the shim in the grips and Figure 28 shows a new locus of failure. There is some fracture in patches of both adherends, but now there is a significant contribution from the glue-line. Adhesive areas show plastic deformation and high-area, brittle cleavage cracking. There are very large voids in the bond line, and perhaps they acted, together with the "no-shim" geometry to nucleate failure in a zone that absorbed more energy in failure than the previous example.

Failure is entirely in the adhesive layer at 250°C (Figure 29). Void area is dominant and softening and flow of the adhesive under stress is obvious: thick void-cell walls have deformed plastically in the stress direction. The actual area of material fracture is small, and appears ductile and splintered, with a few brittle cleavage cracks. The addition of aluminum powder filler improved high-temperature strength on titanium adherends (8,9), and also doubled strength on composite adherends. Figure 30 shows that the locus and features of fracture are also changed. About half the failure is in the composite adherend with the familiar fiber/matrix interfacial mechanism dominant. In the glue line fracture is characterized by very fine plastic deformation and ductile fracture in the walls of microvoids around the aluminum filler particles. The very large volume of stretched polymer that results is likely to contribute to the observed strength.

Unexpected problems arise when the number of components in an adhesive joint increases. For example, Figure 31 shows that the solvent was trapped in a myriad of tiny voids at the surface of the fiber glass cloth-supported adhesive film, when this sample was tested at high temperature.

The use of P13N as the matrix polymer for HT-S graphite fiber composites gave good, reproducable strength even when the locus of failure shifted from the adherend to the adhesive layer, shown in Figure 32. Again, composite failure proceeds via fiber/matrix interfacial failure and brittle fracture of the P13N matrix between the fibers. This matrix polymer is continuous and fractures like NR-150B2, whereas Skybond 710 is distinctly different.

Figure 27. Four magnifications (20X, 1000X, 2000X, 5000X) of the fracture surface of a LARC-3/Skybond 710 sample that gave 2200 psi lap shear strength at room temperature.

About 95% failure in composite substrate. The discontinuous, chunky nature of the Skybond 710 matrix is clearly illustrated on the right; fracture is essentially interfacial between the fibers and resin. The glue line appears to be about 25µm on the bottom left.

59-a

FIGURE 27.

Four magnifications (20X, 1000X, 2000X, 5000X) of the fracture surface of a LARC-3/Skybond 710 sample that gave 2200 psi lap shear strength at room temperature.

5mm

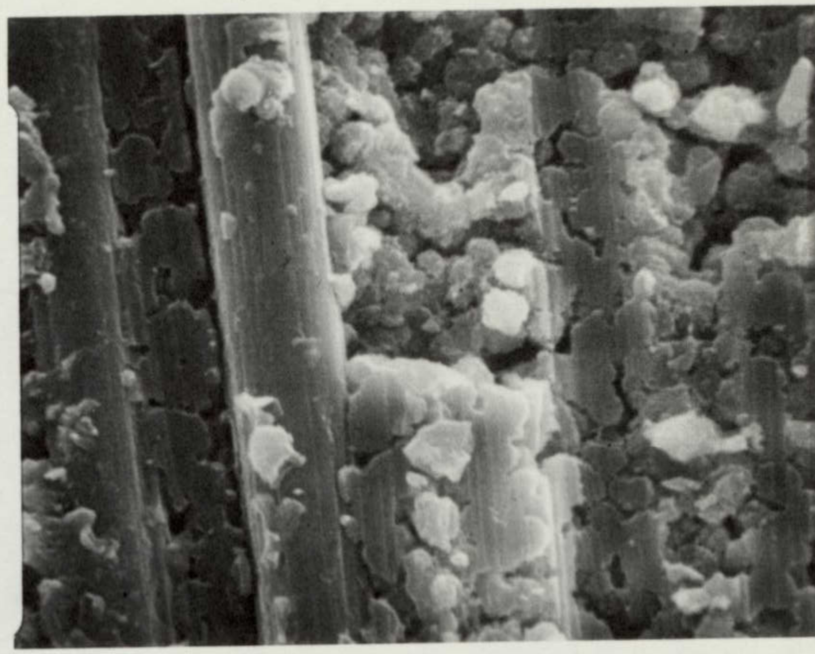

50 μm

596

100 μm

20 μm

FIGURE 28.

Three magnifications (20X and 2 @ 200X) of the fracture surface of a LARC-3/Skybond 710 sample that gave 3300 lap shear strength at room temperature.

Figure 28. Three magnifications (20X and 2 @ 200X) of the fracture surface of a LARC-3/Skybond 710 sample that gave 3300 psi lap shear strength at room temperature.

This sample was fractured without the usual shim in the shear tester grips, and the strength increased 50% over the previous example. The locus of failure is now more than half in the very voidy (0.2 - 2 mm in size) glue line, where there seems to be considerable plastic deformation and high-area, louvered, brittle fracture.

60a

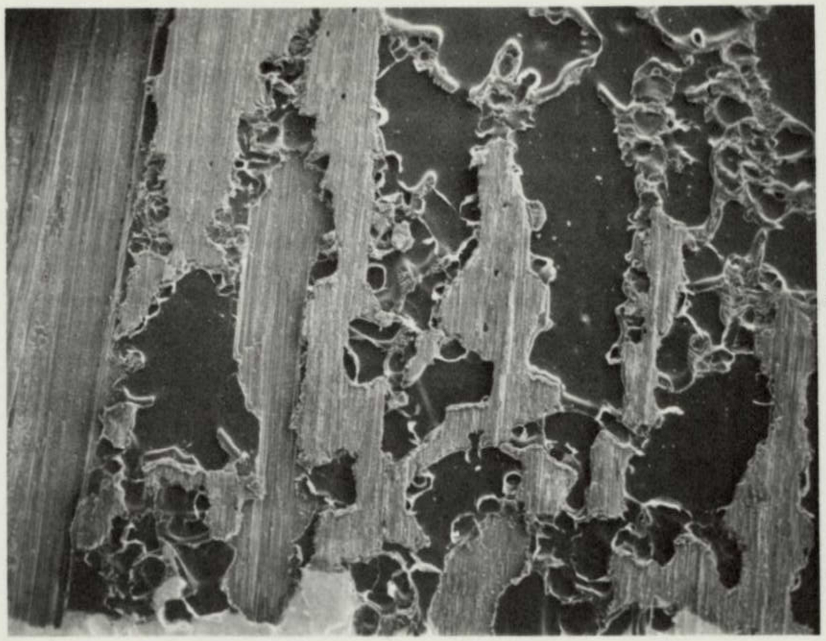

5mm

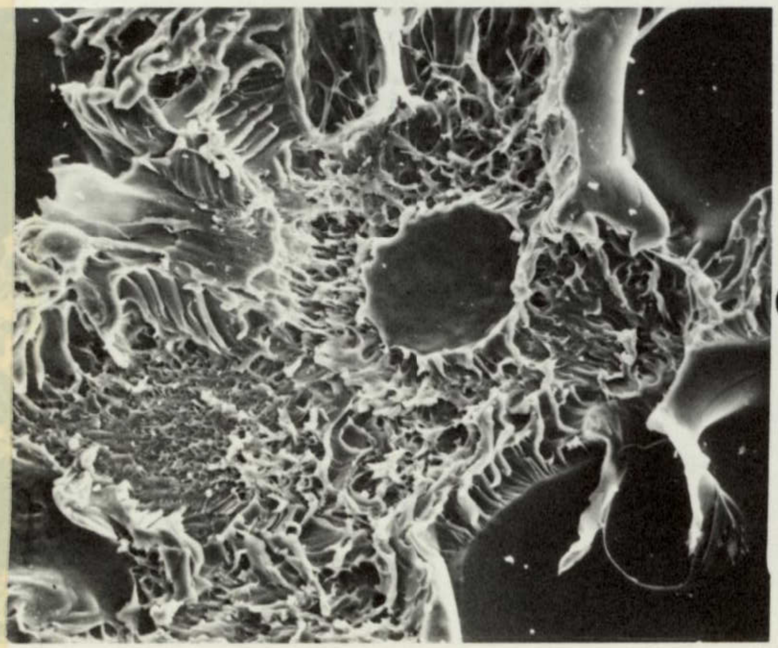

0.5mm

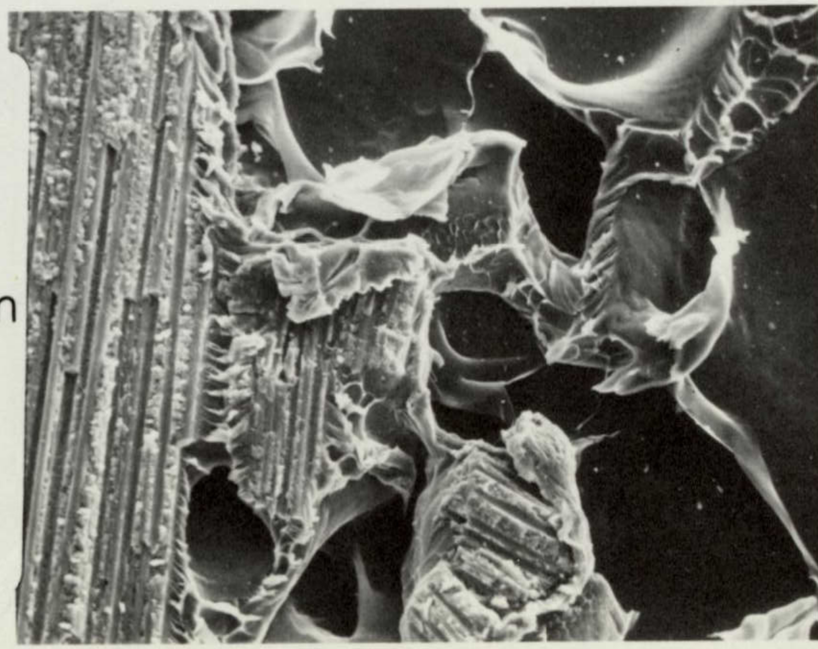

0.5mm

FIGURE 29.

Two magnifications (20X, 200X) of the fracture surface of a LARC-3/Skybond 710 sample that gave 1300 psi lap shear strength at 250°C.

<u>Figure 29</u>. Two magnifications (20X, 200X) of the fracture surface of a LARC-3/Skybond 710 sample that gave 1300 psi lap shear strength at 250°C.

At least 75% void area and flow of adhesive in the direction of stress is obvious. The strength is accounted for by gross plastic deformation of thick (0.1 - 1 mm) void-cell walls and ductile, splintery fracture.

19-a

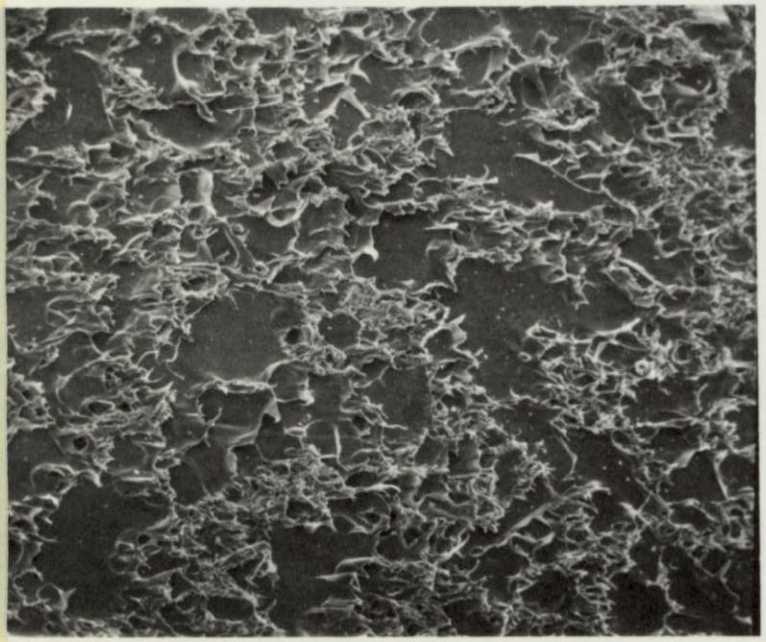

5mm

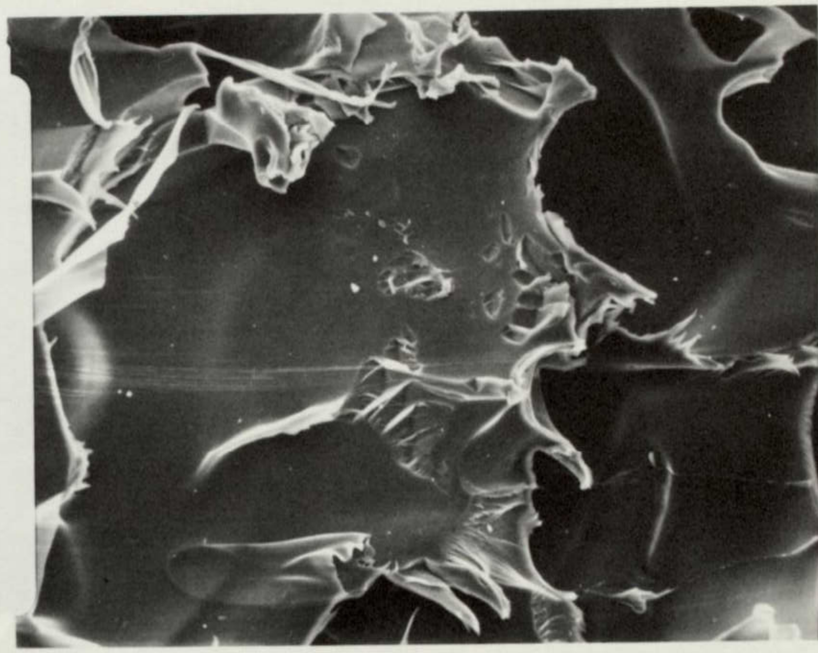

0.5mm

Φ-19

FIGURE 30.

Four magnifications (20X, 200X, 2 @ 2000X) of the fracture surface of a LARC-3 (with Al powder filler)/Skybond 710 sample that gave 2400 psi lap shear strength at 250°C.

Figure 30. Four magnifications (20X, 200X, 2 @ 2000X) of the fracture surface of a LARC-3 (with Al powder filler)/Skybond 710 sample that gave 2400 psi lap shear strength at 250°C.

Including filler doubled strength compared to the previous example. About half the failure is in the composite surface with the same interfacial mechanism seen before. Fracture in the glue line is characterized by very fine plastic deformation and ductile fracture apparently nucleated by the aluminum filler particles, similar to that observed earlier with Ti 6-4 adherends(8).

0.5mm

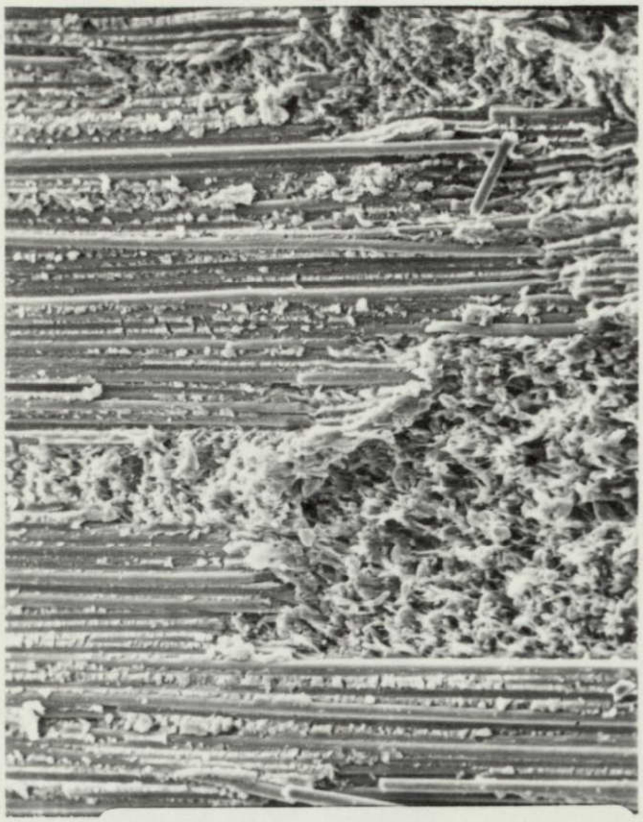

50 μm

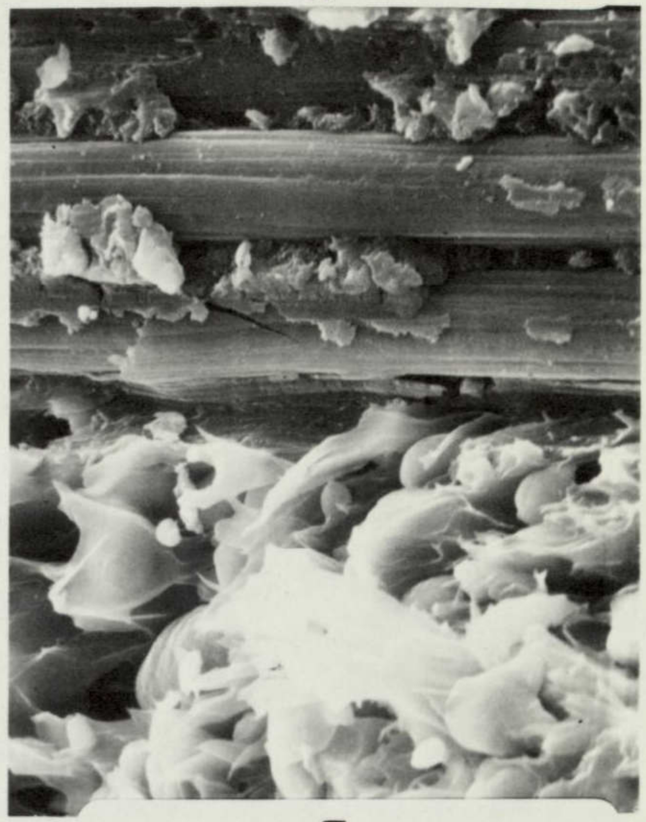

5mm

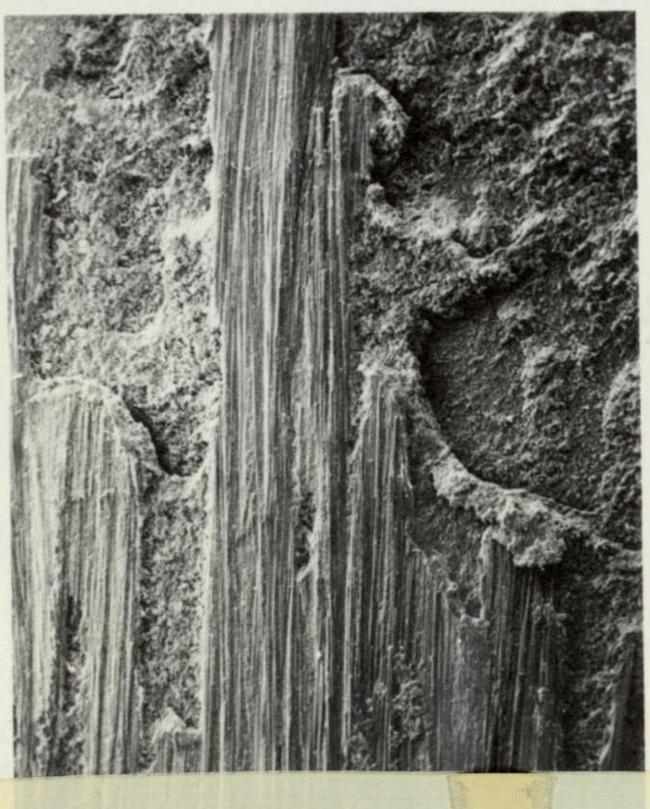

50 μm

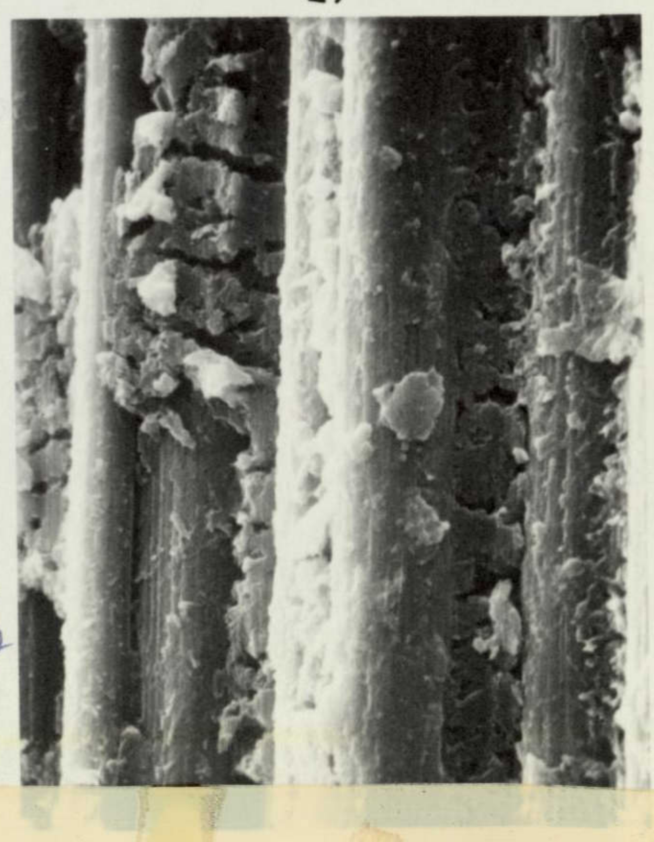

62b

FIGURE 31.

Three magnifications (20X, 200X, 1000X) of the fracture surface of a LARC-3 (with Al filler and scrim cloth)/ Skybond 710 sample that gave 600 psi lap shear strength at 250°C.

Figure 31. Three magnifications (20X, 200X, 1000X) of the fracture surface of a LARC-3 (with Al filler and scrim cloth)/ Skybond 710 sample that gave 600 psi lap shear strength at 250°C.

Voids (d ∿ 0.2mm) cover the surface and limit the fracture area to very thin, micro-void (10-20μm) walls.

63-a

100 µm

5mm

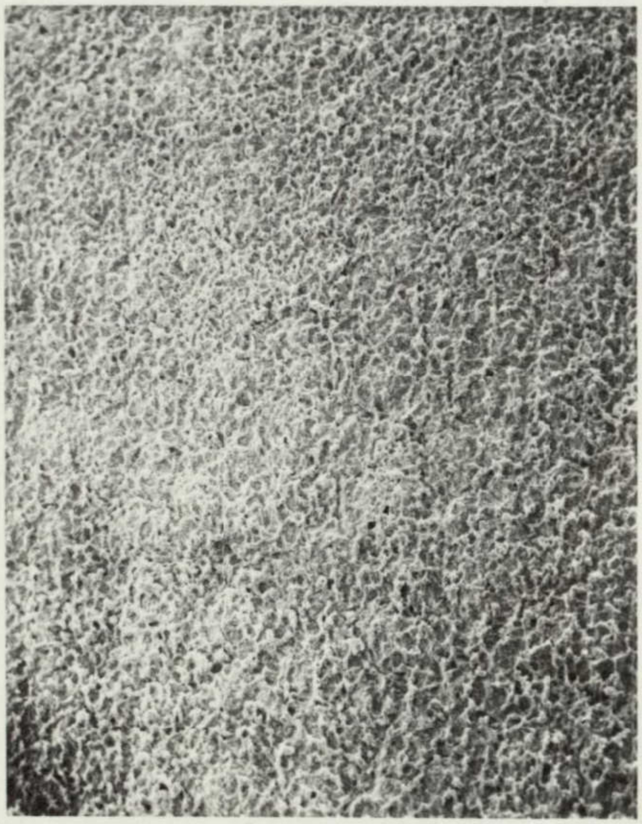

0.5mm

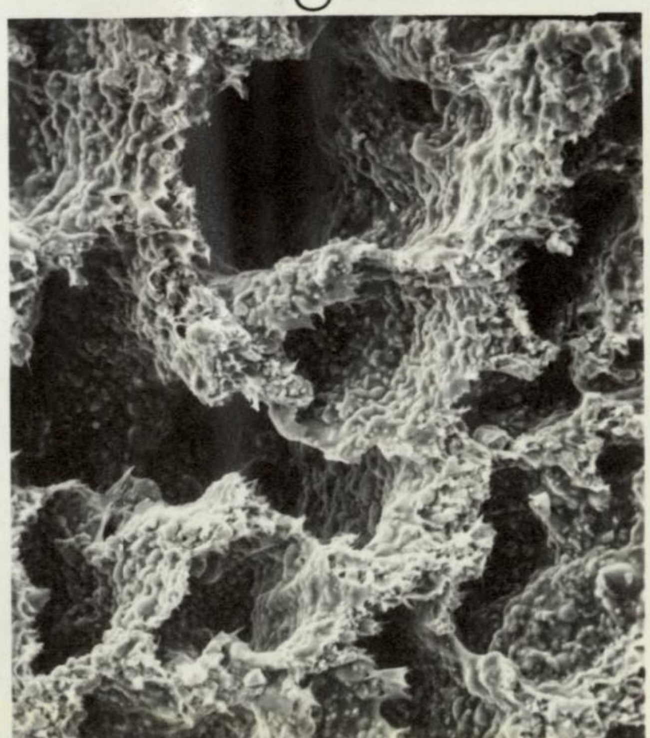

63-b

FIGURE 32.

Four magnifications (2 @ 20X, 1000X, 5000X) of the fracture surface of a LARC-3/P13N sample that gave 3500 psi lap shear strength at room temperature.

Figure 32. Four magnifications (2 @ 20X, 1000X, 5000X) of the fracture surface of a LARC-3/P13N sample that gave 3500 psi lap shear strength at room temperature.

The same strength occurred by either of two mechanisms; in the voidy glue line (top left) or in the composite, where brittle matrix fracture and fiber/matrix interfacial failure occur.

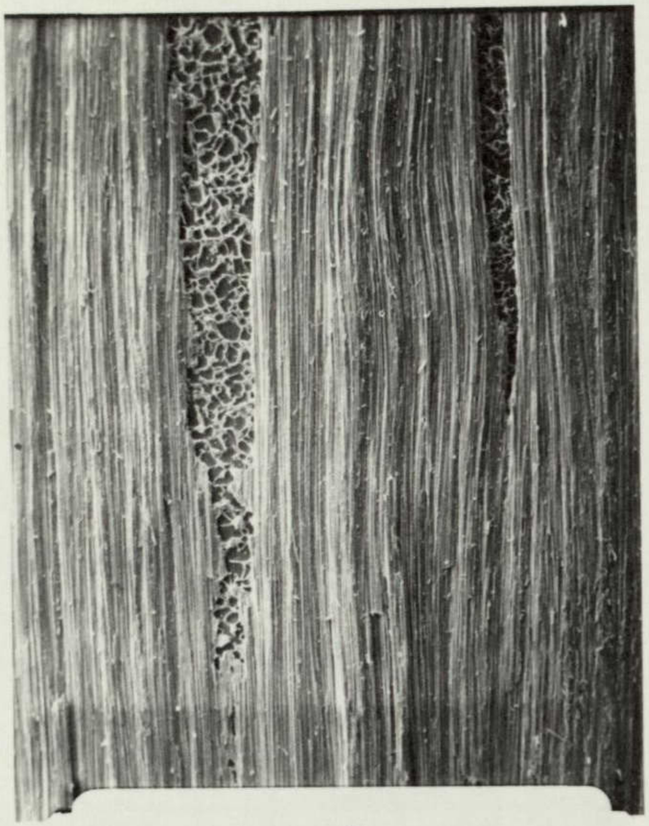

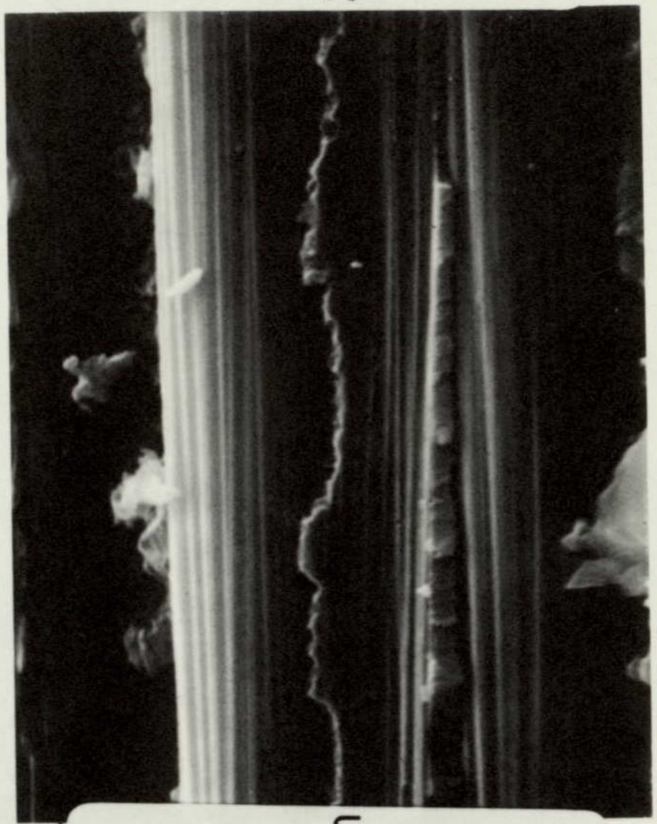

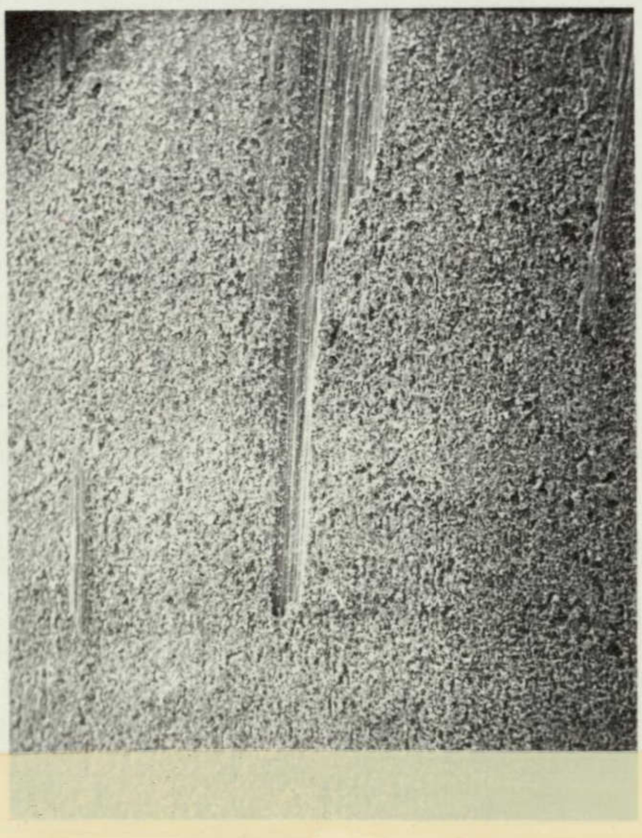

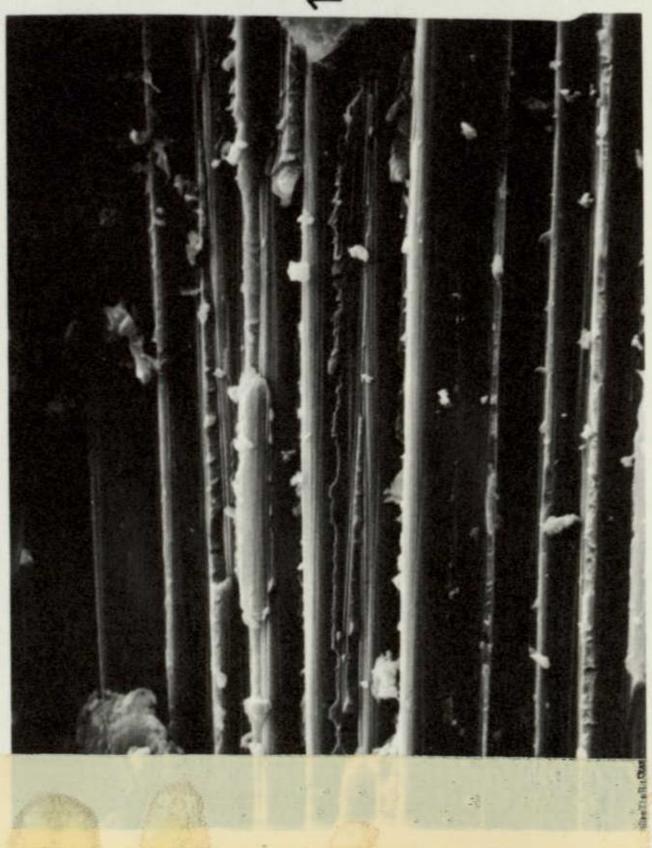

64b

B. Electron Spectroscopy for Chemical Analysis (ESCA)

1. Titanium 6-4

Previous reports included ESCA data on titanium 6-4 adherends and a variety of treatment steps used to prepare the surface for adhesive bonding (4-8). Those data were collected by "narrow scans" of 20 electron-volt wide sections where specific peaks were expected in the ESCA spectrum. Elemental identification and oxidation state data were determined, providing characterization of chemical composition, structure and bonding of the sample surface

Valuable information is contained in the relative intensities of ESCA peaks, but accurate and general quantitative methods are still in the development stage as indicated in the literature review in the Introduction. Therefore, few quantitative ESCA publications are available, although practical ESCA laboratories (particularly in industrial R and D) routinely draw conclusions based on comparisons among peak intensities for two or more specimens.

By collecting the photoelectron spectrum over a range of about 0-700 eV, all elements can be detected. The "wide-scan" ESCA spectra, especially when collected before and after in situ ion etching, at a glance provides a useful characterization of the composition of the surface region. This type of "fingerprint" for a recent phosphate/fluoride adherend is shown at the bottom of Figure 33. A few representative narrow scans are superimposed on this figure, better illustrating the connection between this and previous reports (4-8). Because photoelectron cross sections and escape depths vary, peak heights cannot be taken as directly proportional to elemental concentration. Nevertheless, changes in relative intensity between similar samples can be significant.

Figures 34 and 35 show wide scan ESCA spectra of titanium 6-4 adherends treated by the phosphate/fluoride process last year and this year, respectively. Also the effect of in situ ion etching is shown in each case. In 1975, aluminum did not appear until some of the carbon contamination was removed by ion etching. The initially present aluminum signal in 1976 may be due to the residual grit particles observed on this adherend by SEM/EDAX (Figures 7 and 8). It may also be significant that the initial carbon contamination in 1976 is greater than in 1975, even though the latter sample was in storage for a year. In both cases a notable result of etching was the appearance of a major fluorine peak. Presumably the treatment solutions left this element behind, and it has been observed by ISS/SIMS and Auger Spectroscopy on similar substrates (17,18). But then the questions of the disappearance of phosphorous in Figure 34 after etching is puzzling. Chromium appears after etching in both cases and is probably an impurity in the bulk alloy. The cadmium peaks are an artifact of the ion etching procedure. Assignment of an elemental core level to each peak in ESCA wide scans is usually difficult and sometimes arbitrary, especially for low intensity peaks. Thus some peaks are not assigned and others tentatively identified, but without rationalizing why they are components of these systems.

The anodized titanium 6-4 substrates were metallic blue as received and tended toward brown or yellow after storage or handling.

ESCA spectra of these two areas are shown in Figure 36, and the brown color is explained by the presence of a heavy carbon contamination, while the blue area has the lowest carbon-to-titanium ratio of any substrate as received. Also new elements magnesium and potassium, and the sodium and chlorine peaks are more pronounced than in the case of phosphate/fluoride treatment. Presumably these changes derive from process differences. After etching the carbon contamination has increased surprisingly, obscuring most other surface components. The appearance of fluorine is hard to rationalize unless it is part of the anodizing treatment bath. Obviously, a data base derived from systematic studies of this type will be required to better understand these observations.

Gold is a reference standard in many types of analysis, and is especially suitable as sample supports for ESCA. As a control on wide-scan, ion etching studies, the results on gold are shown in Figure 37. The relatively inert nature of gold compared with titanium is dramatized by the very small carbon signal from adsorbed contaminants before ion etching, and its virtual disappearance after etching. Titanium cannot be made this clean in the present apparatus limited to $>10^{-7}$ torr. The cadmium peak on gold after etching clearly identifies it as an artifact of the etching process. Cadmium is easily sublimed and sputtered. It was used in this equipment before, and is apparently still a contaminant inside the apparatus.

FIGURE 33.

Wide scan ESCA spectrum of a titanium 6-4 adherend after phosphate/fluoride treatment (1976).

Figure 33. Wide scan ESCA spectrum of a titanium 6-4 adherend after phosphate/fluoride treatment (1976).

Superimposed above the wide (743 eV) scan are eight narrow (20 eV) scans taken in the regions indicated. Signal-to-noise ratio could be improved by longer counting times, but is not necessary for most qualitative analysis. The width of the oxygen peak reflects different oxidation states for the surface metal oxide and adsorbed contaminants. The 20 eV spectra for phosphorous and fluorine show that the wide scan may not detect elements in low concentration, although it is very useful for a quick estimate of the relative atomic composition of the major constituents of the surface.

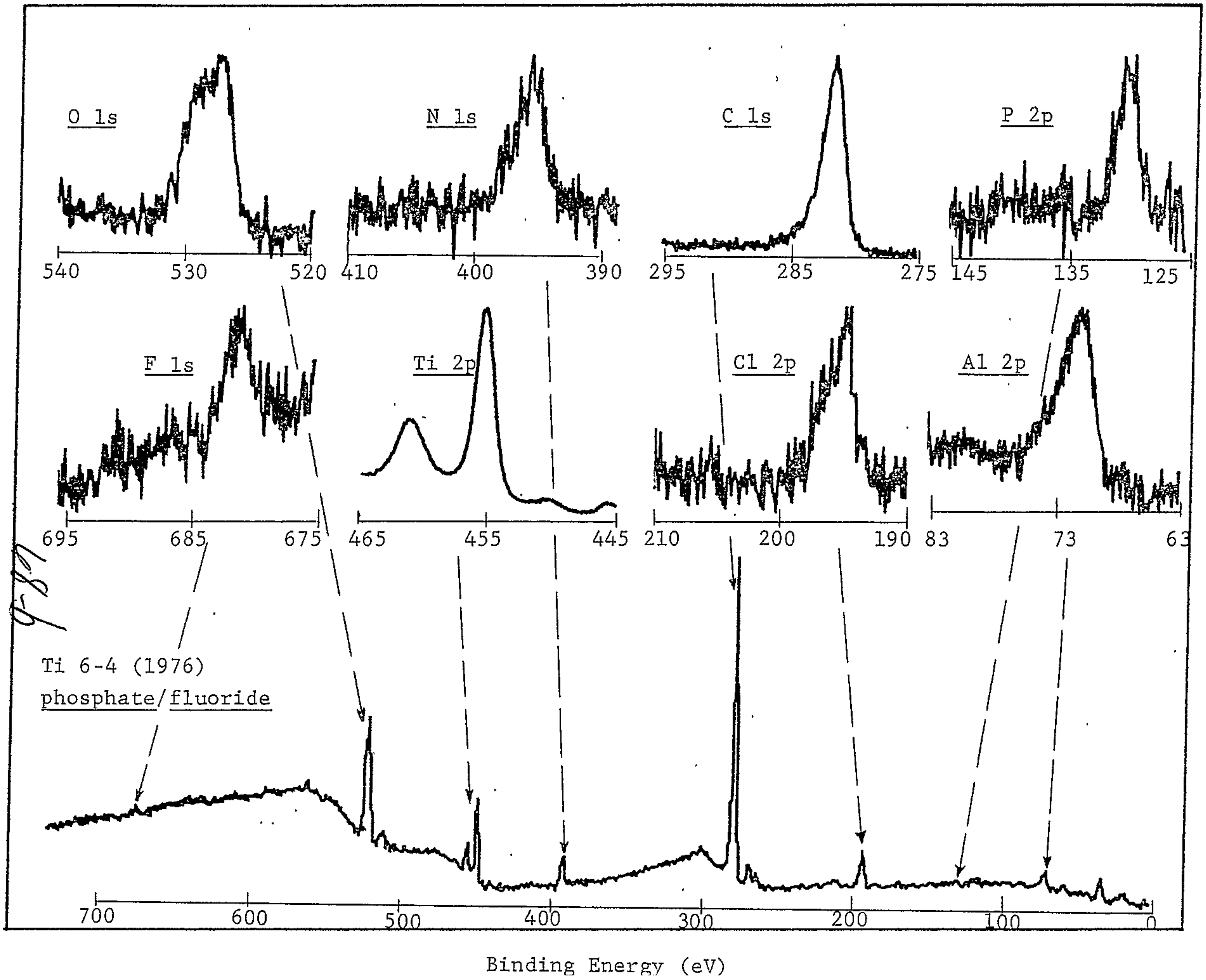
O 1s
N 1s
C 1s
P 2p
F 1s
Ti 2p
Cl 2p
Al 2p
Ti 6-4 (1976)
phosphate/fluoride
Binding Energy (eV)

Figure 34. Wide scan ESCA spectra, before and after in situ ion etchings, of a titanium 6-4 adherend after phosphate-fluoride treatment (1975).

Initially there is considerable contamination, although vanadium from the alloy gives a peak as well as titanium. After etching, the carbon peak is reduced and calcium and phosphorous are eliminated, but titanium and vanadium appear unchanged. New surface constituents fluorine, aluminum, barium, and cadmium appear. (The latter is shown to be an artifact - see Figure 37). The chromium peaks are increased. Presumably the fluorine was deposited during surface treatment and the chromium is an impurity in the alloy. The other peaks are unexplained.

FIGURE 34.

Wide scan ESCA spectra, before and after *in situ* ion etching, of a titanium 6-4 adherend after phosphate-fluoride treatment (1975).

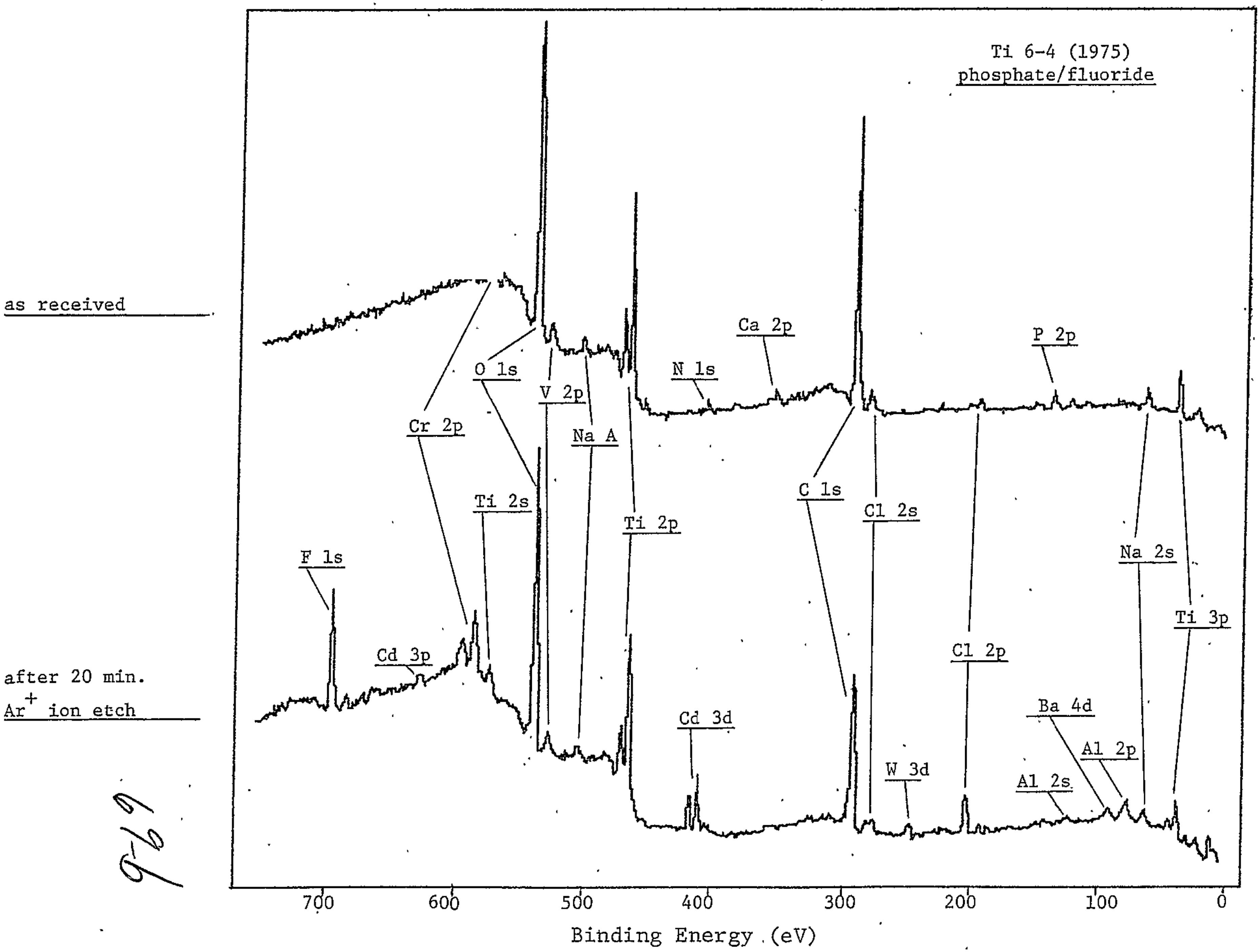
Ti 6-4 (1975)
phosphate/fluoride
as received
after 20 min.
Ar+ ion etch
O 1s
V 2p
Na A
Cr 2p
Ti 2s
Ti 2p
N 1s
Ca 2p
C 1s
Cl 2s
P 2p
Cl 2p
Na 2s
Ti 3p
F 1s
Cd 3p
Cd 3d
W 3d
Ba 4d
Al 2s
Al 2p
700
600
500
400
300
200
100
0
Binding Energy (eV)

FIGURE 35.

Wide scan ESCA spectra, before and after *in situ* ion etching, of a titanium 6-4 adherend after phosphate/fluoride treatment (1976).

Figure 35. Wide scan ESCA spectra, before and after *in situ* ion etching, of a titanium 6-4 adherend after phosphate/fluoride treatment (1976)

Initially the contamination is heavy, almost obscuring the titanium signal. The oxygen peak is also smaller before etching proving that metal oxide contributes significantly to the oxygen peak. Despite the contamination, an aluminum signal shows and may be related to the particles observed by SEM/EDAX (Figures 7 and 8). After etching, the carbon contamination was reduced by more than 50% and the same main features characterize the spectrum as the previous example.

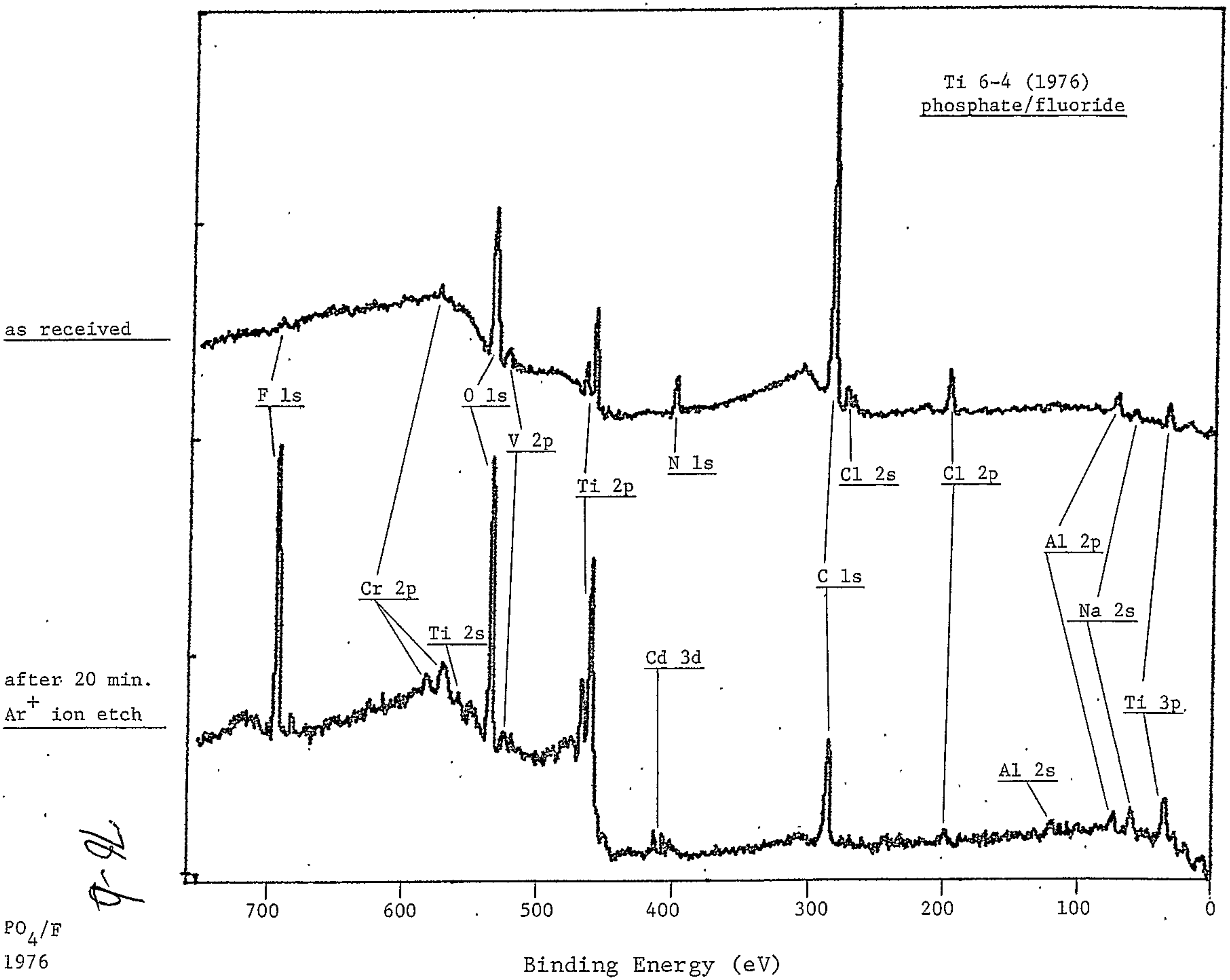

Ti 6-4 (1976)
phosphate/fluoride
as received
after 20 min.
Ar^+ ion etch
F 1s
O 1s
V 2p
Ti 2p
N 1s
Cl 2s
Cl 2p
Cr 2p
Ti 2s
C 1s
Cd 3d
Al 2p
Na 2s
Ti 3p
Al 2s
700
600
500
400
300
200
100
0
Binding Energy (eV)

PO_4/F
1976

Figure 36. Wide scan ESCA spectra, before and after *in situ* ion etching, of two areas of a titanium 6-4 adherend after anodizing treatment.

Spectra from the blue and brown areas of the adherend as received indicate that the brown color is a result of heavy carbon contamination that virtually obscures the ESCA peaks from the substrate. The blue area has the least relative carbon of any of the adherends studied. New peaks due to potassium and magnesium may derive from the anodizing treatment. The spectrum after ion etching is surprising as it appears that carbon contamination increased, and the appearance of fluorine is hard to rationalize.

FIGURE 36.

Wide scan ESCA spectra, before and after *in situ* ion etching, of two areas of a titanium 6-4 adherend after anodizing treatment.

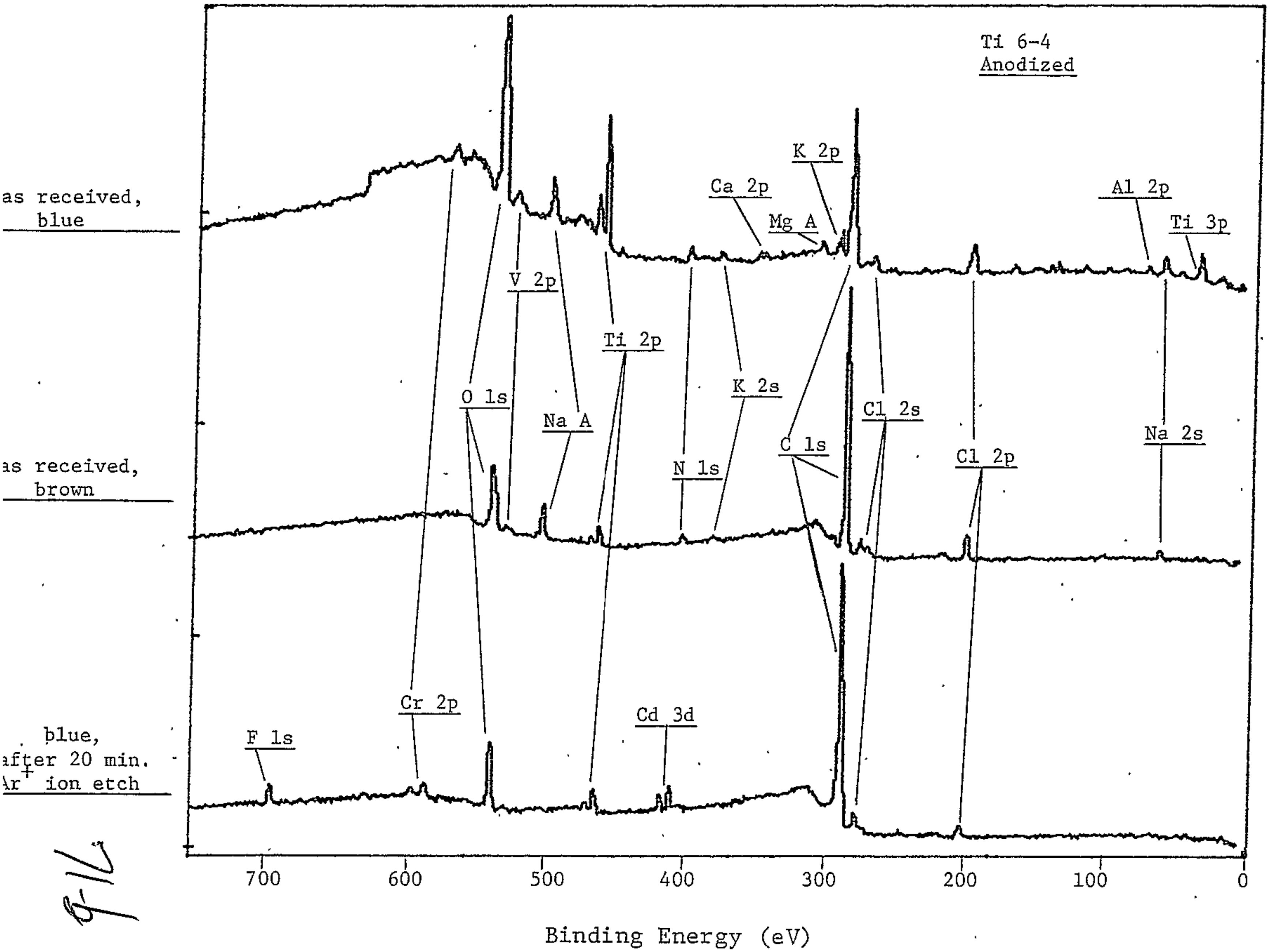
Ti 6-4
Anodized
as received,
blue
as received,
brown
blue,
after 20 min.
Ar$^+$ ion etch
K 2p
Ca 2p
Mg A
Al 2p
Ti 3p
V 2p
Ti 2p
O 1s
Na A
K 2s
N 1s
C 1s
Cl 2s
Cl 2p
Na 2s
F 1s
Cr 2p
Cd 3d
700
600
500
400
300
200
100
0
Binding Energy (eV)

9-16

FIGURE 37.

Wide scan ESCA spectra, before and after _in situ_ ion etching, of a gold reference standard.

Figure 37. Wide scan ESCA spectra, before and after *in situ* ion etching, of a gold reference standard.

There is a small carbon contamination originally that is diminished by etching. Most important is the appearance of the cadmium signal, clearly identifying this feature as an artifact of the ion etching procedure.

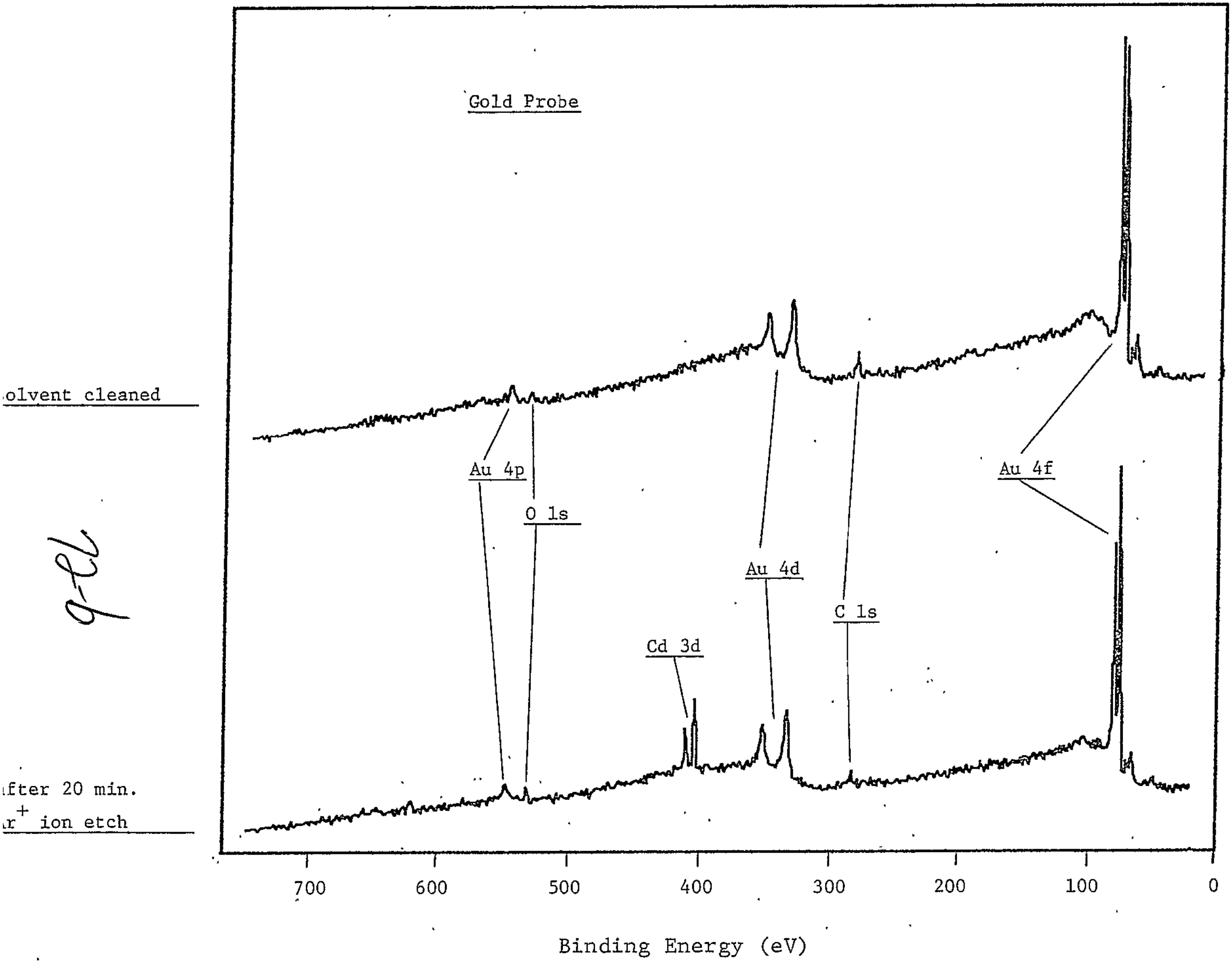

Gold Probe
olvent cleaned
fter 20 min.
r+ ion etch
Au 4p
O 1s
Au 4d
C 1s
Au 4f
Cd 3d
700
600
500
400
300
200
100
0
Binding Energy (eV)

2. Polymers

During the current grant period, ESCA spectra were collected mainly using thin films of well-characterized polymers, cast from solvents directly on a gold reference probe. These studies serve as controls for future studies of fracture surfaces, where the composition is unknown. Furthermore, the use of ESCA for qualitative analysis of polymers has only recently been published for limited classes of similar polymers (40,53-56), but our results to date on a variety of different types of polymers indicate that fundamental ESCA correlation charts may provide identification of most polymers by studying the position, intensity and shape of the ESCA core level peaks.

Representative spectra of five polymers are juxtaposed in Figure 38. The data are presented exactly as obtained, i.e. without correcting for variations in charging and work function. When peak positions were subsequently calculated, our standard procedure assumes that the main carbon peak is always 285.0 eV (53) and the other peaks in the sample are adjusted by the same increment. In Figure 38, the individual peaks have been normalized to the same height to facilitate rapid visual comparison of shape and position. The relative atom percent appears beside each peak. These were calculated from peak-height measurements, adjusted for line sensitivities with Wagner's coefficients (32). Even cursory inspection reveals a unique set of ESCA parameters associated with each polymer. Some of these features are quantized in Table V.

The two polyamic acid samples are very similar in structure, but still are clearly differentiated by the shape of the C 1s peak as well as peak-width in general. The asymmetry of the carbon peak suggests that deconvolution procedures should be used to make more detailed determination of the binding energy and intensity associated with each type of carbon in the polymer.

The NR-150B2/HT-S graphite fiber composite sample was cut from a typical adherend. Since this is a different class of sample from the other four, detailed comparison of peaks cannot be made. All peaks are broad which is probably due to the thick, insulating sample. The amount of oxygen present is a little hard to understand unless it derives from fiber surfaces that are usually given an oxidative surface treatment as the final production step.

Polycarbonate and polysulfone samples have significantly different elemental composition from polyimides, and provided confidence that our first results were not fortutiously accurate for materials of about 75% carbon. Furthermore, these thermoplastic elastomers have relatively high-temperature stability and may be useful to toughen polyimides (Professors J. E. McGrath and T. C. Ward, in the Chemistry Department at V.P.I. & S.U., have an active synthesis and characterization program utilizing these systems). These results are especially interesting because of the discovery of shake-up satellites in carbon, illustrated on expanded scale in Figure 38. Only one literature report exists at this point showing this phenomenon in polymers with <u>pendant</u> aromatic systems (55), and assigning the feature $\pi^* \leftarrow \pi$ transitions in the rings. Our results are the first report of shake-up satellites in <u>backbone</u> aromatic polymers. In consultation with Professor J. C. Schug about the theoretical quantum mechanical basis for $\pi^* \leftarrow \pi$ transitions, there appears to be no reason why all local aromatic systems should not have characteristic shake-up satellites. The problem lies more in the counting statistics required to separate these low intensity features from background. Nevertheless, it seems that an exciting new dimension of structural information is on the horizon.

The other notable features of the polycarbonate and polysulfone data are the high binding energy of oxygen in the former and sulfur in the latter. This is consistent with other carbonate and sulfate structures (59), and is a reflection of low electron density or high oxidation state of the atoms.

Calculations were made of the atom percent of the polymers from idealized stoichiometric formulas. These results, and the difference from values determined from ESCA peak heights, are compared in Table VI. Clearly the potential complications of quantitative ESCA have a small effect on these polymer samples.

FIGURE 38.

Narrow scan ESCA spectra of five

polymeric substrates.

Figure 38. Narrow scan ESCA spectra of five polymeric substrates.

Consideration of the position, intensity and shape of the core level bands determined by ESCA allows a distinct identification to be made of each polymer. Moreover, the atom percents calculated from intensities are accurate; in fact, ESCA may become the method of choice for quantitative elemental analysis of organic solids (35). Further, the "shake-up satellites" for polysulfone and polycarbonate, illustrated on expanded scale, promise a new dimension of structural information on localized π-systems in aromatic polymers.

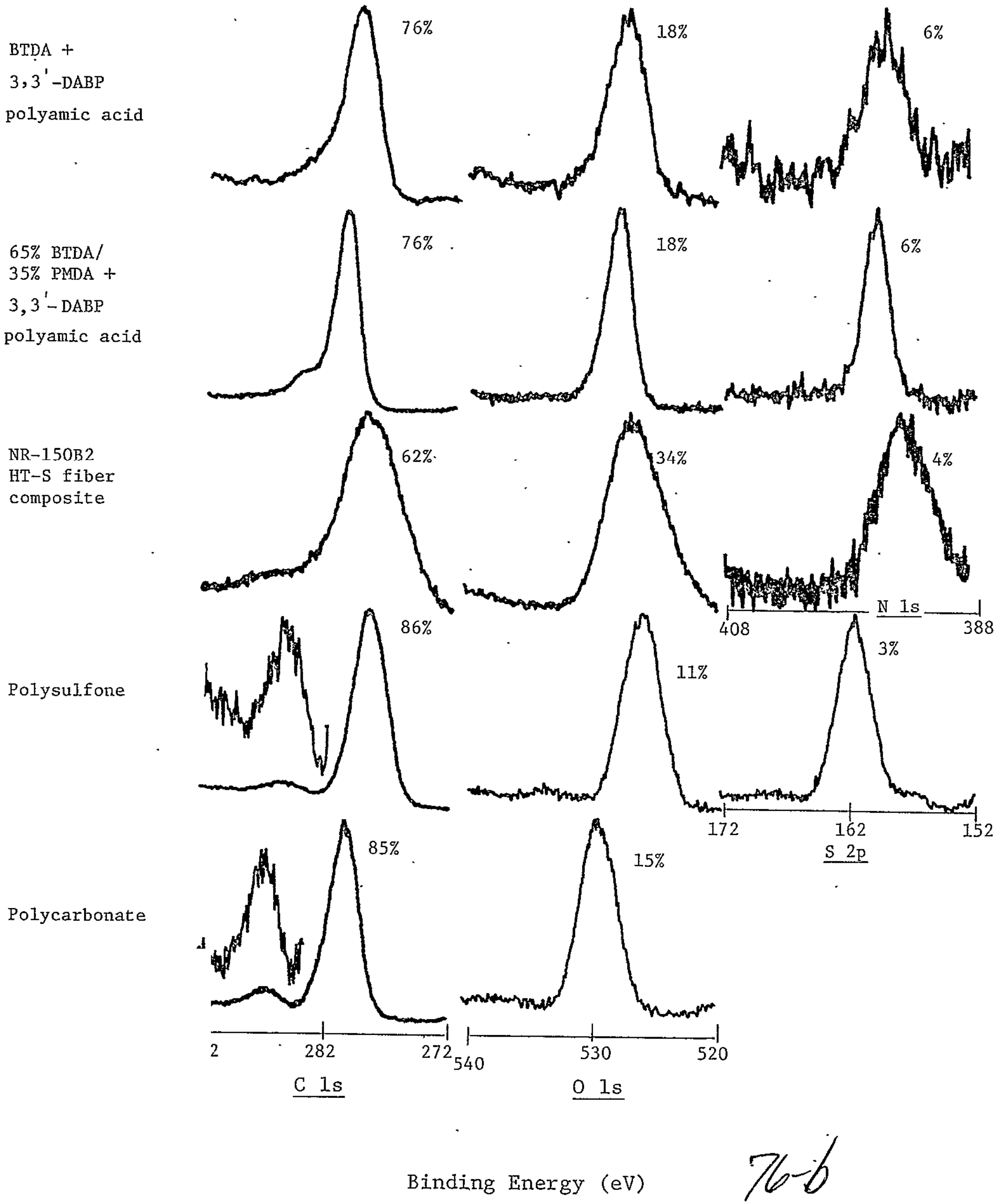
BTDA +
3,3'-DABP
polyamic acid
65% BTDA/
35% PMDA +
3,3'-DABP
polyamic acid
NR-150B2
HT-S fiber
composite
Polysulfone
Polycarbonate
76%
18%
6%
76%
18%
6%
62%
34%
4%
86%
11%
3%
85%
15%
408
N 1s
388
172
162
152
S 2p
2
282
272
540
530
520
C 1s
O 1s
Binding Energy (eV)

TABLE V

Position, Atom Percent and Width Determined From
Core Level ESCA Spectra of Polymers

Polymer	C 1s B.E.*	C 1s W*	C 1s Atom %	O 1s B.E.*	O 1s W*	O 1s Atom %	N 1s B.E.*	N 1s W*	N 1s Atom %	Work Function
BDTA + 3,3'-DABP polyamic acid	285.0	3.1	76	531.4	3.6	18	399.2	3.2	6	4.2
65% BDTA/35% PMDA + 3,3'-DABP polyamic acid	285.0	2.3	76	532.1	2.5	18	400.3	2.4	6	4.5
NR-150B2/HT-S fiber composite	285.0	5.3	62	532.7	5.2	34	399.8	5.0	4	5.9
							S 2p			
polysulfone (satellite)	285.0 292.1	3.3 -	86 -	532.8	3.6	11	168.2	3.1	3	6.6
polycarbonate (satellite)	285.0 291.2	2.7 -	85 -	534.3	3.4	15	-	-	-	4.8

*W = Width at 1/2 height (eV)

*B.E. = Binding Energy (eV)

TABLE VI

Calculated Stoichiometry (Atom %) vs. ESCA Determination

Polymer	Carbon		Oxygen		Nitrogen	
	Calc. (%)	Error (%)	Calc. (%)	Error (%)	Calc. (%)	Error (%)
BDTA + 3,3'-DABP polyamic acid	75	1	20	2	5	1
65% BDTA/35% PMDA + 3,3'-DABP polyamic acid	74	2	21	3	5	1
					Sulfur	
polysulfone	84	2	13	2	3	0
polycarbonate	84	1	16	1	-	-

IV. Summary and Conclusions

Scanning Electron Microscopy/Energy Dispersive Analysis of X-rays and Electron Spectroscopy for Chemical Analysis provided detail characterization of surfaces of interest to NASA-LaRC. Basic data were collected from adherends before bonding to detect contamination or provide reference standards. High Tensile Strength graphite fiber composites using three different matrix polymers, and titanium 6-4 with two different surface treatments, were the adherends. Joints were made with three adhesives, and lap shear strengths determined at NASA-LaRC. Surface analyses were performed on the fractured specimens to determine the proportions of the basic failure mechanisms operating to produce the observed strength (or weakness) in each case. These results are summarized in Table VII. Overall, the results so far lead to the following conclusions:

1. Surface preparation of composites by sanding creates a surface with myriads of potential sites to initiate fracture.

2. When composites are used, failure is almost always in the adherend (interlamellar fracture).

3. Composite failure is generally characterized by separation between the HT-S fibers and the polymer resin matrix.

4. Matrix polymers P13N and NR-150B2 fracture by high-area, brittle cleavage cracking between the fibers. Skybond 710 formed a discontinuous, chunky matrix and did not appear to make a bulk contribution to strength.

5. Composite adherends seem to be more sensitive to the location of flaws and stresses during bonding, and the distribution of strains during shear testing.

6. Particles were left on some titanium 6-4 adherends after a grit blast step, and subsequently initiated failure at low strength.

7. The anodizing surface treatment for titanium 6-4 gives a unique, new physical structure and some new chemical components in the oxide surface layer.

8. Fiberglass cloth adhesive carrier or "scrim" introduces the potential for stress concentration and interfacial separations; glass was usually a component of fracture surfaces.

9. Good strength was obtained under the best conditions with all three adhesives.

10. Some PPQ 413 formulations may have been in error, causing poor flow in some cases and thermal decomposition in others.

11. PPQ 413 was thermoplastic at high temperatures, as was LARC-13 to a lesser extent.

12. Aluminum powder in LARC-3 doubled high-temperature strength, apparently by acting as nuclei for a large volume of finely drawn polymer.

13. In relatively low-strength samples, fractography is very powerful for identifying the cause of weakness.

14. A predominant failure mode was interfacial separation between polymer resins and either glass fibers in adhesive scrim or HT-S graphite fibers in composite adherends.

15. Most bulk polymer failure was by brittle cleavage cracking; therefore, a promising direction for improved strength is toughening via incorporation of an elastomeric phase. Future improvement in strength of adhesively bonded composites will require

more compatible resin/fiber interfacial regions. This is also true for scrim-supported adhesive films.

16. Wide-scan ESCA spectra provided a rapid, "finger-print" characterization of the relative elemental compositon of the sample surface. More useful information was obtained by a second wide-scan after removing surface layers by ion-etching.

17. The change from blue to brown in anodized titanium 6-4 substrated derived from a layer of organic contamination, and not changes in chemical composition.

18. ESCA spectra of four neat polymer films provided a unique set of peak positions, shapes and intensities for each.

19. This is the first report of shake-up satellites in aromatic-back bone polymers, opening a new dimension of structural information on local π- systems in these macromolecules.

Table VII

Summary of Test Parameters, Strength and Fractography

NASA LaRC #	Adhesive	Adherend	Test Temp., °C	Lap Shear Strength, psi	Fig. No.	Components and Modes of Failure
1173	PPQ 413	Titanium 6-4, PO_4/F (1976)	25	1400	9,10	5% delamination, 95% interfacial particles initiate failure
1170 & 1174	PPQ 413 on A-1100/ #112 fiberglass cloth	Titanium 6-4, Anodized	25	1400-2000	12,13	40% interfacial 60% scrim cloth insufficient resin flow
PH-A-1	PPQ 413 on A-1100/ #112 fiberglass cloth	Titanium 6-4 PO_4F (1975)	25	4400	14	good resin penetration 100% scrim cloth resin/glass interface high-area, brittle matrix
1126.1	PPQ 413	NR-150B2 Composite	25	6200	15	100% composites resin/HT-S fiber interface high-area, brittle matrix
1126.2	PPQ 413 on A-1100/ #112 fiberglass cloth	NR-150B2 Composite	25	2100	-	80% composite 20% scrim cloth

Table VII CONT'D

NASA LaRC #	Adhesive	Adherend	Test Temp., °C	Lap Shear Strength, psi	Fig. No.	Components and Modes of Failure
1126.3	PPQ 413 on A-1100/ #112 fiberglass cloth	NR-150B2 Composite	25	2300	-	60% Composite 40% scrim cloth
-	PPQ 413	NR-150B2 Composite	286	2500	16	plastic deformation in glue line 100% composites resin/HT-S fiber interface large, brittle louvers in matrix
-	PPQ 413	NR-150B2 Composite	316	1000	17	decomposition & deformation in glue line 80% ductile + brittle resin in composite surface 20% brittle/ductile cracks in adhesive
1126.4	PPQ 413 on A-1100/ #112 fiberglass cloth	NR-150B2 Composite	25	4000	18	70% composite 30% scrim cloth poor resin penetration
-	PPQ 413	Skybond 710 composite	25	3400	19	100% composite resin/HT-S fiber interface around chunks in matrix
	PPQ 413	Skybond 710 composite	286	4200	20	100% composite (as above) plastic deformation of glue line

Table VII. CONT'D

NASA LaRC #	Adhesive	Adherend	Test Temp., °C	Lap Shear Strength psi	Fig. No.	Components and Modes of Failure
	PPQ 413	Skybond 710 composite	316	3000	21	100% composite (as above) plastic deformation of glue line
1132.1	LARC-13(30% Al powder) on A-1100/#112 fiberglass cloth	NR-150B2 Composite	25	5000	23	80% composite 20% voids at scrim cloth interstices
1132.2	LARC-13 (30% Al powder) on A-1100/#112 fiberglass cloth	NR-150B2 Composite	286	3200	24	50% composite 15% voids 35% scrim cloth
1132.4	LARC-13 (30% Al powder) on A-1100/#112 fiberglass cloth	NR-150B2 Composite	316	1700	25	90% scrim cloth 10% composite
1046-4	LARC-3	Skybond 710 composite	25	2200	27	100% composite
1046-1	LARC-3	Skybond 710 composite	25	3300*	28	50% voids 20% composite 30% high area, brittle adhesive

Table VII CONT'D

NASA LaRC #	Adhesive	Adherend	Test Temp., °C	Lap Shear Strength, psi	Fig. No.	Components and Modes of Failure
1046-2	LARC-3	Skybond 710 composite	286	1300	29	70% void 20% composite 10% plastically drawn adhesive, ductile
1044-2	LARC-3 (63% Al powder)	Skybond 710 composite	250	2400	30	40% composite 60% very fine, plastically deformed adhesive.
1044-1	LARC-3 (63% Al powder)	Skybond 710 composite	25	2400*	-	100% composite
1044-4	LARC-3 (63% Al powder)	Skybond 710 composite	25	2200	-	100% composite
1045-2	LARC-3 (63% Al powder) on A-1100/#112 fiberglass cloth	Skybond 710 composite	250	600	31	90% void 10% very fine, plastically deformed adhesive
1045-1	LARC-3 (63% Al powder) on A-1100/#112 fiberglass cloth	Skybond 710 composite	25	2300*	-	80% composite 20% scrim cloth surface
1045-4	LARC-3 (63% Al powder) on A-1100/#112 fiberglass cloth	Skybond 710 composite	25	1100		60% composite 40% scrim cloth surface

Table VII CONT'd

NASA LaRC #	Adhesive	Adherend	Test Temp., °C	Lap Shear Strength, psi	Fig. No.	Components and Modes of Failure
946-1	LARC-3	P13N Composite	25	3400	32	50% void 40% brittle adhesive 10% composite
948-1	LARC-3	P13N Composite	25	3800	32	90% composite 5% voids 5% brittle adhesive
947-1	LARC-3	P13N Composite	25	3700	-	70% composite 15% voids 15% brittle adhesive

*Spacer removed from strength-test grip

V. References

1. T. L. St. Clair and D. J. Progar, in "Adhesion Science and Technology", (L.-H. Lee, Ed.), p. 187, Plenum Press, New York, 1975.

2. A. K. St. Clair and T. L. St. Clair, Org. Coat. Plast. Chem. Preprints, 35, 185 (1975).

3. D. J. Progar and T. L. St. Clair, SAMPE Mat. Rev., 7, 53 (1975).

4. T. A. Bush, "Characterization of the Titanium Alloy Adherend Surface for Bonding with a Polyimide Resin," M. S. Thesis. Virginia Polytechnic Institute and State University, 1973.

5. T. A. Bush, M. E. Counts, T. C. Ward, J. P. Wightman, "Effect of Polymer Properties and Adherend Surfaces on Adhesion," NASA Final Report, NASA Contract NAS1-10646-14. November, 1973.

6. M. E. Counts and J. P. Wightman, "Effect of Adherend Surfaces on Adhesion," NASA Final Report, NASA Contract NAS1-10646-25, November, 1974.

7. Thurman A. Bush, Mary Ellen Counts and J. P. Wightman, "The Use of SEM, ESCA and Specular Reflectance IR in the Analysis of Fracture Surfaces in Several Polyimide/Titanium 6-4 Systems" in Adhesion Science and Technology, Part A, L.-H. Lee, Editor, p. 365, Plenum Press, New York (1975).

8. D. W. Dwight, M. E. Counts, and J. P. Wightman, "Effect of Polymer Properties and Adherend Surfaces on Adhesion," NASA Final Report, NASA Grant NSG-1124, December, 1975.

9. D. W. Dwight, M. E. Counts and J. P. Wightman, "Surface Analysis and Adhesive Bonding. II. Polyimides." in Colloid and Interface Science, Vol. V. III, M. Kerker, Ed., p. 143, Academic Press, New York (1976).

10. "Fluoropolymer Surface Studies. II." Presented in the Symposium on Advances in Characterization of Metal and Polymer Surfaces, A.C.S. Centennial Meeting, New York, April, 1976.

11. "Quantitative Aspects of ESCA." Presented in the Symposium on Advances in Characterization of Metal and Polymer Surfaces, A.C.S. Centennial Meeting, New York, April, 1976.

12. "Surface Analysis and Adhesive Bonding. I. Fluoropolymers", presented in the Kendall Award Symposium Honoring R. J. Good,

13. "Surface Analysis and Adhesion in Fluoropolymers", presented in the 29th Annual Summer Symposium, A.C.S. Analytical Division, Tempe, Arizona, June 1976.

14. "Surface Analysis and Adhesive Bonding. II. Polyimides." Presented in the International Conference on Colloids and Surfaces, (I.U.P.A.C. and A.C.S.), San Juan, P.R., June 1976.

15. W. A. Brainard and D. H. Buckley, Technical Note #D-6524, NASA Lewis Research Center, Cleveland, Ohio, October 1971.

16. D. H. Buckley and W. A. Brainard in "Advances in Polymer Friction and Wear, Vol. 5A (L.-H. Lee, Ed.), Plenum Press, New York, p. 315, 1974.

17. J. S. Solomon, J. A. Mescher, T. J. Wild, T. P. Graham, and R. G. Keil, Technical Report #AFML-TR-76-128, Wright-Patterson Air Force Base, Ohio, July 1976.

18. W. L. Baun, N. T. McDevitt and J. S. Solomon, Technical Report #AFML-TR-76, 29, Part II, Wright-Patterson Air Force Base, Ohio, September 1976.

19. M. J. Marmo, M. A. Mostafa, H. Jinnal, F. M. Fowkes, and J. A. Manson, Ind. Eng. Chem., Prod. Res. Dev., 15 (3), 206 (1976).

20. H. B. Hopfenberg and V. Stannett, in "The Physics of Glassy Polymers", (R. N. Howard, Ed.), Applied Science Publishers Ltd., London, 1973, p. 504.

21. H. B. Hopfenberg, L. Nicolais and E. Drioli, Polymer, 17, 195 (1976).

22. J. N. Sultan, R. C. Laible and F. J. McGarry, Appl. Polym. Symp., 16, 127 (1971).

23. J. N. Sultan and F. J. McGarry, Polym. Eng. Sci., 13 (1), 29 (1973).

24. R. C. Laible and F. J. McGarry, Polym.-Plast. Technol. Eng 7 (1), 27 (1976).

25. W. D. Bascom, C. O. Timmons and R. L. Jones, J. Mater. Sci 10 (6), 1037 (1975).

26. F. J. McGarry and T. J. Suen, U. S. Patent 3,853,690, December 10, 1975.

27. S. Mostovoy and E. J. Ripling, in Adhesion Science and Technology, (L.-H. Lee, Ed.), Plenum Press, p. 513, New York, 1975.

28. W. G. Knauss, App. Mech. Rev., 1973; 1.

29. R. P. Kusy and D. T. Turner, Polymer, 17, 161, (1976)

30. G. P. Koo, Plast. Eng., 30 (5), 33 (1974).

31. S. Bagrodia and G. L. Wilkes, J. Biomed. Mater. Res., 10, 101 (1976).

32. C. D. Wagner, Anal. Chem., 44, 1050 (1972).

33. K. T. Ng and D. M. Hercules, J. Electron Spectrosc., 7, 257 (1975).

34. J. M. Delaney and J. W. Rabalais, Anal. Chem., 48, 920 (1976).

35. K. L. Cheng and J. W. Prather, Crit. Rev. Anal. Chem., 37, May 1975.

36. H. Ebel and M. F. Ebel, X-ray Spectrometry, 2, 19 (1973).

37. P. H. Holloway, J. Electron Spectrosc., 7, 215 (1975).

38. R. J. Baird, C. S. Fadley, S. K. Kawamoto, M. Mehta, R. Alvarez and J. A. Silva, Anal. Chem., 48, 843 (1976).

39. J. T. Armstrong and P. R. Buseck, Anal. Chem., 47, 2178 (1975).

40. R. S. Swingle and W. M. Riggs, Crit. Rev. Anal. Chem., 267, October 1975.

41. H. Berthou and C. K. Jorgensen, Anal. Chem., 47, 482 (1975).

42. M. Janghorbani, M. Vulli and K. Starke, Anal. Chem., 47, 2201 (1975).

43. D. T. Clark, in Electron Emission Spectroscopy (W. Dekeyser, L. Fiermans, G. Vanderkelen and J. Vennik, Eds.), D. Reidel Publishing Co., Boston, 1973, p. 373.

44. T. Farrell, J. Phys. E. Sci. Inst., 6, 977 (1973).

45. M. Mehta and C. S. Fadley, Phys. Lett. A, 55, 59 (1975).

46. M. F. Ebel, J. Electron Spectrosc., 8, 213 (1976).

47. K. Asami, J. Electron Spectrosc., 9, 469 (1976).

48. R. Bouman, J. B. Van Mechelen and A. A. Holscher, Surf. Sci., 57, 441 (1976).

49. L. J. Brillson and G. P. Ceasar, Surf. Sci., 58, 457 (1976)

50. R. F. Reilman, A. Msezane and S. T. Manson, J. Electron Spectrosc., 8, 389 (1976).

51. M. Valli, M. Janghorbani and K. Starke, Anal. Chim. Acta, 82, 121 (1976).

52. G. K. Wertheim and S. Huefner, J. Inorg. Nucl. Chem., 38, 1701 (1976).

53. D. T. Clark, in Advances in Polymer Friction and Lubrication, 5A (L. H. Lee, Ed.), Plenum Press, New York, 1974, p. 241.

54. D. T. Clark, J. Peeling and J. M. O'Malley, J. Polym. Sci., Polym. Chem. Ed., 14, 543 (1976).

55. D. T. Clark, D. B. Adams, A. Dilks, J. Peeling and H. R. Thomas, J. Electron Spectrosc., 8, 51 (1976)

56. D. J. Progar and T. L. St. Clair, "Preliminary Evaluation of a Novel Polyimide Adhesive for Bonding Titanium and Reinforced Composites," presented at the 7th National SAMPE Technical Conference, Albuquerque, New Mexico, October 1975.

57. A. K. St. Clair and T. L. St. Clair, "Structure-Property Relationships of Isomeric Addition Polyimides Containing Nadimide End Groups," Presented at the Symposium on Molecular Engineering-- -Au Interface Between Polymer Chemistry and Polymer Engineering, 170th A.C.S. Meeting, Chicago, August 1975.

58. P. M. Hergenrother and D. J. Progar, "High Temperature Composite Bonding with PPQ," presented at the 22nd National SAMPE Symposium.

VI. APPENDIX

"Surface Analysis and Adhesive Bonding. II. Polyimides"

by

David W. Dwight, Mary Ellen Counts and James P. Wightman

(Reference 9)

ACADEMIC PRESS, INC.

SURFACE ANALYSIS AND ADHESIVE BONDING. II. POLYIMIDES

David W. Dwight, Mary Ellen Counts and
James P. Wightman
Virginia Polytechnic Institute and State University

I. ABSTRACT

Surface analysis by SEM/EDAX shows effects upon fracture surfaces of adhesive formulation, process, and test variables. Empirical correlations between shear strength and structure of the fracture surface are promoted by qualitative fracture mechanics theory. Interfacial and bulk failure, viscoelastic, plastic and brittle mechanisms, and the distribution of initial flaws are the controlling factors. A series of experimental polyimide adhesives was tested on titanium 6-4 adherends, and voids in the glue line appear to be a prime factor limiting strength and reproducibility. Strength varies inversely with temperature of testing. SEM shows a corresponding increase in interfacial failure and decrease in plastic and brittle mechanisms. Improved high-temperature strength was obtained by filling the adhesive with aluminum powder; interfacial separation was eliminated and much finer features characterize the microtopography. High-temperature failure appears to proceed farther from the interface, judging by estimates of the residual adhesive thickness using EDAX. Changes in solvent, amine and anhydride in the adhesive formulation also are characterized by unique fracture surfaces.

II. INTRODUCTION

Adhesive bonding of aerospace systems and components is increasing at a rapid pace (1). Substantial cost savings are possible with the reduction in weight and in manufacturing costs. Other advantages over riveted or bolted structures are facile joining of thin and contoured sheets, and reduced stress concentration and galvanic corrosion; adhesives are the only practicable way to join fiber-reinforced composites and honeycomb structures. However, new service requirements (10,000 hours at 600°F [316°C]) exceed the property limits of most synthetic organic polymers. The total system also must withstand exposure to high humidity and severe temperature cycles. Furthermore, restrictions are placed upon polymer synthesis by the need for good processability with very low

volatiles under stringent autoclave conditions.

Our interdisciplinary program has synthesis and strength-testing of novel high-temperature polymers as its primary focus (2), with detailed surface analyses of substrates and fracture surfaces to aid in interpreting the results (3). This report integrates some of the results of the preliminary studies with new data derived from changes in solvent, amine and anhydride during adhesive formulation. Also we have studied the effects of aging and strength-testing at high temperatures, and the improvement in these properties with aluminum powder adhesive filler. Interpretation and correlation of the strength-testing and SEM results is facilitated by reference to qualitative fracture mechanics theory (4). This approach identifies: (1) inherent flaws, (2) viscoelastic and plastic deformation, (3) crazing and crack propagation, and (4) interfacial failure as the main factors contributing to overall strength. Changes in parameters of adhesive formulation, processing, and testing alter the proportions of each of these failure mechanisms. Results from SEM combined with energy-dispersive x-ray fluorescence analysis (EDAX) suggest that, in some cases, useful estimates of the thickness of residual adhesive layers may be made. For improvements in strength, it is first important to know the details of crack-initiation, and the extent and morphology of the failure zone (5).

III. EXPERIMENTAL

Photomicrographs were obtained with the Advanced Metals Research (AMR) Corporation Model 900 Scanning Electron Microscope operating at 20 kV. The specimens were cut to approximately 1 x 1 cm with a high pressure cutting bar and fastened to SEM mounting pegs with adhesive-coated, conductive copper tape. To enhance conductivity, a thin (~200Å) film of Au/Pd alloy was vacuum evaporated onto the samples. Photomicrographs were taken with the samples inclined 20° from incident electron beam.

Rapid elemental analysis was obtained by energy-dispersive x-ray fluorescence with the EDAX International Model 707A unit attached to the AMR-900 SEM.

Adhesive synthesis and testing has been described elsewhere (2).

<u>Abbreviations of Monomers and Solvents</u>

BTDA-Benzophenone Tetracarboxylic Acid Dianhydride
DABP-Diaminobenzophenone
PMDA-Pyromellitic Dianhydride

ODPA-Oxidiphthalic Anhydride
EHA-13-m,m''-Diamino Terbenzylone
DG-Dyglyme, DMAC-Dimethylacetamide, DMF-dimethylformamide

IV. RESULTS AND DISCUSSION

A. Aging and Testing at Elevated Temperatures

A series was prepared with a standard BTDA + m,m'-DABP/DG adhesive and exposed to 295°C for 30 days in air, and then shear tested at 25°, 225°, 250° and 270°C, respectively. Little thermal- or oxidative-degradation occurred during the severe exposure (joints were not stressed during aging), but strength dropped rapidly at higher test temperatures. SEM examination (Figures 1-5) indicates that two processes occur as the test temperature increases: (1) the percentage of interfacial failure increases, and (2) the amount of plastic deformation and brittle fracture decreases.

The same general features characterize the fracture surface of the sample tested at room temperature (Figure 1) as

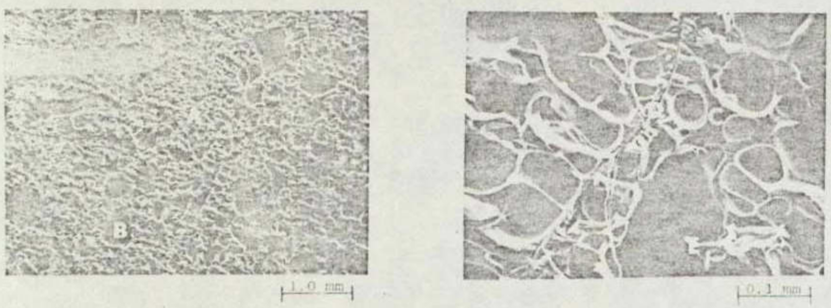

Fig. 1. Photomicrographs of the fracture surface of BTDA + m,m'-DABP/DG adhesive after aging 30 days at 295°C; 3570 psi shear strength at room temperature. Features similar to previous, (unaged) room temperature results (3).

have been seen in previous (unaged) high strength samples (3). At lower magnification there is a fairly uniform distribution of raised material that forms a filigree pattern "A" superimposed upon lower, smooth, oblong areas "B" that have dimensions ranging from 0.02 to 0.5 mm, approximately. The low areas are the bottoms of voids that were probably created during the formation of the joint and expanded during fracture. The filigree is composed of void-cell walls that have undergone plastic deformation and finally fractured, primarily by a brittle cleavage-crack propagation mechanism. It is

93

only the deformed areas that provide strength. Some of the cracks are smooth and quite parallel to the substrate, such as in area "C" on the higher magnification photomicrograph, but also fine louvers, tilted at an angle to the adherend, appear along the curved line that comes down the center "D". Localized "hot spots" that could promote ductility indicated at "E" may arise from adiabatic fracture processes. Note that only a very small amount of interfacial failure appears, and many, thin walls result from plastic deformation.

Generally similar features are seen in the 225°C sample (Figure 2) but the proportion of interfacial failure "A", and

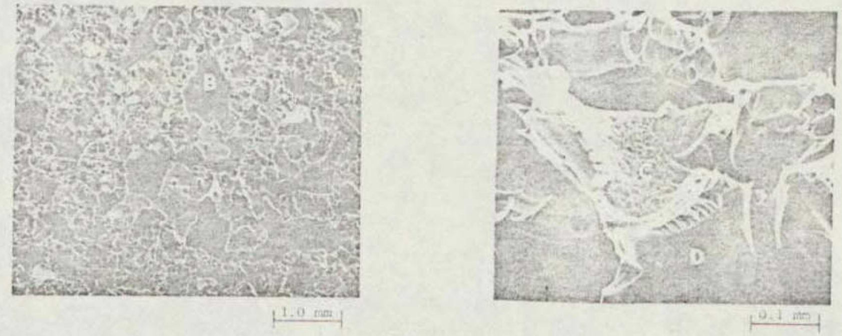

Fig. 2. Same as Fig. 1 except 2065 psi strength, tested at 225°C.

void area "B" has increased. Areas of adhesive that have detached from the opposite adherend show that original interfacial contact was good, because the polymer faithfully replicates the detailed surface features of the titanium (area "C"). Comparing Figures 1 and 2, it appears that the voids have coalesced in the latter, sometimes reaching dimensions over 1 mm. Correspondingly, void-cell walls are thicker; area "D" at higher magnification provides a striking example of a plastically-drawn void-cell wall, circumscribed by brittle cleavage cracks.

Figure 3 shows that interfacial failure and void area increase with temperature (250°C). Large void spaces are almost completely interconnected across the sample. At higher magnification, some strength across the interface is indicated by continuity where the brittle, cleavage-crack louvers meet the exposed substrate. Interfacial failure predominates in the 270°C test. The opposite sides of mating fracture surfaces are shown in Figure 4; it is quite simple and instructive to locate the matching features. There is very little plastic deformation, hence little strength. Brittle cleavage cracks without much louvering account for the failure that is

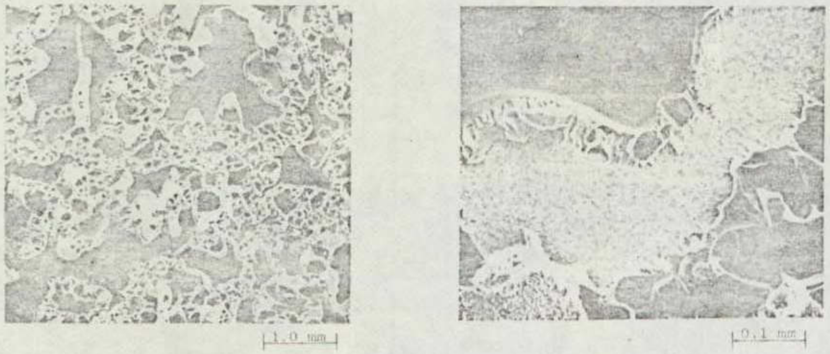

Fig. 3. Same as Fig. 1 except 1465 psi strength, tested at 250°C.

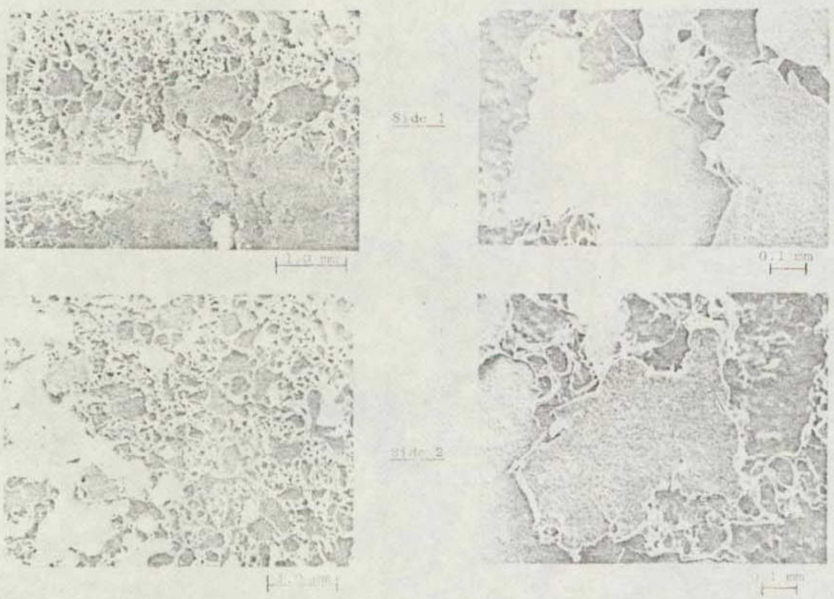

Fig. 4. Same as Fig. 1 except 760 psi strength, tested at 270°C; opposite sides of mating fracture surfaces.

not interfacial. The circled area of Side 1 is shown at higher magnification in Figure 5, illustrating a discontinuity (low forces) at the polymer/metal interface.

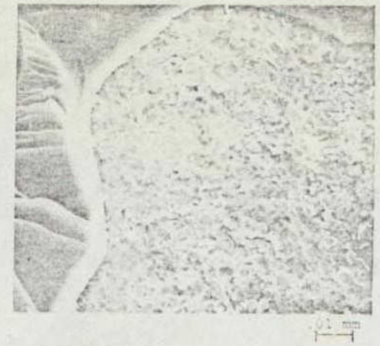

Fig. 5. High magnification view of area circled in Fig. 4. Note the brittle cleavage-crack louvers on the left and the discontinuity at the polymer/metal interface.

Apparently high temperature reduces interfacial forces, probably through differential thermal expansion, and the polymer experiences less stress. In other words, without sufficient bonding at the polymer/metal interface, mechanisms that provide adhesive strength (elastic deformation, crazing, etc.) will not come into play. From this point of view, it seems reasonable that overall strength would be the product of an interfacial bonding term and a term that sums the contributions to the strength of bulk materials.

Progar and St.Clair found a two-fold improvement in high-temperature strength (65/35 BTDA/PMDA + m,m'-DABP) was obtained by using aluminum powder as an adhesive filler (2). Figure 6 shows typical surface features of filled-adhesive samples fractured at room temperature. The aluminum filler is apparent as lumps about 1-10 μm in diameter, covered with at least a thin layer of polyimide. Fracture-surface features are much smaller than with unfilled adhesive. At high magnification it appears that the fracture initiates in a myriad of minute voids (or nucleation sites) existing in the walls of the larger void areas, and the fracture surface is composed of very thin, plastically-deformed microvoid-cell walls. This feature is unique to the filled adhesive.

No interfacial failure occurred, in contrast to the results at 250°C with unfilled adhesive. Perhaps the aluminum filler prevents interfacial failure at high temperature by adjusting relative thermal expansion. Another effect of filler is to increase the amount of fracture surface area by expanding the filigree pattern into a more continuous area.

EDAX provided information on the thickness of adhesive film remaining on the substrate after fracture, since the 20 kV electron beam should penetrate about 1 μm of organic polymer. EDAX results from two magnifications of the room temperature

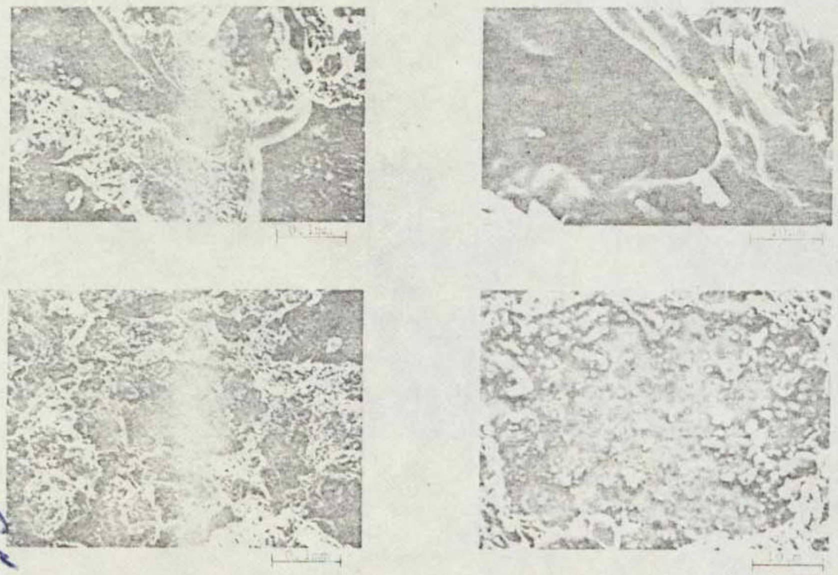

96

Fig. 6. Photomicrographs of the fracture surface of 65/35 BTDA/PMDA + m,m'-DABP/DG adhesive filled with 50% (top) and 70% (bottom) aluminum powder.

samples are shown in Figure 7. The gold and palladium peaks are due to the ~200 Å conductive coating layer; they are useful for approximate internal standards. The aluminum filler actually gave the largest peak in the original spectra, omitted here for clarity. In line A (50% Al), all the adherend (Ti) signal was found to be coming from small holes, seen in Figure 6 (top) at high magnification; no Ti signal could be obtained at the bottom of voids. The opposite was true at 70% Al. More Ti appears on the survey scan, and it dominates the spectrum from void bottoms. Figure 6 (bottom) shows the area from which the last EDAX spectrum was taken. Clearly there is a layer of polymer there, but it seems to be so thin that titanium surface features show through vaguely. EDAX examination of both high temperature samples failed to uncover a Ti signal at any magnification. Thus it can be concluded that the room temperature fracture occasionally penetrates nearer to the adherend than the high temperature fracture, which can hardly come closer than 1μm.

The combination of SEM and EDAX provides most of the essential information on the locus and micromechanics of fracture. It is true that the SEM electron beam can penetrate several hundred Angstrom units of adhesive and give an EDAX signal from underlying adherend. However the combination between the EDAX spectra and the SEM photomicrographs usually leaves little doubt about the details of fracture, as illus-

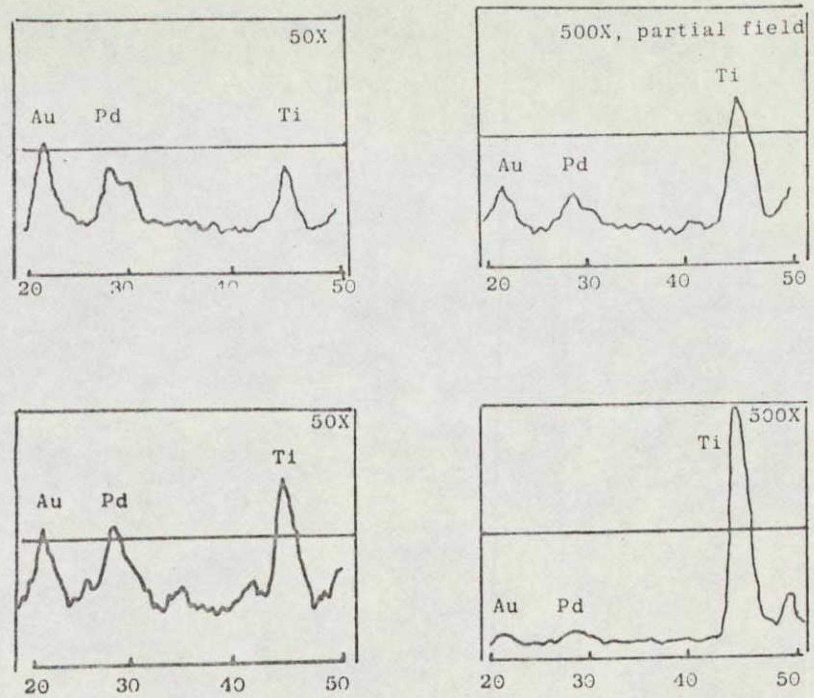

Fig. 7. Elemental analysis, using EDAX at two magnifications, of the same samples shown in Fig. 6. Top - Some adherend shows through on the 50X "survey" on the left, but all the Ti signal originated from holes like the one shown in Fig. 6. Bottom - More adherend signal at 50X, and it dominates the spectrum when the beam was focussed into the void bottom.

trated in Figures 6 and 7. Moreover, by variation of the beam voltage and use of calibration samples of known thickness, it may be possible to make more quantitative measurements of residual adhesive film thickness. An important advantage of SEM/EDAX is the ability to focus the electron beam and analyze only very small, selected areas.

B. Anhydride, Amine and Solvent

Several adhesive formulation parameters were varied, and good shear strengths obtained with changes in comonomer and solvent (except for the use of p,p'-DABP, which gave 1400 psi). Figures 8-10 display the micro-mechanics of fracture for these samples. The shear strength results can be rationalized in terms of the proportion of voids, interfacial and brittle failure, and plastic deformation.

The use of DMF as solvent for standard polyimide gives little interfacial failure, but a large proportion of connected-void area compared to fracture area, shown in Figure 8.

96

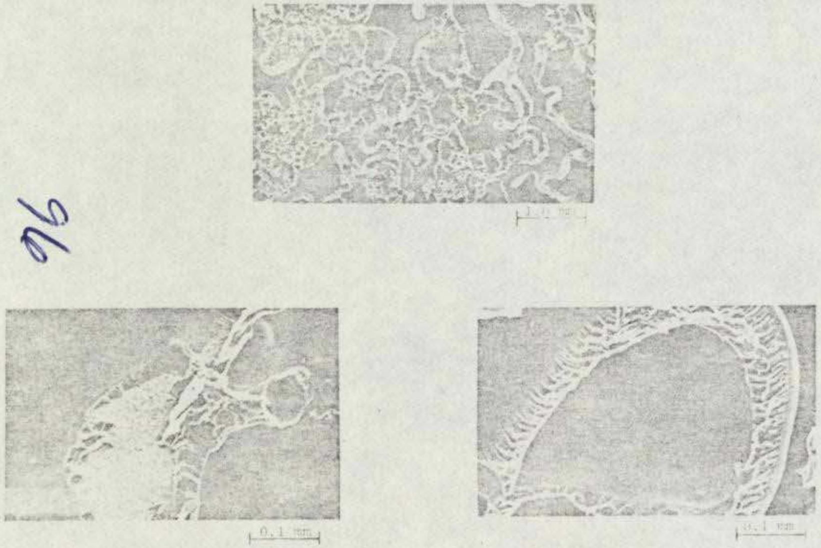

Fig. 8. Photomicrographs of the fracture surface of BTDA + m,m'-DABP adhesive in DMF solvent; 3700 psi shear strength.

Apparently the 3700 psi strength is developed by the initiation and annihilation of a large number of brittle cleavage cracks illustrated by numerous louvers in the higher magnification photomicrographs. Figure 9 shows a large proportion

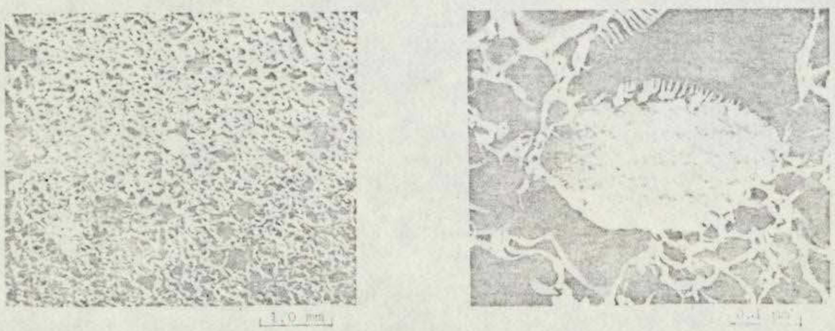

Fig. 9. Photomicrographs of the fracture surface of OPDA + m,m'-DABP/DG adhesive; 4500 psi shear strength.

of drawn and fractured polymer in a high-strength sample prepared with anhydride comonomer, ODPA. At higher magnification, a balance between moderate plastic deformation and brittle fracture is apparent, as well as exposed substrate and an indication of strong polymer/metal bond (continuity at the interface).

EAH-13 comonomer was used to provide a totally imidized, film adhesive with enough flow at high temperature so that good interfacial contact occurred during pressing at 200 psi and 300°C for an hour. The photomicrographs in Figure 10 show

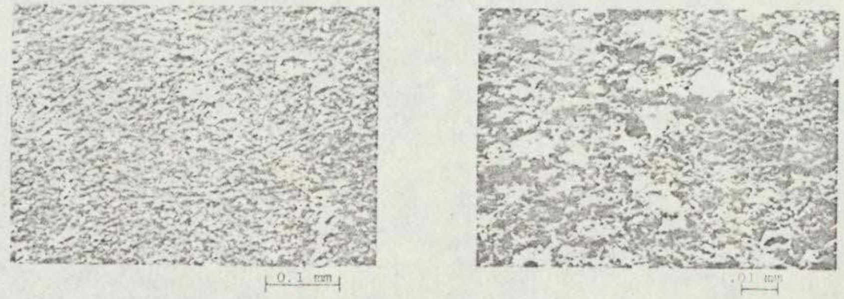

Fig. 10. Photomicrographs of the fracture surface of BTDA + EAH-13/DMAC, "imidized flow-bonding" adhesive; 3500 psi shear strength. Note the replication of the titanium adherend surface, and the absence of voids or plastic deformation: failure was completely interfacial.

that the polymer has formed a detailed replica of the titanium surface. Failure is totally interfacial on one side of the joint. It is unusual for good strength to be obtained without contributions from plastic and brittle mechanisms. Perhaps elastic deformation occurred. Otherwise, the true area over which polymer/metal polar and dispersion forces interact must be many times the geometrical joint area, due to the adherend roughness. Most important is the absence of the typical void structures so characteristic of joints prepared by imidization during bonding.

V. SUMMARY AND CONCLUSIONS

The basic findings to date of our interdisciplinary adhesive program are summarized in Table 1. Lap shear strength decreased when the test temperature increased; interfacial failure and void area increased and plastic and brittle mechanisms decreased. Interfacial bonding must be weakened by

TABLE 1
Variations in Adhesive Formulation, Test Parameters, Strength and Fracture Surfaces

Variable		Lap Shear Strength (psi)†	Fracture Surface Analysis: Figure No.	Fracture Surface Analysis: Comments
Temperature (BTDA + m,m'-DABP)				
Aging, °C	Testing, °C			
295	25	4320	1	∿50/50 filigree and and void, almost no interfacial failure; thin plastic deformation, brittle fracture with louvers.
295	225	2060	2	More interfacial and void area; thicker-wall deformation, brittle fracture with louvers.
295	250	1460	3	Similar except more void and interfacial area.
295	270	850	4,5	∿60/30/10 interfacial/void/filigree; small plastic deformation and brittle fracture surface area.
Aluminum Powder (65/35 BDTA/PMDA + m,m'-DABP DG)				
% Al	Testing, °C			
50	25	3780	6,7	∿60/40 void and filigree; much finer features at hi mag.—microvoids in walls, thin plastic deformation area large; lumps of Al seem covered with polymer. EDAX:Ti

TABLE 1 (continued)

Variable		Lap Shear Strength (psi)†	Fracture Surface Analysis: Figure No.	Fracture Surface Analysis: Comments
%Al	Testing, °C			
50	250	1210	--	Similar at 20X, but melting rather than drawing. EDAX:No Ti
70	25	3720	6,7	Fracture area continuous instead of filigree, low void and no interfacial area; detail similar to above EDAX:Ti
70	250	2340	--	Similar, except EDAX:no Ti
Solvent (BTDA+mm'-DABP)				
DG		5280	6*,9*	∿50/50 filigree and void, almost no interfacial failure; thin plastic deformation, brittle fracture with louvers.
DG		3860	10*, 11*	Similar except more interfacial and void area.
DMAC		2510	7*,8*	Large void area and interfacial failure, no filigree; little deformation or brittle fracture surface
DMF		3860	8	∿20/70/10 filigree/void/interfacial; little deformation but high area of brittle fracture with louvers.

97

TABLE 1 (continued)

Variable	Lap Shear Strength (psi)†	Fracture Surface Analysis: Figure No.	Fracture Surface Analysis: Comments
Anhydride (m,m'-DABP/DG)			
BTDA	5280	6*,9*	Similar to line 1
PMDA	0	15*,16*	60/40 interfacial and void; small brittle fracture area.
ODPA	3250	9	High % filigree; short, thin deformation and brittle louvers.
Amine (BTDA/DG)			
m,m'-DABP	5280	6*,9*	Similar to line 1
m,p'-DABP	2070	12*,13*, 14*	50/50 void and interfacial; some hackled brittle fracture
EAH-13/DMAC	3500	10	100% interfacial; no voids, deformation, or brittle failure.

*Reference 3. †Average of three samples.

differential thermal expansion. Filling the adhesive with aluminum powder doubled the high-temperature shear strength; interfacial failure was eliminated and features of fracture surfaces were an order of magnitude smaller.

DG and DMF promoted good contact with the adherend, but DG resulted in plastic deformation while DMF gave high-area, brittle fracture. DMAC appeared to give poor adherend contact and little deformation or brittle fracture surface. Changes in solvent may effect polymer physical properties through variations in chain entanglement.

Adhesive formulations with either the anhydride PMDA or para-structure in the amine appeared more brittle than when anhydrides BTDA or ODPA or m-amines were used. Plastic deformation decreased and interfacial failure and low-area brittle cracks (without extensive louvering) increased in the

former cases. The totally pre-imidized "flow-bonding" adhesive film, employing the amine EAH-13, produced no voids in the glue line during the bonding step, and failed interfacially (with good strength in spite of the absence of brittle and plastic mechanisms.)

In all other cases, voids were generated during cure either by residual solvent or water of imidization. The distribution of void sizes and locations within the glue line seems to be random and probably was the main cause of poor reproducability and lowered shear strengths. Not only is the area of drawing and fracture limited by void areas, but also they serve as nucleation sites for crack initiation. When strength results varied anomalously on replicate samples, there was usually a corresponding variation in void area.

Currently work is in progress to eliminate voids, synthesize more effective polymers, employ high-modulus fiber composites as adherends, expand durability tests, and refine the semi-empirical approach to understand adhesive bonding by quantitative analysis of fracture-surface data and rheological (WLF) measurements.

VI. ACKNOWLEDGMENTS

NASA support (Grant No. NSG-1124), program coordination by Norm Johnston, and expert SEM/EDAX operation of Frank Mitsianis are gratefully acknowledged.

VII. REFERENCES

1. Dauksys, R. J., SAMPE Quarterly, 1 October 1973.
2. a. St.Clair, T. L. and Progar, D. J., in "Adhesion Science and Technology" (L.-H. Lee, Ed.), p. 187, Plenum Press, New York, 1975.
   b. St.Clair, A.K. and St.Clair, T.L., SAMPE Mat. Rev., 7, 53 (1975).
   c. Progar, D. J. and St.Clair, T. L., Organic Coatings and Plastics Chemistry Preprints 35, 185 (1975).
3. Bush, T. A., Counts, M. E. and Wightman, J. P., in "Adhesion Science and Technology" (L.-H. Lee, Ed.), p. 365, Plenum Press, New York, 1975.
4. Dwight, D. W., in "Kendall Award Symposium, 1976", to be published in J. Colloid Interface Sci.
5. Good, R. J., J. Adhesion, 4, 133 (1972).